INAUGURAL-DISSERTATION

zur
Erlangung der Doktorwürde
der
Naturwissenschaftlich-Mathematischen
Gesamtfakultät
der
Ruprecht-Karls-Universität
Heidelberg

vorgelegt von
Tina Wiegand (M. Sc.)
aus Ilmenau

TAG DER MÜNDLICHEN PRÜFUNG:
2. FEBRUAR 2018

RECEPTOR-MEDIATED FORCES FOR CELL SENSING OF EXTRACELLULAR LIGANDS AND FOR VIRUS PARTICLE UPTAKE

Gutachter:

Prof. Dr. Joachim Spatz
Prof. (apl.) Dr. Reiner Dahint

ABSTRACT

Mechanical forces between cells ensure organic development and homeostasis, but they are also associated with diseases such as cancer or viral infections. The absolute forces in nature can be as high as 1.5 kN, which allows the mantis shrimp to smash oysters, down to a few pN transduced by single cellular receptors. However, these small forces are strong enough for cells to probe their local environment. While the mechanism, which enables cells to investigate the stiffness of their surrounding, is already well elucidated, information on how cells sense spatial distribution of ligands is missing.

In this thesis I established a method, which allows to measure cellular traction forces on elastic substrates with varying nano-spacing of extracellular ligands. In contrast to previous studies on stiff substrates, adhesion complexes and tractions were larger for longer distances between extracellular adhesion sites. This can be theoretically explained by the force load on individual integrin receptors, which has to exceed a certain threshold value to promote adhesion growth through conformational changes in a protein of the "clutch complex".

In order to experimentally access the force load per integrin heterodimer, I combined molecular tension fluorescence microscopy (MTFM) with traction force microscopy (TFM). For the first time, I could assess a homogeneous distribution of forces > 19 pN underneath the adhesion area of cells on soft substrates. Simultaneously, macroscopic tractions up to 2.7 kPa were observed at the cell edges. Applying stronger tension probes and analyzing tractions in the z-direction will help to cross-validate the results obtained from these two state-of-the-art methods in biomechanics as a next step.

In the second part I investigated the mechanical parameters of virus particle uptake by cells. Many intracellular pathogens, such as mammalian reoviruses as employed in this thesis, mimic extracellular motives to interact with host cells and initiate their internalization. This leads to the assumption that host cells sense this specific ligand presentation, engage the endocytic machinery and generate forces, which are able to overcome the bending and tension energy of their plasma membrane.

I demonstrated that these forces exerted on single reovirus particles on the basolateral side of cells are strong enough to break down the biotin-NeutrAvidin bond used for virus immobilization on stiff and soft substrates. I quantified the forces to exceed 40 pN by kinetic analysis of the tearing of viruses from these surfaces and single MTFM with covalently immobilized reoviruses.

The herein presented methods are powerful tools to study forces exerted by individual receptors as well as on single particles e.g. during endocytosis. The involvement of the actin cytoskeleton, specific receptors or molecules of the endocytic machinery was examined. Inhibition of the ligand-receptor interactions between reoviruses and cells did not significantly change the rate of virus uptake. Interestingly, bare nanoparticles of comparable diameter lacking specific binding sites were torn off at a similar rate and thus with the same forces as viruses. Hence, specific receptors seem to be dispensable for virus particle uptake.

ZUSAMMENFASSUNG

Mechanische Kräfte zwischen Zellen gewährleisten die Entwicklung von Organen und deren Selbstregulierung, können aber auch zu Krankheiten wie Krebs oder Virusinfektionen führen. Die absoluten Kräfte reichen dabei von 1.5 kPa, was es dem Fangschreckenkrebs ermöglicht Austern zu zerschlagen, bis hinab zu wenigen pN, die von einzelnen zellulären Rezeptoren übertragen werden. Diese sehr geringen Kräfte sind ausreichend für Zellen um ihr lokales Umfeld zu untersuchen. Dabei ist der Mechanismus, welcher es Zellen ermöglicht die Steifigkeit ihrer Umgebung zu ermitteln, bereits gut aufgeklärt. Allerdings fehlen Informationen darüber, wie Zellen die räumliche Verteilung von Liganden wahrnehmen.

In dieser Dissertation habe ich eine Methode etabliert, die es erlaubt zelluläre Traktionskräfte auf elastischen Substraten mit verschiedenen Nano-Abständen der extrazellulären Liganden zu messen. Im Gegensatz zu früheren Studien auf steifen Substraten waren die Adhäsionskomplexe und Zugkräfte größer, wenn die Abstände zwischen den extrazellulären Ankerpunkten anstiegen. Dies kann theoretisch durch die Belastungskraft auf einzelne Integrinrezeptoren erklärt werden. Übersteigt sie einen gewissen Schwellenwert, wird das Adhäsionswachstum durch eine Konformationsänderung in einem Protein des "Kupplungs-Komplexes" gefördert.

Um die Belastungskraft auf ein Integrin-Heterodimer experimentell zugänglich zu machen, habe ich molekulare Spannungs-Fluoreszenz-Mikroskopie (MTFM) mit Traktionskraft-Mikroskopie (TFM) kombiniert. Dadurch konnte ich zum ersten Mal eine homogene Verteilung von Kräften > 19 pN unterhalb der Adhäsionsfläche von Zellen auf weichen Materialien nachweisen. Gleichzeitig wurden makroskopische Zugspannungen bis zu 2.7 kPa an den Zellrändern beobachtet. Stärkere Spannungssonden und Analysen der Zugkräfte in z-Richtung werden im nächsten Schritt eine Kreuzvalidierung dieser modernsten Methoden in der Biomechanik erlauben.

Im zweiten Teil habe ich die mechanischen Faktoren der Viruspartikelaufnahme in Zellen untersucht. Viele intrazelluläre Pathogene, wie Reoviren, die in dieser Arbeit verwendet wurden, imitieren extrazelluläre Motive, um mit Wirtszellen zu interagieren und ihre Internalisierung zu initiieren. Dies führt zu der Vermutung, dass Zellen diese spezifische Ligandenpräsentation spüren, die endozytotische Maschinerie herbeiziehen und Kräfte generieren, welche die Biege- und Spannungsenergie der Plasmamembran überwinden können. Ich konnte zeigen, dass die Kräfte, die auf einzelne Reoviren von der basalen Seite von Zellen ausgeübt werden, stark genug sind, um die Biotin-NeutrAvidin Bindung zu brechen, welche für die Immobilisierung der Viren auf harten sowie weichen Materialien genutzt wurde. Mit Hilfe kinetischer Analyse des Abreißens der Viren von der Oberfläche und Einzel-MTFM Messungen mit kovalent immobilisierten Viren ermittelte ich Kräfte, die 40 pN überstiegen.

Die hier vorgestellten Methoden sind mächtige Werkzeuge zur Untersuchung von Kräften während der Endozytose und der Beteiligung des Aktinzytoskeletts, spezifischer Rezeptoren oder von Molekülen der endozytotischen Maschinerie. Die Hemmung der Rezeptor-Liganden-Interaktion hat die Rate, mit der Reoviren aufgenommen wurden, nicht signifikant geändert. Interessanterweise wurden sogar bloße Nanopartikel mit vergleichbarem Durchmesser aber ohne spezifische Bindestellen mit ähnlicher Rate und somit ähnlichen Kräften wie Viren aufgenommen. Daher scheinen spezifische Rezeptoren für die Virusaufnahme entbehrlich zu sein.

The mantis shrimp can deliver a blow with fifteen hundred Newtons of force, which tells you what a sissy punch Newton must have had.

— Ze Frank

ACKNOWLEDGMENTS

Many thanks to Prof. Joachim Spatz for providing an excellent and challenging research facility and gathering fantastic scientists in the PCI and MPI in Heidelberg as well as in Stuttgart. Besides the larger framework he also constantly provided creative approaches towards new experiments and specific questions regarding my work and I feel very honored to have been allowed to join our super cool retreats to Antholz, which I already enjoyed five times - maybe once I will have stayed with Familiy Brunner more often than Joachim has.

I want to thank Prof. (apl.) Reiner Dahint for reviewing this thesis as well as Prof. Freddy Frischknecht and my forth examiner for agreeing to be part of my committee.

Thank you PD Ada Cavalcanti-Adam for this exciting topic, all the efforts to fulfill the desired experiments, introducing me to many other researchers of the field and pushing our fruitful collaborations. This four years in your group, which has been constantly changing and developing, have been very supportive and crazy in a positive way.

In our group there are so many people without whom this work would not have been possible, but my fattest thank is dedicated to Rebecca "das Böse" Medda. She corrected this thesis, which was extremely helpful, and was always around to help with whatever question might occur providing sound answers, psychological as well as physiological advice and globuli. Furthermore she is the madest in the zoo. Blobb. Of *Horst*, I want to thank ALL my collegues in Heidelberg and in Stuttgart, who made it such an enjoyable time, especially Maria Ott, Chiara Zambarda, Dirk Ollech, Julia Ricken and Paulina Wysmołek alias HalPig, Å, Dark, Hals-Nase-Beinbruch and the YouTube-Pro for deep scientific discussions, proofreading and help, but most importantly for all the fun and craziness during lunch, coffee, cake, beer, Glühwein, (Aprés-) Ski, Hiking, lab-party and so on. As already Mama Medda pointed out I hope that we will find such an inspiring group of people to work with in future, however I doubt it.

Next, I want to thank my numerous collaborators. First and foremost Marta Fratini, who has gone through the PhD together with me. Thanks for billions of viruses, dozens of cell culture flasks whenever I

got a contamination again, shared posters and conferences. Of course I want to thank Steeve Boulant for the insights and help in virology and the hospitality in his lab as well as being part of my thesis advisory committee. I am also thankful to his lab members Pranav Shah, Delia Bucher and Markus Mukenhirn who supported this work with viruses and cells.

Prof. Ulrich Schwarz, Felix Frey and Dimitri Probst gave support in the theoretical part during TAC meetings, personal debates, modeling and analysis, respectively.

Klaus Yserentant did not only become a close friend but also an highly valued collaborator for single-molecule imaging and analysis.

Pere-Roca Cusachs and Roger Oria presented ever-growing beard-styles in Heidelberg during our Skype meetings and did not stop believing in our big story, which made it a pleasure to send tons of nanopatterned substrates for successful experiments to Barcelona.

A huge thank you is going to Khalid Salaita, Yang Liu and Kornelia Galior, who hosted me as warm as one could wish at Emory University, Atlanta and taught me the beauty and tricks of Molecular Tension Fluorescence Microscopy.

Stefanie Neubauer from the lab of Horst Kessler in Munich assisted with synthesis of peptidomimetic molecules and supported me during the first year with advice and synthesis for the polyethylene glycol-based tension sensor.

Christoph Niemeyer, Alessandro Angelin and Klavdiya Gordiyenko from the Karlsruhe Institute of Technology introduced Paulina Wysmołek and me to the world of DNA-origami and I wish them all the best for the continuation of the project.

Aldo Ferrari and Tobias Lendenmann contributed by elegant nanoprinting techniques and gave me a warm and slow welcome at the ETH in Zürich.

I also want to thank all the students I had the privilege to work with and who had to make the experience that experiments do not always work: Annika Behrend, Phillip Kleinert, “dipping” Nico Spiller, “fresh” Luca Blicker, Kirsten Emler, Lena Thärichen, “chillige” Julia Ohmes and Maurizio Wack.

My dear friends Tobias Schmidt, Tim Enke, Julia Peukes, Klaus Yserentant and Anna-Sophia Pinck are going through the same trouble of a PhD as I do - sometimes even more ;) Thanks for delicious Tatorte, cool Motto-party’s when we were young, lame evenings, on which we “versacken” nowadays, “interesting” holidays and much more, which makes our friendship special.

Last but not least, I want to thank my family Sylke, Götz, Roya, Siegrun, Elisabeth and my boyfriend Matthias, who added thousands of commas to this work. Vielen Dank, dass ihr mich immer unterstützt habt und immer für mich da seid. Auch wenn ich nicht immer anrufe: Ich liebe euch!

CONTENTS

Part I

INTRODUCTION

There is a growing awareness of the importance of forces in biology for the vast majority of processes. In this thesis I will focus on the forces between single cells and their extracellular environment as well as forces during the binding and the uptake of small particles such as viruses.

1

FORCES BETWEEN CELLS AND THEIR ENVIRONMENT

The ability of cells to sense and transmit not only biochemical but also physical cues, such as temperature, light, electricity and mechanical forces is crucial for their viability. In particular the mechanical properties of the local environment were shown to have influences on cell proliferation, differentiation and survival [1–4]. The extracellular matrix (ECM) surrounding cells is a complex network of secreted macromolecules such as collagen, laminin or fibronectin and mainly provides support [5]. Specific binding sites on these proteins serve as ligands for cellular receptors, which mediate the adhesion and signaling between the inside and the outside of the cell.

In order to sense the stiffness and the distribution of ligands, cells are probing their extracellular environment by pulling or pushing. In the first place forces have to be generated in the interior of the cell.

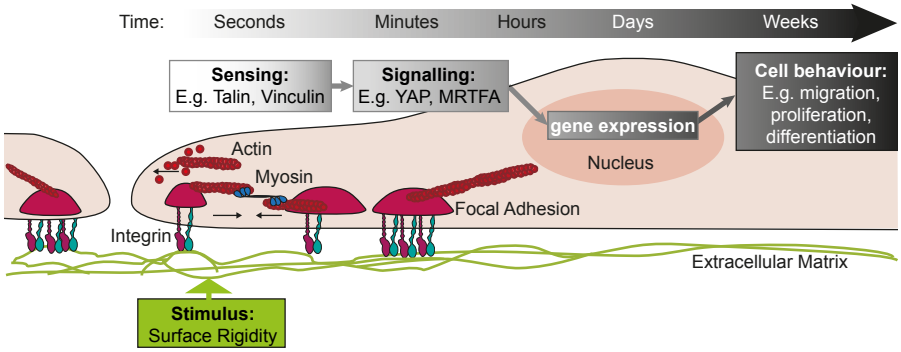

Figure 1.1: Mechanosensing and force transduction. Extracellular mechanical cues, like substrate rigidity, can be sensed by tension sensitive proteins such as talin and vinculin. Therefore the cell probes the extracellular matrix by pushing and pulling through integrin-based adhesion sites, with forces generated by the cytoskeleton. This mechanical signal is transduced into a chemical signal by binding of signaling molecules such as YAP and MRTFA, which can induce gene expression that ultimately alters the cell behavior. Adapted from [6].

1.1 CELLULAR FORCE GENERATION

Cellular forces are built up by the cytoskeleton, which consists of actin, intermediate filaments and microtubules. While intermediate filaments can efficiently resist tensile forces, they do not contribute to the generation of cellular stress [7]. Pushing forces are mainly

generated by actin polymerization, while pulling forces are originating in the contractility of the cytoskeletal network through bundling of filaments and power-strokes of molecular motors [8]. The polymerization of globular actin to its filamentous form was shown to generate up to 0.76 pN per single filament [9], bundling of filaments 0.2 pN [10]. Between $2 - 4$ pN are generated by kinesins and myosin II motors, which are pulling on microtubules and actin filaments respectively [11, 12].

The contractility of the whole cytoskeleton adds up to "global" traction forces that are deforming their environment and leading to the rearrangement of the ECM. The cytoskeleton reinforces itself by the formation of contractile actin stress fibers throughout the cell [13–15].

"Local" forces, on the other hand, are limited to the regions of actin polymerization such as in lamellipodia at the leading edge of the cell or in filopodia beneath the plasma membrane. In lamellipodia, actin polymerization is mediated by the Arp2/3 complex, which attaches to preexisting filaments and branches new filaments in an angle of 70 °, forming a "dendritic" array of actin, that can push the plasma membrane in dependence of its contact angle to the membrane with nanonewton forces (see Figure 1.1) [8, 16–18].

In contrast to these networks, actin filaments in filopodia are assembled in elongated parallel bundles by formins. They can bind the barbed ends of actin and withstand the forces from the growing filament pushing orthogonally against the membrane. Per actin filament ~1.3 pN [19] and in total >10 pN are generated through the assembly of several filaments to extend a filopod [20, 21].

The mechanical work W for actin polymerization is the same in both cases, however the displacement δ of the membrane induced by the addition of actin monomers ($\delta = 2.75$ nm for one monomer) depends on the angle of action and thus the force F differs according to $W = F \times \delta$ [22].

1.2 CELL ADHESION AND FORCE TRANSMISSION

The forces generated by the actin cytoskeleton are transmitted to the extracellular matrix via integrin-based focal adhesions [3]. Integrins are transmembrane proteins that form hetero-dimers of an α and β subunit. 24 different types of integrins are encoded in the human genome with specific physiological tasks [5]. The $\alpha_5\beta_1$ integrin, for example, transduces forces across the plasma membrane. Therefore it binds extracellularly to fibronectin via the conserved peptide motive Arg-Gly-Asp (RGD) and intracellularly is is linked to the actin cytoskeleton [23]. In the resting state integrins are in a bent conformation, which straightens upon binding of extracellular ligands or through the intracellular connection to the actin cytoskeleton (see Figure 1.2). These different forms of integrin activation are titled inside-

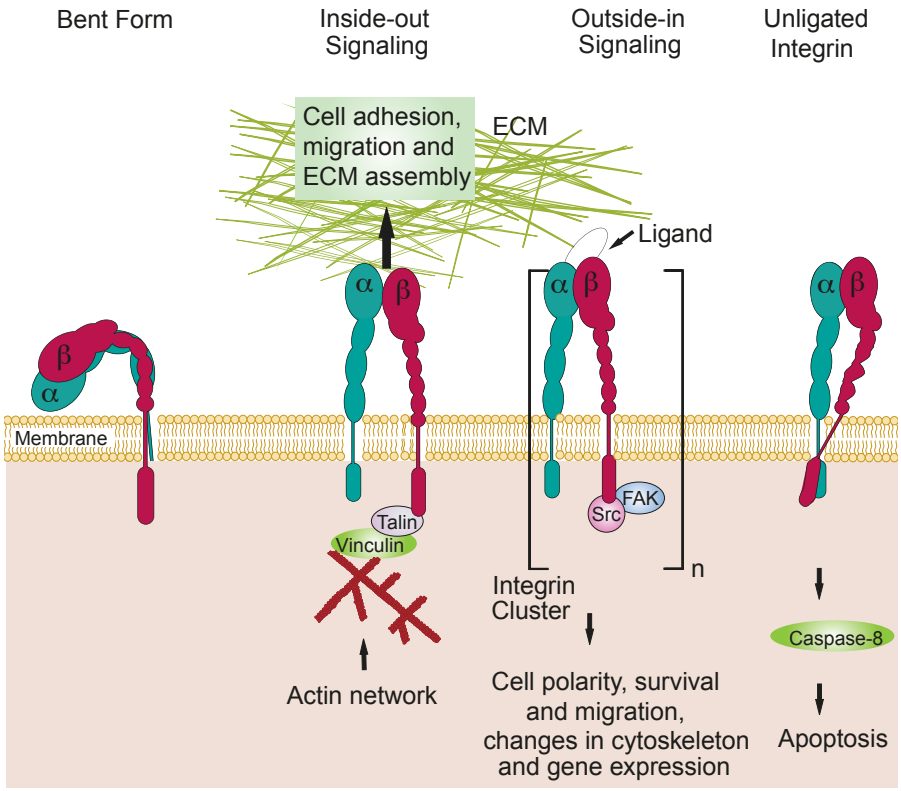

Figure 1.2: Integrin activation by inside-out signaling via coupling to the actin cytoskeleton or outside-in by binding of ECM ligands. Detachment of cells leads to unligated integrins that are not in the resting state (bent form). This can induce integrin mediated death by activation of caspases. Adapted from [24].

out and outside-in signaling, respectively, and allow cell sensing of extracellular cues such as ECM composition and stiffness [25]. Depending on specific peptide sequences and their flanking sites of extracellular proteins, particular integrin types are engaged. For example $\alpha_1\beta_1$ and $\alpha_2\beta_1$ integrins bind specifically the collagen peptide motive Gly-Phe-Hyp-Gly-Glu-Arg (GFOGER) while all α_V integrins, two β_1 integrins (α_5, α_8) and $\alpha II_b\beta_3$ share the ability to recognize ligands containing the RGD motive [26, 27]. Their clustering recruits intracellular proteins like talin, paxillin or focal adhesion kinase (FAK), which are promoting the adhesion growth. Integrin-based anchor points mature under tension from $30-40\,\text{nm}$ small nascent adhesions over transient dot-like contacts called focal complexes ($\sim 0.1-1\,\mu\text{m}$ in diameter) to focal adhesion (FA) sites (oval, $2-5\,\mu\text{m}$ in length) [28, 29]. During this maturation process, up to 160 different proteins including vinculin, zyxin and Src-family kinases are orchestrated. This induces signal cascades that can, among other things, activate the transcription factor yes-associated protein 1 (YAP), which is thereupon translocated to the nucleus and influences cellular behavior at the gene expression level (see Figure 1.1) [30–34].

FAs are primary responsible for adhesion but they also promote migration [35], rearrangement of the extracellular matrix [36] and mechanosensing [28, 37]. One can imagine these specialized adhesions as "molecular clutches" which regulate the actin retrograde flow and thereby regulate the traction forces applied to the substrate [38]. Individual proteins can serve as mechanosensors such as the actin adaptor protein talin, which was previously identified as force-sensitive clutch molecule [32, 39]. Talin unfolds under sufficient force load, which opens a binding pocket for vinculin enabling adhesion growth and YAP nuclear translocation. Rigidity sensing by FAs was found to be mediated by α_V-class integrins. They accumulate in areas of high traction force with specific bond dynamics and hence they adjust the cellular contractility to the rigidity of the substrate [23, 40].

Model systems with biomimetic surfaces showed that a defined ligand distribution at the nanoscale is needed to allow stable cell adhesion [41]. It was hypothesized that some FA molecules could serve as rulers [42–45], but the exact mechanism how cells can sense extracellular ligand density and distribution remains unclear.

Each integrin bears on average a few pNs within FAs [46]. However, due to a process known as catch bond behavior and cyclic mechanical reinforcement the fibronectin-integrin bond can strengthen itself up to 100 times [47, 48] and withstand at least 54 pN of constant tension outside [49, 50] and up to 120 pN in FAs [51]. Even forces that lead to biotin-streptavidin dissociation have been observed [52], which is known as one of the strongest non-covalent bond in nature with an equilibrium association constant $K_0 \approx 4.3{\times}10^7 M^{-1}$ [53]. Depending on the loading rate, rupture forces between ~25 and 200 pN have been measured [54–56].

1.3 UNBINDING FORCES

Macromolecular binding within or between cells such as receptor-ligand complexes are non-covalent and therefore reversible. Their binding and unbinding usually follows first order kinetics and the binding rate k can be thus described by the Arrhenius equation:

$$k = A \cdot e^{-\frac{\Delta E_a}{k_B T}} \tag{1.1}$$

with A being the pre-exponential factor, ΔE_a the activation energy, k_B the Boltzmann constant and T the absolute temperature.

$k_B T$ is often referred to as a unit of the thermal energy state of molecular bonds. In biological systems the change in Gibbs free ΔG of e.g. receptor-ligand bonds is usually in the range of a few $k_B T$, which promotes the reversibility and dynamics of the system [57]. The thermal energy of $1\,k_B T$ equals at room temperature ($T = 298.15\,\mathrm{K}$) a mechanical energy of $E_m = F \cdot \Delta x \approx 4.1\,\mathrm{pN \cdot nm}$. Hence, the forces that individual nanometer-sized proteins can with-

stand are in the piconewton range [39, 58]. In figure 1.3, the relation for different types of bonds between unbinding forces and the characteristic length scale of the action of force depending on their binding energy is depicted.

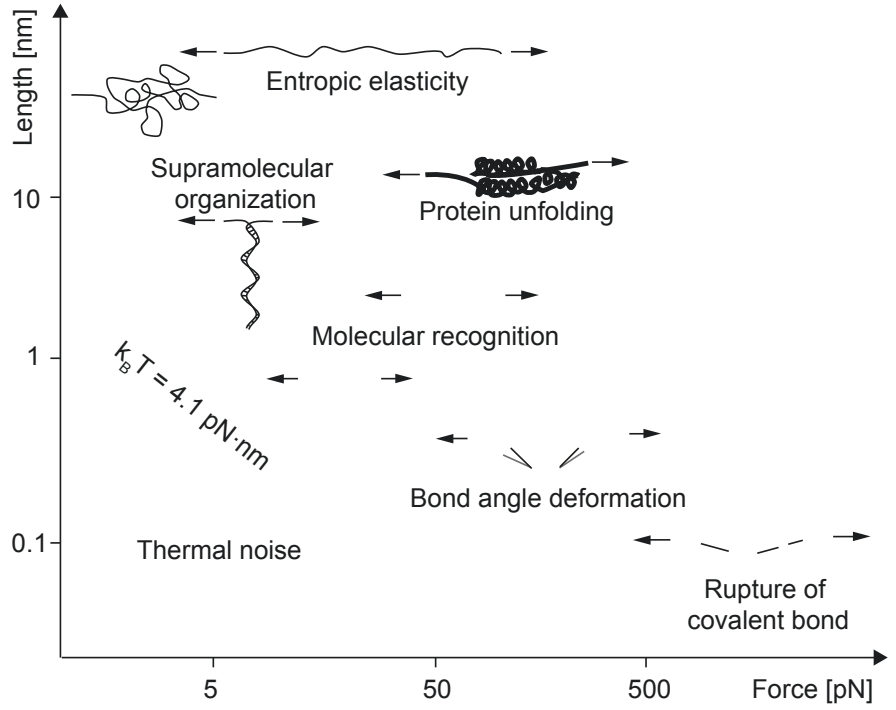

Figure 1.3: The potential length versus force for molecular complexes. Adapted from [59].

Pulling two molecules apart along the reaction coordinate with a constant force F reduces the energy barrier and therefore the probability for unbinding increases (see Figure 1.4) [60]. This was theoretically described by Bell in 1978 [62] and can be expressed as the Arrhenius equation for the dissociation constant k_{off} for single bonds under external force load:

$$k_{off}(F) = \upsilon \cdot e^{-\frac{\Delta G + \Delta E_a - F\Delta x}{k_B T}} = k^0_{off} \cdot e^{\frac{F\Delta x}{k_B T}} \tag{1.2}$$

where υ is the natural vibration frequency of the bond, k^0_{off} is the off-rate at equilibrium without external force and Δx is the interaction range [59]. It has to be noted that due to the stochastic Maxwell-Boltzmann distribution of thermal energy among individual molecules, every bond will brake after a sufficient long time. Thus, the mean force that leads to an unbinding event strongly depends on the duration of action. To acknowledge this fact, the loading rate $f = \mathrm{d}F/\mathrm{d}t$ became a crucial measure for the strength of molecular adhesions. For the biotin-streptavidin unbinding force, values of more than 170 pN have been reported for a loading rate of 10^4 pN/s, while only 5 pN were needed with a pulling rate of

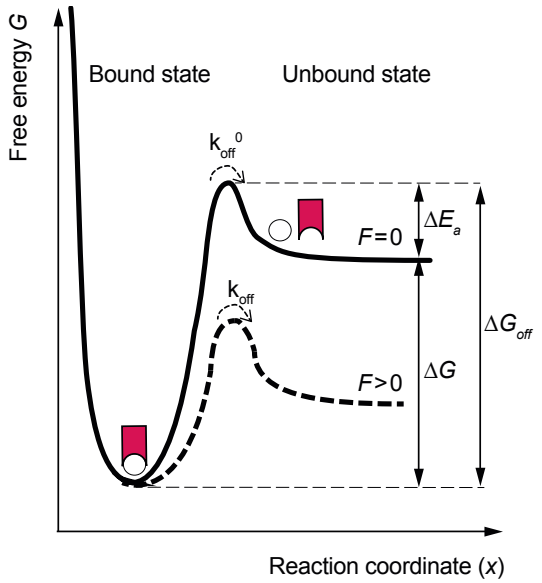

Figure 1.4: Energy landscape of molecular bonds under external force load. The receptor-ligand complex (purple-green) resides in its bound state in an energy valley. To separate the ligand from the receptor, the energy barrier ΔG_{off} has to be overcome, which consists of the change in Gibbs free energy ΔG and the activation energy ΔE_a. This energy barrier is significantly reduced when a force F is applied and the dissociation rate under zero force, k^0_{off}, increases to k_{off}. Adapted from [59, 61].

10^{-2} pN/s [55]. This relation between the most probable unbinding force F and the loading rate f is defined by the Bell-Evans model [60, 63, 64]:

$$F(f) = \frac{k_B T}{\Delta x} \cdot \ln(f \cdot \frac{\Delta x}{k_{off} \cdot k_B T}) \tag{1.3}$$

1.4 CELLULAR FORCE MEASUREMENT TECHNIQUES

A simple method for characterizing cellular forces is embedding cells in collagen gels. Contraction of the gel can be measured by the change in diameter and gives an estimate over the forces of cellular ensembles (see Figure 1.5) [65]. First measurements of single cellular traction forces have been conducted in the 1980s by Harris and Stopak with wrinkling silicone sheets [66]. Since then, many elaborated methods have evolved, of which the most common and state-of-the-art techniques are briefly discussed in the following chapter.

1.4.1 *Traction Force Microscopy*

Traction force microscopy (TFM) is based on the deformation of an elastic substrate upon cellular tractions. One option is to grow cells

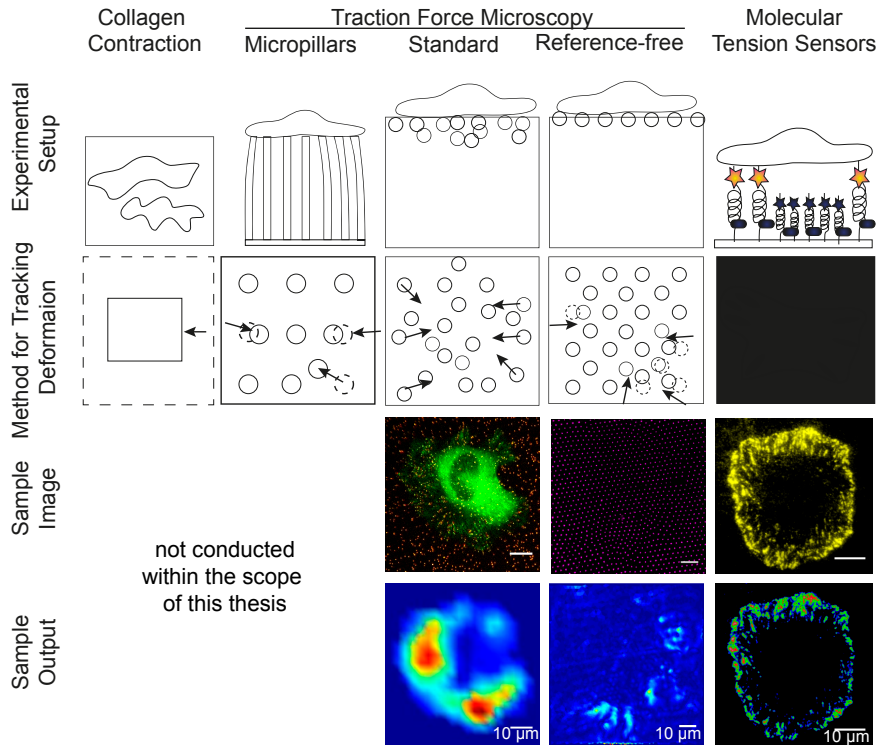

Figure 1.5: Cellular force measurement techniques. Adapted from [65] with own, unpublished sample images.

on top of a bed of elastic micropillars, which allows the quantification of local forces underneath the cells by tracing the deformation of the pillars [67]. This technique enables to isolate individual tractions within the cellular adhesion area, however it is limited in resolution and to discrete adhesion sites by the microfabrication of the pillars to several microns (see Figure 1.5) [68].

The most commonly form of TFM utilizes continuous elastic 2D substrates, which are deformed upon cell adhesion and visualized by embedded fluorescent marker beads [69]. Traction forces can be reconstructed from the displacements of the markers compared to a reference-state without cells by particle image velocimetry (PIV) and Fourier transform traction cytometry (FTTC) algorithms [70, 71]. If the adhesion sites are known one can circumvent the underestimation of tractions at small adhesion sites inherent to FTTC through a traction reconstruction with point forces [46, 72]. Improvements of the substrates with multicolor beads and combination with super-resolution microscopy led to lateral resolution up to ~1 µm [73].

TFM even allows to measure forces in 3D matrices [74], however, this is experimentally as well as computationally very demanding.

A recent development that facilitates the actual measurement uses nano-printing techniques to distribute the marker beads in a systematically defined manner. Thereby the step of cell removal can be omitted, which is referred to as confocal reference-free traction force

microscopy (cTFM) [75]. Here, a nano-ink composed of quantum dots (Qdots) and gold nanoparticles (AuNPs) is applied on top of silicon substrates via electrohydrodynamic NanoDrip-printing, which allows to detect in- and out-of-plane deformations with high precision. Tractions are obtained using finite element analysis circumventing the delicate regularization steps present in PIV.

1.4.2 *Molecular Tension Sensors*

Another type of measurement is offered by molecular tension sensors, that are directly coupled to the protein of interest inside or at the membrane of the cell. One can distinguish between (i) genetically encoded molecular sensors, that are expressed in the cell and report intracellular forces between $1 - 10\,\mathrm{pN}$ (see Section 1.4.2.1) and (ii) synthetic molecular sensors that are coupled to an extracellular ligand and have a range of $1 - 100\,\mathrm{pN}$ (see Section 1.4.2.2) [76, 77].

The principle is based on the extension of a molecular "spring" with a known spring constant in the piconewton scale, that can be observed by spectroscopic rulers with fluorescence microscopy. The most widely used spectroscopic ruler is the Förster resonance energy transfer (FRET) sensor, that consists of two fluorophores attached to the opposite ends of the tension sensitive molecule. In close proximity, a non-radiative dipole-dipole coupling allows an energy transfer from the excited donor fluorophore to the acceptor fluorophore, which as a result emits photons at its emission wavelength. This energy-transfer is distance (d)-dependent and follows a $1/d^6$ relationship, allowing for a dynamic radius of $\sim 5 - 15\,\mathrm{nm}$ depending on the spectra of the fluorophores [78]. Furthermore, nanometal surface energy transfer (NSET) has been utilized as spectroscopic ruler [79]. Here, a fluorophore (dipole) is quenched by a nearby metallic surface proportional to $1/d^4$ [80], which allows for a longer dynamic range of $\sim 5 - 25\,\mathrm{nm}$ and thus tension magnitudes that are not accessible by FRET-based tension sensors [79, 81, 82]. Further quenching mechanisms can or have been exploited for molecular tension probes such as proximitry imaging (PRIM) [83], fluorescence loss [49], or homo-FRET [84].

1.4.2.1 *Genetically Encoded Molecular Sensors*

As sensing elements various molecules have been proposed. For the genetically encoded tension sensors, obviously proteins accomplish the task. The spider silk flagelliform protein, which consists of repeats of the peptide sequence GPGGA, is known as an elastic linker in nature, and was thus chosen by Grashoff et al. for their vinculin force sensors [85]. It was further applied to characterize the tension beard by cadherins, platelet endothelial cell adhesion molecules (PECAM-1) and β-spectrins [76, 86–88]. Other polypeptides like $(GGS)_n$ or spec-

trin repeats have been used to target myosin II and α-actinin, respectively [83, 89].

While genetically encoded force sensors allow for measurements of intracellular forces, they can also be purified from e.g. bacteria and immobilized on a substrate to measure the forces transduced by transmembrane proteins such as integrins [90, 91]. A mechanically much more robust protein with well characterized unfolding properties is titin, the largest protein known in the human body. It anchors the thick myosin filaments to the Z disc in the sarcomers of striated muscle tissue and it consists of individual Ig domains that can be unfolded and refolded upon mechanical stress [5]. The I27 domain of titin was used by Galior et al. as a sensor molecule that unfolds depending on the loading rate at $40 - 150\,\mathrm{pN}$, which is $10 - 20$ times higher than the forces accessible with the polypeptide sensors [51].

1.4.2.2 *Synthetic Molecular Sensors*

Synthetic tension sensors are composed from polymers such as polyethylene glycol (PEG), which can be considered as a worm-like chain (WLC) to model their extension upon mechanical tension. Extracellular ligands, such as the epidermal growth factor (EGF) [92] or the peptide RGD [79], are coupled to the synthetic sensors in order to target the EGF receptor and integrins, respectively. This approach has been pioneered in the group of Prof. Khalid Salaita at Emory University, Atlanta and was termed molecular tension fluorescence microscopy (MTFM). The combination with patterns of gold nanoparticles obtained by block copolymer micelle nanolithography (BCML) [93–95] further allowed to dissect the effect of ligand spacing on individual molecular force load [82].

Another class of synthetic sensors is based on force-induced rupture or shearing of DNA duplexes [96]. Hereby one of the DNA strands is either ruptured completely by the cells (referred to as tension gauge tethers (TGT) [49]) or it is covalently attached to its complementary strand through a hairpin loop [97, 98]. The unfolding of DNA duplexes is reported at precise threshold forces. Hence, these sensors provide digital information if the force load on individual molecules exceeded a certain threshold force or not.

1.5 MOTIVATION

1.5.0.1 *Sensing of extracellular ligand density*

Physical parameters like stiffness, roughness and nano-distribution of cellular anchor points of the ECM are modulating cell functions. While there are many theories and studies on rigidity sensing of cells [23, 32, 37, 40, 99–101], little is known about how and why certain extracellular ligand spacings and distributions are preferred over oth-

ers. Hypothetically both mechanisms seem to be force-driven and depend on the transduction of forces across the cell membrane.

In classical TFM these two aspects are often intermingled because stiffer substrates are usually achieved by higher cross-linking of polymers, which, as a result, allows more ECM proteins to bind. In studies on stiff glass substrates nanopatterned with adhesive ligands, however, a clear dependence of cell spreading and thus force generation on ligand density and distribution has been observed [41, 43, 102–104]. For a mechanistic understanding of the processes allowing cells to measure physical parameters, it is necessary to combine both, extracellular ligand distribution and stiffness of the environment.

This study was performed in collaboration with the groups of Prof. Pere Roca-Cusachs, in Barcelona and Prof. José Manuel García-Aznar in Zaragoza, Spain. In this thesis I will therefore combine, for the first time, classical TFM with BCML to obtain elastic substrates with defined nano-spacing of extracellular ligands in order to measure the cellular tractions in different scenarios.

1.5.0.2 *Comparison of global traction forces and local single receptor force load*

For the force load on individual integrin receptors, values have been reported, which differ several orders of magnitude from each other mainly depending on the measurement technique [49, 67, 79, 105, 106]. While TFM allows to probe cells on soft, and thus physiological substrates, the force load per single integrin can be only estimated by dividing the total tractions by the number of receptors, which gives an average force load of a few pN [46]. With MTFM, which allows to investigate the force load per single molecule but has been limited to glass substrates so far, forces of up to 120 pN have been observed [51, 52, 90]. In this study I will combine TFM with MTFM in order to understand the discrepancy between both techniques and cross-validate their results.

2

MECHANICS OF ENDOCYTOSIS

Endocytosis is the process of internalization of molecules, particles or pathogens by cells, that are too big (> 10 nm) or otherwise hindered to penetrate the plasma membrane. The lipids of the membrane are thereby bending around the obstacle and engulfing the cargo until a membrane-bound vesicle pinches off and can be intracellularly transported to its final destination by the help of motor proteins and the cytoskeleton [109]. Understanding the physical principles of endocytic pathways can help to prevent entry of pathogens into host cells and is therefore significant for the development and accessing the risks of nanoparticular drug delivery tools [110].

2.1 ENDOCYTIC PATHWAYS

Since there are many different types of substances that have to cross the membrane, cells have evolved many different strategies for their internalization. One can distinguish (a) phagocytosis, which comes from the ancient greek word $\varphi\alpha\gamma\omega$ = to eat and refers to the internalization of bigger particles, and pinocytosis (ancient Greek $\pi\iota\nu\omega$ = to drink), describing the uptake of soluble materials and small particles. Pinocytosis can be further distinguished in (b) macropinocytosis, (c) clathrin-dependent endocytosis, (d) caveolin-dependent endocytosis and (e) clathrin- and caveolin-independent pathways mainly by the size and surface properties of the cargo and the protein machinery that facilitates the uptake [108] (see Figure 2.1).

(a) Phagocytosis occurs in all type of organisms from unicellular amoeba to mammalians, where it is conducted only by specialized cells, such as macrophages, upon binding of certain ligands. Particles, or even whole cells, e.g. bacteria, of $0.5 - 10\,\mu m$ in diameter can be engulfed by this pathway, which is of particular importance for the immune system [111, 112].

(b) Via Macropinocytosis bigger quantities of extracellular fluid and micrometer-sized particles are internalized by membrane ruffling, which closes over the cargo and forms so-called macropinosomes [107].

(c) The pathway best studied for small particles in the nanometer range is clathrin-mediated endocytosis (CME). Clathrin is a protein that consists of three light and heavy chains forming a triskelion, which can self-polymerize into flat lattices or cages. The first stage of CME is the formation of a membrane invagination called clathrin-coated pit (CCP). This might be either induced by binding of recep-

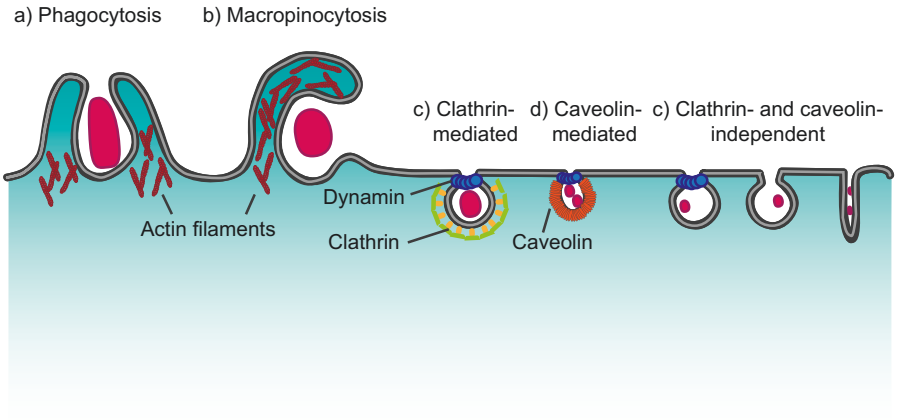

Figure 2.1: Endocytic pathways. The internalization of particles and extracellular fluid is achieved via different pathways: a) phagocytosis and b) macropinocytosis are capable of taking particles in the micrometer range, which involves actin-driven membrane remodeling; nanometer-sized particles are endocytosed by c) clathrin-mediated, d) caveolin-mediated or e) clathrin- and caveolin-independent pathways. The involvement of the cytoskeleton is not clear in all cases. Adapted from [107, 108].

tors via the clathrin-adaptor protein AP2 or by the formation of a nucleation module including FCH domain only Proteins (FCHO), which can sense low curvatures through their F-BAR domains [113]. To date it remains unclear if clathrin assembles on the flat membrane and gets curved as it grows to vesicles [114–116], or if CCPs are forming with a constant curvature [117–120]. The cargo is recruited into the CCP by binding of AP2 to cargo-specific adaptors and clathrin assembles in hexagons and pentagons to form a clathrin-coated vesicle (CCV). The GTPase dynamin is recruited to the neck of the vesicle to conduct the scission and resealing of the separated membranes [113]. While the typical diameter of a CCV is ~ 80 nm, particles up to 200 nm in diameter have been found to be internalized by CME [121].

(d) Caveolae are $50 - 80$ nm sized, flask-shaped membrane invaginations with an enrichment of sphingolipids and cholesterol as well as caveolin proteins in the membrane [108]. Contradictory to this typical size even particles as big as 500 nm have been observed to be internalized via caveolae [121]. Like in CME, dynamin helps to pinch off the vesicles, which are intracellularly trafficking to intermediate compartments (caveosomes) or directly fusing with early endosomes [122].

(e) In addition to clathrin- and caveolin-mediated endocytosis there are several other pathways identified to date, which are also dynamin-dependent (CLIC/GEEC-type, IL2Rβ-pathway) or dynamin-independent (Arf6-, or flotilin-dependent) [123].

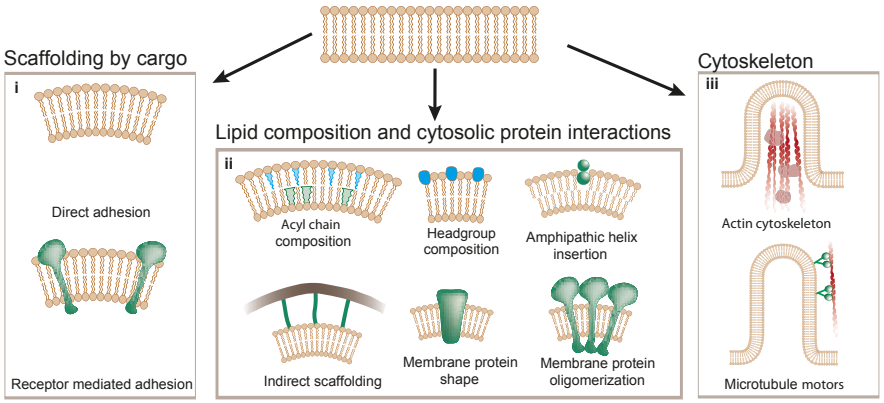

Figure 2.2: Membrane shaping mechanisms. Deformation of the membrane during endocytosis as well as other processes like movement or division costs bending energy. This can be obtained from binding an extracellular cargo to the membrane (i), the lipid composition and interaction with cytosolic and membrane proteins (ii) and the cytoskeleton (iii). Adapted from [127].

2.2 FORCES DRIVING ENDOCYTOSIS

For the big reorganization and formation of larger membrane ruffles both, phagocytosis and macropinocytosis clearly require actin polymerization. For the other endocytic pathways the involvement of actin is not that clear [124–126], however, also the bending of the plasma membrane around smaller cargos requires energy that can be obtained from (i) direct binding of the cargo or binding to receptors in the cell membrane, which releases free binding energy or (ii) from binding of cytosolic proteins to the membrane or alteration of the lipid composition, which stabilizes the curvature and (iii) from the cytoskeleton pushing against the membrane to form protrusions and invaginations (see Figure 2.2). The energy barrier that has to be overcome depends on the size and shape of the cargo. The smaller the particle the higher is the energetic cost for membrane bending.

(i) Extracellular Cargo Binding

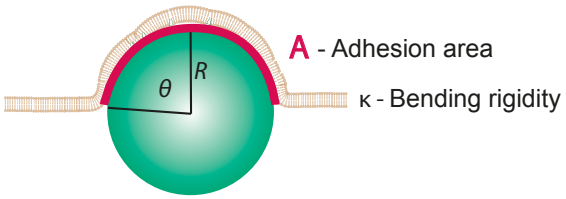

Figure 2.3: Adhesion energy between an object and the cell membrane.

The driving force for engulfment of extracellular objects is the adhesion force F_{ad} between an object and the cell, which depends on the work of adhesion W, the elasticity composed of the elastic modulus E and the Poisson´s ratio ν as well as the dimensions d of the adhesion area in the following way (with n being a constant):

$$F_{ad} = n\sqrt{\frac{WEd^3}{1-\nu^2}} \tag{2.1}$$

Interestingly, it was proposed that although receptor-ligand interactions have an effect on W, the highest adhesion force is expected for smooth surfaces without specific adhesion molecules, depending exclusively on van der Waals forces [128]. Neglecting further the elasticity of the cargo, the energy E_{ad} that is gained by adhesion over an area A is defined as:

$$E_{ad} = |W|\, A \tag{2.2}$$

and depicted in figure 2.3. This gain in adhesion energy is partially counteracted by the energetic cost required for bending the plasma membrane, which can be calculated as an integral over the total surface A :

$$E_{bend} = \int dA 2\kappa C^2 \tag{2.3}$$

with κ being the bending rigidity and $C = \frac{1}{R}$ the curvature, which is defined by the dimensions of the cargo assumed to be spherical, assuming complete adhesion and neglecting the formation of the neck at the bottom of the membrane invagination. Thus, the smaller the particle, the higher is C and the more energy it takes to bend the membrane. Assuming a spherical particle, the adhesion area for a spherical cap with the opening angle θ would be $A = 2\pi R^2(1-\cos(\theta))$ and thus:

$$E_{bend,sphere} = 4\pi\kappa(1-\cos(\theta)) \tag{2.4}$$

Membrane bending is favored if the total energy $E_{total} = E_{ad} - E_{bend}$ becomes negative:

$$E_{total} = 4\pi\kappa(1-\cos(\theta)) - |W|\, 2\pi R^2(1-\cos(\theta)) \leq 0 \tag{2.5}$$

$$2\kappa \leq |W|\, R^2 \tag{2.6}$$

Thus, in order to initiate its uptake purely by adhesion forces, the particle radius has to exceed a critical value defined by the bending rigidity of the membrane and the adhesion work:

$$R_{crit} = \sqrt{\frac{2\kappa}{|W|}} \tag{2.7}$$

The adhesion energy per unit area of attractive van der Waals forces between the lipid bilayer and a particle are typically in the order of

$1\,k_BT/a^2$, with a being the molecular length scale. For a membrane with $\kappa \cong 20\,k_BT$, this leads to the estimate $R_{crit} \cong 6\,a$. Assuming a being comparable to the size of a lipid head group of $a \cong 0.8\,\text{nm}$, one obtains a critical radius of $R_{crit} \cong 5\,\text{nm}$ [129]. Specific adhesion molecules at the surface of nanoparticles can interact with cellular receptors and thereby contribute with high binding energies. However, they also induce roughness, which causes separation between the membrane and the particle and thus dramatically reduces van der Waals forces. Since cellular receptors are limited in their concentration, specific adhesion molecules are rather reducing than enhancing the adhesion force compared to smooth surfaces [128]. As we will see later (cf. 2.3.1), the adhesion energy obtained by specific but sparse receptor-ligand interactions presented by virus particles might be three orders of magnitude smaller than the adhesion energy density, which would be obtained for a smooth nano-sphere. While high adhesion forces allow for stable attachment and free energy to overcome the energetic cost of membrane bending, they also hinder the particles such as viruses to release the membrane for their further journey into the cytosol. Thus, it is to assume that particles, which gain entry into the cytosol, have a total adhesion energy in the order of ~1 k_BT, which allows for a reversible binding to the cellular membrane under physiological conditions (cf. Section 1.3).

(ii) Membrane Shaping Proteins and Lipids

Membrane-deforming proteins such as Bin-Amphiphysin-Rvs (BAR) superfamily proteins, dynamin and epsin have the capability to stabilize and drive membrane curvatures upon their binding and have been identified to be involved in endocytic pathways. BAR proteins show an intrinsic banana-shaped curvature domain that peripherally binds to the membrane surface via electrostatic interactions [130]. As they impose different curvatures, F-BAR proteins bind to shallow membranes in early steps of CME, whereas at later stages N-BAR proteins (endophilin and amphiphysin) bind to the neck of the bud [131]. In clathrin-independent endocytosis endophilin is important for the tubulation of the membrane as well as its scission [132]. Dynamin is recruited in several pathways to the neck of membrane vesicles, where it oligomerizes in a helical lattice and upon GTP hydrolysis a conformational change provides force for vesicle scission [133, 134].

Like the adhesion of extracellular ligands, the binding of intracellular proteins reduces the bending energy E_{bend} of the membrane and induces a spontaneous curvature. In presence of BAR proteins the local membrane curvature is matched as good as possible to the intrinsic curvature, imposed by the protein, in order to minimize the energy density [135].

Further the membrane compositions itself can impose a certain curvature. If one layer of the lipid bilayer is enriched with lipids, conically shaped lipids or transmembrane proteins this will induce a "positive" curvature with the centre of curvature on the opposite side of the membrane [131]. But not only the shape of lipids, defined by their acyl chains and size of the head groups is important, also their recruitment of proteins comes into play. They can further modify the shape of lipid head groups. Especially phosphoinositides (PtdIns) can be easily modified and are, amongst other things, essential for the budding of CCVs by binding of adaptor proteins such as epsin [127]. Likewise, the concentration of certain curvature favoring lipids and membrane-associated proteins can be used as a sensing mechanism of extracellularly induced curvatures e.g. by cargo molecules [130].

(iii) Role of the Cytoskeleton

Actin dynamics are involved in a number of membrane shaping processes such as filopodia, axonal growth cones and phagocytic cups. They keep the membrane tension and thus its local decrease can promote curvature [127]. In cells with turgor, such as yeast, additional force has to be generated by the endocytic machinery for membrane deformations and here the role of actin is well studied [125, 136–138]. In mammalian cells however, neither the role of the cytoskeleton for CME nor for clathrin-independent pathways is well understood although a number of endocytic accessory proteins and lipids are known to regulate actin dynamics [139–142]. E.g. membrane phospholipids, especially PtdIns(4,5)P_2, were found to enhance actin-binding proteins that promote filament assembly, such as Arp2/3 and formin, while repressing the binding of actin-filament destabilizing proteins (e.g. cofilins) [134]. Clathrin can interact with actin filaments via the light-chain-bound Hip1R, which becomes important as soon as the membrane tension impedes with vesicle formation, e.g. by mechanical stretching [143]. Actin polymerization at CME sites was found to be regulated by cortactin, N-WASP and Arp2/3 [140, 144]. Further also dynamin binds cortactin and activates Arp2/3-mediated actin polymerization cooperating in the vesicle scission [134]. However, despite all these evidences, endocytosis is often impaired but not completely stalled upon actin disruption [145–148] suggesting alternative actin-independent routes.

Also other cytoskeletal proteins like microtubules might be involved. Intracellularly, many vesicles and viruses are translocated along microtubules by kinesin motors, which have been proposed to be also involved in pulling the vesicle inside the cell [127, 149].

2.3 VIRUS PARTICLE UPTAKE

Viruses are obligate intracellular pathogens [150]. Therefore, they hijack endocytic processes in order to be internalized into a host cell where they capture the transcription machinery for their replication. As a first step, they attach to receptors at the cell surface, which allow a stable adhesion, bending of the cell membrane and interaction with further receptors that ultimately lead to their uptake. Primary attachment is often mediated by electrostatic or non-specific interactions with lipids or glycosaminoglycans, that are ubiquitously expressed in eukaryotic cells and brings them into close contact with the cell membrane [151]. Hereafter specific interactions between cellular receptors and ligands on the virus capsid are established by mimicking certain extracellular cues such as the fibronectin peptide sequence RGD. In fact, the RGD motive has been found on a number of viruses on their glycoproteins of the envelope or in case of non-enveloped viruses in their capsid proteins. Representatives are herpesviruses, ebolaviruses, adenoviruses or reovirus [152]. While the interaction with certain integrins has been studied and structurally elucidated, the role of integrin receptors for the virus attachment and/or entry is not well understood.

One mechanism might be the force transduction via integrins leading to an outside-in signaling, which recruits endocytic proteins such as clathrin. The turnover of $\beta 3$ integrins by CME was found to be mutually exclusive at sides with high traction forces [153], suggesting that the binding between integrins and a loose object such as a virus particle might lead to the hijacking of receptor recycling pathways.

On the other hand, the highly ordered nanostructure of viruses displayed as nanopatterned ligands could also induce receptor clustering in the host cell, which is associated with higher traction forces [154–156]. This could be either a signal recruiting the endocytic machineries or induce clathrin- and dynamin-independent endocytosis by the initiated bending of the membrane around the particle [126].

2.3.1 *Endocytosis of Mammalian Reovirus*

Mammalian orthoreovirus (called "reovirus" in the following) is a non-enveloped, double-stranded RNA virus in the familiy of *Reoviridae*. It is capable of infecting humans but has not been described to cause a specific human disease. Thus, infections are either asymptomatic or linked to minor respiratory and gastrointestinal illness in early childhood [158, 159]. Reovirus was used in this study, as it is well characterized and serves as a model for pathogenic viruses such as rotavirus, adenovirus and other non-enveloped viruses concerning the virus uptake. It is entering cells, amongst other pathways, via CME [160]. Further, reovirus is in current clinical trials as viral anti-

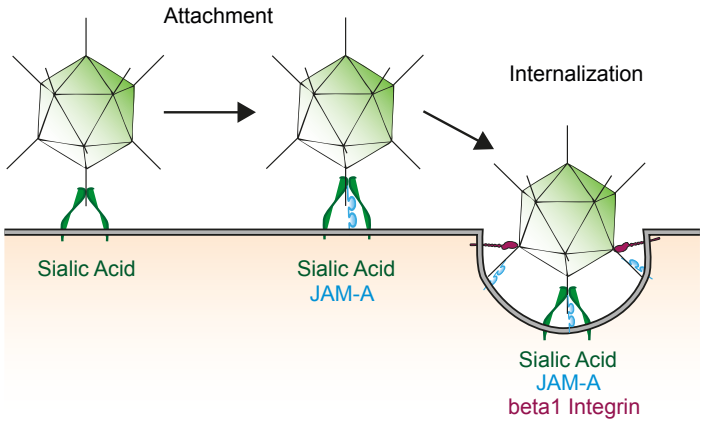

Figure 2.4: Attachment of reovirus to host cells. Reovirus establish primary adhesions with sialic acids on the cell membrane. Specific ligand-receptor interactions are formed between JAM-A and the viral the attachment protein $\sigma 1$. $\beta 1$ integrins have been proposed to mediate the internalization. Adapted from [157].

cancer therapy and thus its exact entry strategies are of increasing interest to exclude interactions combined oncolytic agents [161].

Its outer capsid displays an icosahedron of ~ 85 nm in diameter and is mainly composed of the proteins $\mu 1$ and $\sigma 3$. The viral attachment protein $\sigma 1$ forms trimers and is located at each of the 12 vertices. During infection the intact virion undergoes conformational changes involving the loss of the capsid protein $\sigma 3$, cleavage of $\mu 1$ and the extension of the compact form of $\sigma 1$ to a flexible fiber, leading to the so-called intermediate subviral particle (ISVP) [162]. The initial adhesion is mediated by binding to sialylated glycans on the host cell membrane via the attachment protein $\sigma 1$ [163, 164].

The junctional adhesion molecule A (JAM-A), which is expressed at tight junctions at the cell-cell interface as well as on leukocytes, was identified to serve as a specific receptor interacting with $\sigma 1$. While it is dispensable for infection of the intestine in mice, it promotes infection of endothelial cells [165] and its expression allows the infection of non-permissive cells [166]. Blocking of JAM-A in endothelial cells prevents almost completely their infection with reovirus, however infectivity does not depend on the intracellular interactions of JAM-A mediated by its cytoplasmic tail [157]. Suggesting that the role of the $\sigma 1$-JAM-A interaction is mainly for an efficient attachment rather than signaling events, which are leading to the internalization of reovirus.

Coming back to the theoretical adhesion energy (cf. 2.2) one can evaluate the local gain in adhesion energy between JAM-A and $\sigma 1$, which is the main receptor-ligand interaction for reovirus particles. It exhibits a dissociation constant of $K_d = 9 \cdot 10^{-8}\,\mathrm{M}$ [166], accounting for a binding energy of roughly $E_{ad,JAM-A} = k_B T \ln(\frac{K_d}{c_0}) \approx -16 k_B T$ per receptor. Due to the 12-fold geometry and the effec-

tive radius of ~42 nm of the reovirus particle plus the $\sigma 1$ spikes of 48 nm in length, the adhesion energy density is given by $|W| = (12E_{ad,JAM-A})/(4\pi r^2) \approx 1.9 \cdot 10^{-3}\,\mathrm{k_BT/nm^2}$. Taking only these interactions into account, only particles with an effective radius exceeding $R_{crit} = \sqrt{\frac{2 \cdot 20 k_B T}{1.9 \cdot 10^{-3} k_B T}} \approx 145\,\mathrm{nm}$ could enter the cell, suggesting the involvement of further adhesion sides (adopted from Felix Frey in the Group of Prof. Ulrich Schwarz at the Institute for Theoretical Physics, Heidelberg University, unpublished).

The outer capsid protein $\lambda 2$ displays the integrin-binding sequence RGD [167]. Blocking and knock-out of integrin $\beta 1$ leads to a reduction in reovirus infectivity, suggesting a role of $\beta 1$ integrins for the internalization of reovirus into the host cell [157, 168]. Assuming a binding energy of $E_{ad,Integrin} \approx -10 k_B T$ per receptor-ligand interaction and the maximal number of 5 integrins binding the RGD sequences at each penton base, the effective adhesion density is given by $|W| = (12E_{ad,JAM-A} + 60E_{ad,Integrin})/(4\pi r^2) \approx 7.8 \cdot 10^{-3}\,\mathrm{k_BT/nm^2}$. This would result in the uptake of particles with $R_{crit} = \sqrt{\frac{2 \cdot 20 k_B T}{7.8 \cdot 10^{-3} k_B T}} \approx 71.6\,\mathrm{nm}$ or bigger, which holds true for reovirus particles.

The RGD sequence is displayed by both, virions and ISVP, which were found to enter the host cells by different endocytic pathways [160, 169]. Thus, the interaction with $\beta 1$ integrins seems not to induce a specific pathway but rather aiding the general uptake. It was suggested, that another integrin binding motive, Ile-Asp-Ser-Ser (IDSS) for $\alpha 4\beta 1$ integrins in the capsid protein $\sigma 3$, could account for the differential uptake, since $\sigma 3$ is present in virions only [160]. Until today however, the mechanism by which integrins mediate reovirus entry remains unclear.

2.4 NANOPARTICLE UPTAKE

Inanimate nanoparticles can largely vary in size, shape, stiffness and surface properties like coatings or roughness. When they come in close proximity to cells, they interact with the cell membrane, generating forces leading to their uptake [107]. The main determinant of the endocytic pathway is again their size as discussed in section 2.1. However, unlike small molecules or viruses, uncoated particles do not interact with specific cellular receptors in order to initiate endocytic pathways. So their cellular uptake depends solely on physical parameters. In contrast, coating of nanoparticles with specific molecules or proteins can activate their cellular uptake via certain pathways e.g. coating with transferring initiates CME [170, 171]. Furthermore, when bare nanoparticles are applied to cells in growth medium or in vivo, serum proteins or other molecules can adhere to their surface especially if charged. This results in an unspecific coating, which was found to be sufficient for initiation of endocytosis [172].

2.5 ENDOCYTIC FORCE MEASUREMENT TECHNIQUES

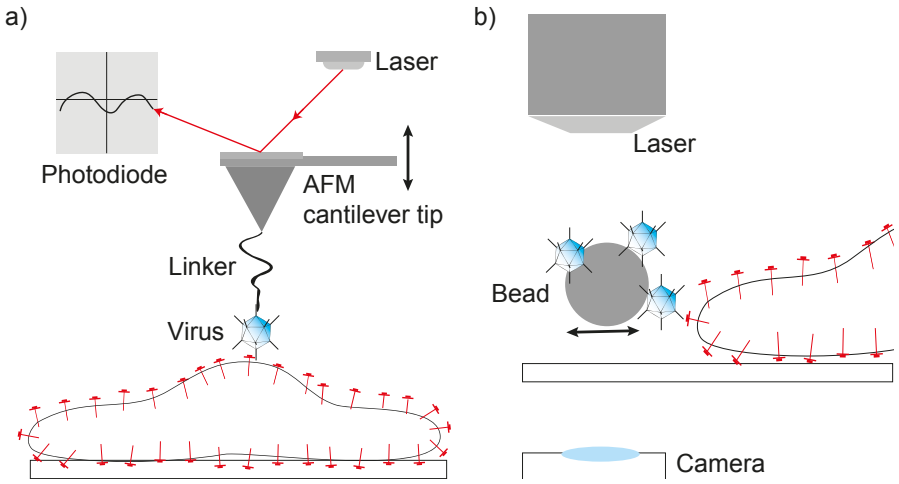

Figure 2.5: . Endocytic force measurement techniques. a) AFM and b) optical tweezers have been applied to perform single virus force spectroscopy. Adapted from [173, 174].

To measure the adhesion strength and the forces due to the invagination and uptake of cargo by a host cell, several biophysical techniques have been applied. In the case of virus particles as cargo, measurements based on AFM and optical tweezers have been summarized by Hermann and Sieben under the term single-virus force spectroscopy (SVFS) [173] and will be briefly discussed in the following. Further, the forces of nanoparticle uptake have been investigated using these techniques [175–177] or by altering cell mechanics on different stiff substrates [178]. Finally, also molecular tension probes (cf. Section 1.4.2) have been utilized to characterize the forces during adhesion and endocytosis of EGF through its receptor [92].

2.5.1 *Atomic Force Microscopy*

The classical force spectroscopy method in biophysics is based on the adhesion of a (functionalized) tip to a substrate (e.g. cells), which is measured by the deformation of a cantilever upon approaching or retracting from the substrate via a deflected laser beam (see Figure 1.5). For the use in endocytic measurements the cargo is typically attached to the tip while interacting with immobilized cellular ligands or whole cells. Rankel et al. tethered human rhinoviruses to an AFM tip and measured binding as well as unbinding forces to surface-tethered receptors and cells of $17 - 110\,\mathrm{pN}$ [179]. They observed increased binding affinities for longer contact times and stepwise rupture events suggesting binding of multiple receptors to the virus and estimated based on these values the kinetic off-rate $k_{off} = 0.05 \pm 0.15\,\mathrm{s}^{-1}$ for rhinovirus 2 with their cellular receptor

*f*MBP-V1-8 and the dissociation constant $K_D \cong 24\,\text{nM}$. Sieben et al. used influenza virus particles interacting with adherent cells from the apical side and retracted the tip at a loading rate of $20 - 1000\,\text{pN/s}$ resulting in rupture forces of $\sim 10 - 20\,\text{pN}$. They also observed force curves with serial rupture events indicating multivalent binding and an off-rate of $k_{off} = 0.12 \pm 1.23\,\text{s}^{-1}$for the interaction with CHO cells [180, 181]. Similarly, Alsteen et al. immobilized virus-like particles to an AFM tip and mapped the early adhesion steps with adherent cells. However, they detected particle rupturing at much higher loading rates up to $10^6\,\text{pN/s}$ and thus higher forces up to 300 pN [174]. Applying the Bell-Evans model (cf. Equation 1.3), they revealed the kinetic off-rate $k_{off} = 20.5 \pm 6.7\ \text{s}^{-1}$ for single virus-receptor bonds. These results suggest a big variety of adhesion forces between viruses and cells most probably depending on the specific receptor-ligand interactions and adhesion times applied in these studies. While so far AFM experiments with whole virus particles focused on the forces during initial adhesion, studies measuring the actual forces during virus endocytosis are lacking. The only studies characterizing the trace peak of AFM during endocytosis of nanoparticles were conducted in the lab of Prof. Hongda Wang with tips functionalized with Qdots or AuNPs [175–177]. They found a particle size-dependent force ranging from $39 - 126\,\text{pN}$ with bigger particles (20 nm) experiencing higher forces compared to smaller ones (5 nm). Actin inhibition by cytochalasin B resulted in depletion of the force signal, while the mechanism of nanoparticle uptake was not elucidated. In overall terms it remains difficult to dissect the contribution of forces originating from adhesion and endocytosis by the use of AFM.

2.5.2 *Optical Tweezers*

The working principle of an optical tweezer lies in the trapping of a bead by a focused laser beam with Gaussian beam profile. When an external force is pulling on the bead, the x-y position of the bead is changing according to the restoration force generated by the momentum change of the refracted light at the edges of the bead [182]. This has been used with influenza virus particles tethered to the bead to probe the interaction strength with cells revealing rupture forces between $10 - 23\,\text{pN}$ at loading rates between $4 - 1000\,\text{pN}$ [181]. Similarly, for the interaction between dengue viruses and cells expressing their receptor DC-SIGN $\sim 44\,\text{pN}$ have been documented [183]. Real endocytic events have been followed by optical tweezers for CME of notch ligands with a mean pulling force exerted by the cell of 10 pN [184]. Here, force generation depended on dynamin, epsin and actin binding and was in the same order of magnitude as the forces reported for EGF endocytosis by molecular tension probes [92].

2.6 MOTIVATION

Besides specific molecular interactions and signaling events, bare biophysical parameters like particle size and plasma membrane tension determine the uptake of viruses and thus their infectivity. A deeper understanding of the mechanical processes of endocytosis is therefore crucial to stop obligate intracellular pathogens from gaining access to cellular hosts. While until today the adhesion strength between virus (-like) particles and host cells has been characterized by SVFS methods, data on the forces during virus uptake itself are still missing. Furthermore, AFM and optical tweezers are limited to probe the interaction of particles and non-polarized cells or from the apical side of adherent cells. However, receptor presentation and actin dynamics vary widely for the adherent vs. non-adherent sides of cells. Moreover, the membrane tension, which is a critical factor opposing endocytosis, is higher at the apical side than on the basolateral side of polarized cells [143, 185].

In this study I will utilize mammalian reovirus particles as a model system for non-enveloped virus particle uptake. The primary infection route of reovirus - and many other pathogens - is oral and thus the viruses are first encountering epithelial layers of the respiratory and intestinal tract [158]. One could assume that the uptake of these viruses is thus mainly occurring from the apical sides of polarized cells. However, like many other viruses, reoviruses depend on the attachment to proteins mediating cell-cell junctions (JAM-A [166]) as well as cell-matrix (β1-integrins [157]) interactions. It can be thus speculated that these viruses first gain access, e.g. via small lesions, to the basolateral side of their host cells or into tight junctions before the initiation of their uptake. During the spreading of reovirus within the body, other cell types such as neurons get infected displaying different receptors and adhesion modes [186], which further underlines the importance of studying virus-cell interactions at the sides of cell adhesion.

The first aim is therefore to establish a method to immobilize reovirus particles on glass substrates to observe in unprecedented detail the interactions between the basolateral side of cells, their adhesion sites and virus particles. It can be assumed that in vivo interactions with the ECM trap virus particles in close contact to cells, which increases their chance of cellular uptake. This is going to be mimicked in vitro by co-presentation of ECM proteins or small peptides and reovirus particles. In addition I will consider the effect of the mechanical properties of the surrounding applying substrates with varying stiffness.

To quantify the absolute forces applied to single-virus particles on the basolateral side of adherent cells I will employ modular tension probes capable of bearing different types of ligands. MTFM has been

previously used to determine the forces between integrins and ECM peptides [79, 82, 97] as well as between EGF and its receptor complex, which is subsequently endocytosed [92]. In the work presented here, I show for the first time successful tethering of complete, infectious virus particles to molecular tension probes immobilized on an adhesive substrate. This method allows one to directly access endocytic forces acting on single virus particles by adherent cells, which had never been possible before.

Finally, I want to elucidate the origin of these forces through the use of small molecule inhibitors, blocking antibodies and knock-out cells. This will allow one to dissect the contribution of cellular receptors, the actin cytoskeleton as well as different endocytic pathways to the mechanics of virus particle uptake.

Part II

MATERIALS AND METHODS

Besides standard biophysical methods such as traction force microscopy or live cell imaging, I herein present new ways to study forces transduced by single cellular receptors and towards single particles such as viruses. I therefore combined block-copolymer nanolithography and molecular tension fluorescence microscopy with traction force microscopy and established a method for non-covalent as well as covalent immobilization of infectious, non-enveloped virus particles.

3 CELLULAR FORCE MEASUREMENTS

To measure cellular traction forces, forces transduced by single receptors and the forces applied to single virus particles during endocytosis, several biophysical methods have been exploited and combined in this thesis, namely: (reference-free) traction force microscopy, block copolymer micelle nanolithography and molecular tension fluorescence microscopy. All chemicals have been purchased from Sigma-Aldrich unless otherwise stated.

3.1 COMBINATION OF TRACTION FORCE MICROSCOPY WITH NANOPATTERNED LIGAND PRESENTATION

In order to yield control over the ligand presentation on elastic hydrogels in the nano-range while accessing cellular traction forces, I developed a two-step protocol combining BCML [95, 187] with polyacrylamide (PAA) hydrogels including fluorescent marker beads for traction force microscopy (TFM) [156].

3.1.1 *Block Copolymer Micelle Nanolithography*

I produced quasi-hexagonal ordered and disordered gold nanopatterns as previously described [41–43, 102, 188, 189]. Therefore, polystyrene(x)-b-poly(2-vinylpyridine)(y) diblock copolymers (PolymerSource Inc., Canada) and Polystyrene standard (Alfa Aesar, USA) were dissolved in toluene and stirred for 24 h at room temperature (RT). To vary the spacing and order of the gold nanopatterns, different compositions of the polymers were used according to table 3.1. Gold(III) chloride trihydrate was added to the micellar solutions with a specific loading parameter ($L = \frac{n[HAuCl_4]}{n[P2VP]}$), which defines the size of the gold nanoparticles. For disordered structures the micellar gold solution was subsequently mixed with a polystyrene solution in a 1:1 volume ratio. 10 µl of the solution were spin-coated (WS-400A-6NPP/Lite, Laurell Technologies Cooperation, USA) on 12 mm round coverglasses (Glaswarenfabrik Karl Hecht, Germany) previously cleaned with freshly prepared piranha solution for 1 h (3:1 mixture of sulfuric acid and hydrogen peroxide (20 %)) to remove organic residues. Samples were treated with oxygen plasma (TePla 100-E, 0.4 mbar, 150 W, 10 min) to remove the polymer matrix and form metal particles with minimal interactions with the glass substrate.

For the transfer of the gold nanoparticles into hydrogels, the BCML substrates were either used directly after plasma treatment or re-

Table 3.1: Preparation details for BCML

GENERATED STRUCTURES	STYRENE UNITS (X)	VINYL-PYRIDINE UNITS (Y)	c IN mg/ml	LOADING PARAMETER L	v (SPIN COATING) IN rpm
100 nm ordered	1824	523	4	0.6	10000
100 nm disordered	a) 1824 b) 123000	523	4 8	0.5	8000
50 nm ordered	1056	495	8	0.5	7000
50 nm disordered	a) 1056 b) 50000	671	9 8	0.3	5000

activated with a UV lamp for 30 min for the coupling of a gold-acryl crosslinker. Substrates were immersed in 30 mM N,N´-bis-(acryloyl)cystamine (Alfa Aeser, USA) in ethanol (99 %) for 1 h in the dark, washed three times for 30 min with pure ethanol and dried in a stream of nitrogen.

3.1.2 *Preparation of Hydrogel Substrates for Traction Force Microscopy*

PAA samples with fluorescent marker beads were used to access the tractions of cells sensing differently spaced extracellular ligands as well as for experiments with cells encountering reovirus particles. The hydrogels were produced inspired by Elsegui-Artola et al. [40] as follows: glass coverslips (20x20 mm², #1, Carl Roth, Germany) were washed by sonication for 10 min in ethyl acetate and dried with compressed nitrogen. They were incubated in a solution of 1.5 ml 3-(Trimethoxysilyl)propyl methacrylate, 1.5 ml acetic acid and 20 ml ethanol (96 %) for 30 min. Afterwards, they were washed three times in ethanol for 10 min and dried with compressed nitrogen. phosphate buffered saline (PBS), acrylamide (40 %) and N,N´-Methylenebis(acrylamide) (2 %) were mixed (according to table 3.2), vortexed and devolatilized with a desiccator for 5 min. Subsequently, 10 µl fluorescent beads (0.2 µm, red or 0.1 µm, blue, diluted and sonicated 1:10 in MilliQ water, FluoSpheres^{TM}carboxylate-modified, Thermo Fischer Scientific, USA), 2.5 µl ammonium persulfate (APS) (freshly prepared 100 mg/ml in MilliQ water) and 1 µl N,N,N´,N´-Tetramethylethylenediamine (TEMED) were added to the mixture. In order to prevent bubbles forming during the polymerization, the solution was not vortexed after degassing but mixed by repeated aspirating and dispensing of a large portion of the volume with a pipette. 10 µl of the solution were placed on the treated glass coverslip and covered with a 12 mm round nanopatterned surface (see section 3.1.1)

Table 3.2: Polyacrylamide mixtures for TFM samples.

STIFFNESS IN kPa / SUBSTANCES IN µl	0.5	1.5	5	13	18	30
PBS	429	414	382.2	367.75	352	299
Acrylamide	50	62.5	93.3	93.75	94.5	150
Bis-acrylamide	7.5	10	11	25	40	37.5
Beads (diluted)	10	10	10	10	10	10
APS	2.5	2.5	2.5	2.5	2.5	2.5
TEMED	1	1	1	1	1	1
Sum	500	500	500	500	500	500

or 7.5 µl of the solution were covered with a purified glass coverslip and allowed to polymerize for 20 min at RT. The reaction was quenched by incubating the sandwich in PBS for 10 min. For the transfer of the nanopattern, these samples were further incubated in PBS at 37 °C for 72 h before removing carefully the nanopatterned glass from the hydrogel [156].

3.1.3 *Immobilization of Ligands for Cell Adhesion*

Cellular adhesion is promoted by peptide ligands, which are immobilized on the AuNPs via short thiol linkers. 25 µM cRGD-thiol (cyclo [Arg-Gly-Asp-D-Phe-Lys(Ahx-Mercaptopropionic Acid), PCS-31062-PI, Peptides International) were incubated on top of the hydrogels at RT for 4 h. Afterward, ligand-conjugated nanopatterned hydrogels were washed 5 times for 10 min each in PBS to remove unbound peptides.

Surfaces of non-patterned hydrogels were further coated with fibronectin for cells to adhere. Therefore, 100 µl of freshly prepared Sulfo-Sanpah (Thermo Fischer Scientific, 1 mg in 10 µl DMSO + 1 ml 4-(2-Hydroxyethyl)piperazine-1-ethanesulfonic acid (HEPES), pH 8.5) was applied on the hydrogel and exposed with UV light for 10 min, after which the color turned from orange to brown. The hydrogels were washed in a big volume of HEPES for 1 min and directly immersed on a drop of 50 µl fibronectin (from human foreskin fibroblasts, dialyzed against PBS overnight via Dispo-Biodialyzer, molecular wight cut-off (MWCO) 1 kDa, 10 µg/ml in HEPES) and incubated overnight at 4 °C.

3.2 COMBINATION OF TFM WITH MTFM

In this thesis I utilized molecular tension probes with different "spring"-molecules and an NSET quenching mechanism. For the im-

mobilization and intrinsic quenching function of the molecular tension probes, gold nanoparticles are needed on top of the classical TFM samples. I therefore exploited transfer of gold nanopatterns into PAA hydrogels as described in the previous section with enlargement of the particles (see Section 3.2.1), as well as cTFM substrates with micropatterned gold/Qdots arrays (see Section 3.2.2).

3.2.1 *Electroless Deposition for the Enlargement of Gold Nanoparticles*

PAA hydrogels with fluorescent marker beads and transferred gold nanopatterns were produced as previously described in section 3.2.1. Since the pure AuNPs showed low binding affinity for the molecular tension probes, another layer of gold was deposited on top of the gold particles to make them readily available. In electroless deposition Au^{3+} is reduced by NH_2OH, which is surface-catalyzed and thus mainly preexisting AuNPs are enlarged rather than new particles being nucleated [190–192]. Therefore, hydroxylamine hydrochloride (0.2 mM in MilliQ water, freshly prepared) and gold(III)chloride trihydrate (0.5 % w/w in MilliQ water) were mixed in a 5:1 volume ratio. 500 µl of the mixture were applied on the hydrogels and incubated for 10 min at RT. Afterwards, coverslips were washed thoroughly in PBS to ensure that no hydroxyl amine traces remain in the gels, which could be toxic to cells and dried carefully from the side with the help of a kimwipe (Kimberly-Clark Professional) for the subsequent reactions.

3.2.2 *Confocal Reference-free Traction Force Microscopy*

Silicone substrates with micro-patterned Qdots and/or AuNPs arrays were produced by Tobias Lendenmann in the lab of Aldo Ferrari, ETH Zürich as previously described [75]. In brief: two component polydimethylsiloxanes (CY52-276 Part A and B, Dow Corning, USA) were mixed, spin-coated on glass coverslips for 1 min at 1500 rpm and cured at 70 °C for 30 min. Afterwards the substrates were kept for 2 weeks at RT before further use, to allow a homogeneous aging of the samples. For immobilization of the molecular tension probes, the composition of the ink was altered from the original protocol to contain (i) Qdots only, (ii) AuNPs only or (iii) a 20:1 mixture of both. Blue CdS/ZnS core/shell Qdots with an emission peak at 457 nm and octanethiol-capped AuNPs were obtained from the lab of David J. Norris, ETH Zürich [193, 194] and transferred from hexane dispersions to tetradecane with an optical density of 0.25 for a 1 mm path, to ensure a reproducible printing process. Electrohydrodynamic nanodrip-printing allows to deposit small volumes of a conductive ink with nanometer-control on a surface [195–197]. Therefore, the silicon substrates were placed on a conducting grounded plate. The ink was

filled in a gold-coated glass capillary with an opening diameter of 1 - 1.5 µm, which was moved above the substrate using a piezoelectric stage. Nanoscale droplets with a diameter of 50 - 100 nm were ejected through application of 200 - 250 V voltage pulses for 100 ms with the custom-built control unit. Several droplets formed a nano-disc of ~200 nm in diameter. These nano-discs were positioned in an hexagonal pattern with 3 µm distance between individual nano-discs and the tetradecane evaporated, leaving behind the nanoparticle content only.

3.3 MOLECULAR TENSION FLUORESCENCE MICROSCOPY

In this thesis I conducted molecular tension fluorescence microscopy adapted from and further developed in cooperation with the lab of Prof. Khalid Salaita (Emory University, Atlanta). Three types have been established and used: tension probes based on (a) an organic PEG spring, (b) deoxyribonucleic acid (DNA)-hairpins and (c) the I27 domain of the protein titin. All of these molecules can be linked to AuNPs via a thiol function on their lower end. This serves as anchor point on a surface and quenches distance-dependently the fluorophore, which is attached to their upper end of the tension probe (see Figure 6.5 and Section 1.4.2).

3.3.1 *Surface Preparation for the Binding of Molecular Tension Probes*

For experiments on glass substrates, surfaces were passivated with a self-assembled monolayer of PEG. This prevented non-specific adhesion of the tension sensors to the background. Thiol modifications on a fraction of the PEGs allowed me to immobilize AuNPs, which serve as adhesion site and quencher of the tension probes. Therefore, glass coverslips (20x20 mm², #1, Carl Roth, Germany) were washed and activated in freshly prepared piranha solution for 1 h. Afterwards, the glasses were rinsed 3 times in MilliQ water, sonicated for 5 min and dried with compressed nitrogen. Silane-PEG-methoxy (molecular wight (MW) ~ 2000 g/mol, Biochempeg, USA) and silane-PEG-lipoic acid (MW ~ 3400 g/mol, synthesized as described in Section 3.3.2) were solved in dry toluene (dried over 3 Å molecular sieves) in a 19:1 molar ratio with total silane concentration > 125 µM to ensure complete coverage of the glass surfaces. Coverglasses were immersed in this solution in a custom-made glass sample holder and the reaction was catalyzed by 25 µM triethylamine (≥99.5 %) and left for 16 h under nitrogen atmosphere at 80 °C. The substrates were subsequently washed in ethyl acetate (p.a., AppliChem, Germany) and methanol (p.a., Carl Roth, Germany) for 5 min each by ultrasonication and dried with compressed nitrogen. 300 µl of gold nanospheres (9 ± 2 nm) in tannic acid (0.05 mg/ml, nanoComposix, USA) were applied on top

of the coverglasses, incubated for 30 min at RT and unbound AuNPs were washed off under a stream of MilliQ water. Successful binding of AuNPs to the surface was evaluated by observation of a red sheen. Samples were immediately used for experiments with tension probes.

3.3.2 *Synthesis of Silane-PEG-Lipoic acid*

$(CH_3CH_2O)_3$Si-PEG-lipoic acid (MW ~3400 g/mol, referred to as silane-PEG-lipoic acid in the following) was synthesized analogously to $(CH_3CH_2O)_3$Si-PEG(2000) in [198]. To a solution of 0.5 g NH_2-PEG-lipoic acid (MW ~3400 g/mol, Biochempeg, USA) in 3 ml dry N,N-dimethylformamide (DMF) (p.a., Carl Roth, Germany), 1.1 equivalents of 3-(triethoxysilyl)-propyl isocyanate were added under nitrogen atmosphere and stirred for 24 h at RT. The PEG-product was cooled to 0 °C, precipitated in an excess of cold diethyl ether and filtered with a porous frit (No. 3). The precipitate was washed with cold diethyl ether and dried under reduced pressure overnight to yield silane-PEG-lipoic acid as a white powder.

3.3.3 *PEG-based Tension Probe*

The synthesis of a PEG-based tension sensor was based on the work of Dr. Yang Liu [79, 82] but designed in a modular way to be able to exchange the ligands for cell adhesion.

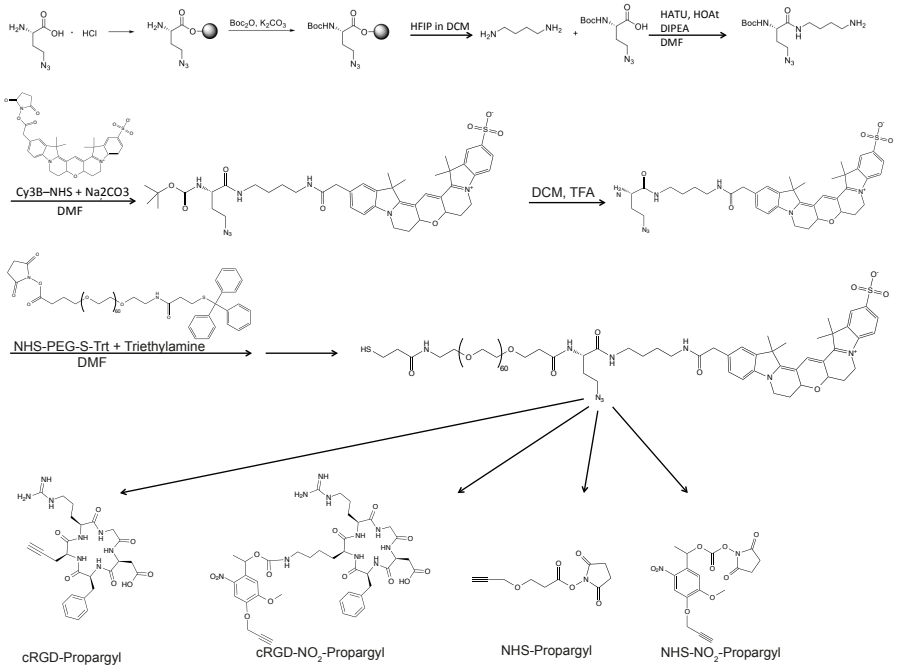

Figure 3.1: Synthesis route of the modular PEG-based tension probe.

The ligand and the fluorophore were attached to the upper end of a long PEG chain via a small, branched molecule. This molecule (Boc-L-Aha-butan-1-amine, $C_{13}H_{26}N_6O_3$) containing an azide function, a free amine group and a Boc-protected amine group was kindly provided by Dr. Stefanie Neubauer from the lab of Prof. Horst Kessler (TU Munich) (see Figure 3.1, upper row). I reacted 0.5 mg of this molecule with 0.9 equivalents of the fluorophore Cy3B-N-hydroxysuccinimide (NHS) (GE Healthcare, UK, solved in 70 µl DMF) in a total volume of 140 µl 1 M $NaHCO_3$ buffer (pH 8.5) overnight at RT. The product was lyophilized (FreezeZone, Labconco, USA) and subsequently purified by high performance liquid chromatography (HPLC) (Äkta pure, GE Healthcare, UK) with a C18 column (Phenomenex, USA, diameter 10 mm, length 250 mm) with buffer A: water + 0.1 % TFA and a gradient of 10 - 90 % buffer B: acetonitrile + 0.1 % TFA at a flow rate of 0.7 ml/min and analyzed by mass spectrometry (see Section 5.4).

In the next step the Boc-protective group was removed by trifluoracetic acid (TFA) in dichloromethane (DCM) for 2 h at 0 °C and 1 h at RT. This allowed the intermediate product to react with 0.9 equivalents of trityl-protected thiol-PEG-NHS (MW ~ 3000 g/mol, Iris biotech, Germany) in a small volume of DMF adjusted to mM concentrations with triethylamine as base for 2 days at RT. The reaction in organic solvents prevents the PEG from forming a mushroom conformation, which would bury its reactive group. Unreacted intermediate product was purified from the PEG containing molecules by HPLC. Impurities from the unreacted PEG-educt were not further purified as they can be considered as additional passivating PEGs strand for tension sensing experiments.

Since the binding efficiency of the PEG-tension sensor to the AuNPs was low in previous studies [79, 82], AuNPs have been pre-incubated with the tension probes and short passivating ethylene glycol $(EG)_8$-thiols, purified in solution and subsequently immobilized on the silane-PEG-lipoic acid surfaces (as described in Section 3.3.1). Therefore, 500 µl of gold nanospheres (9 ± 2 nm) in tannic acid (0.05 mg/ml, nanoComposix, USA) were incubated with 400 nM of the PEG-based tension probe and 1.2 µM EG_8-thiols (O-(2-carboxyethyl)-O-(2-mercaptoethyl) heptaethylene glycol, 95 %) in a total volume of 1 ml at 24 °C overnight in the dark. For purification, the PEG-decorated AuNPs were centrifuged for 45 min at 21000 rcf, the supernatant was removed and the particles resuspended in 1 ml water for 4 times. After immobilization of 300 µl of the PEG-decorated AuNPs on the silane-PEG-lipoic acid surfaces for 10 min, different ligands were attached to the upper end of the PEG-tension sensor by copper-catalyzed azide-alkyne cycloaddition (CuAAC) (see Section 3.3.6).

3.3.4 *DNA-Hairpin-based Tension Probe*

The design of the DNA-based tension sensor was based on a hairpin structure with defined unfolding force as presented by Zhang and co-workers [97]. Adaptations have been made to the previous design in order to immobilize the DNA on AuNPs (thiol-modification at the lower end), covalently bind different types of ligands (azide-modification at the upper end) and prevent shearing of DNA (one force transmitting strand only - see Figure 6.5b). Custom synthesized DNA oligomers were purchased from Integrated DNA Technologies, USA with 3´ and 5´ modifications as follows: 5AmMC6 is a 5´-amino modifier with a C6 spacer arm, 3AmMO is a 3´-amino modifier, 5ThioMC6-D is a 5´-thiol modifier with a C6 spacer arm, 3ThioMC3-D is a 3´-thiol modifier with a C3 spacer arm, 5AzideN is a 5´-azide modifier with a C5 spacer (see table 3.3).

Table 3.3: DNA oligomers for DNA-hp-based tension sensor. Colors indicate complementary bases, which were hybridized to form DNA-hp-based tension sensors.

STRAND	SEQUENCE
top DNA	5AmMC6/CGC ATC TGT GCG GTA TTT CAC
bottom DNA	5ThioMC6-D/TT TGC TGG GCT ACG TGG CGC TCT T/3AmMO
hp DNA (4.2 pN)	5AzideN/GTG AAA TAC CGC ACA GAT GCG TTT GTA TAA ATG TTT TTT TCA TTT ATA C TT TAA GAG CGC CAC GTA GCC CAG CAA A/3ThioMC3-D
hp DNA (12 pN)	5AzideN/GTG AAA TAC CGC ACA GAT GCG TTT GGG TTA ACA TCT AGA TTC TAT TTT TAG AAT CTA GAT GTT AAC CCT TTA AGA GCG CCA CGT AGC CCA GCA AA/3ThioMC3- D
hp DNA (19 pN)	5AzideN/GTG AAA TAC CGC ACA GAT GCG TTT CGC CGC GGG CCG GCG CGC GGT TTT CCG CGC GCC GGC CCG CGG CG T TTA AGA GCG CCA CGT AGC CCA GCA AA/3ThioMC3-D

Fluorophores have been covalently bound to DNA strands with amine modification as follows: top strand DNA and bottom strand DNA were reacted in 0.1 M $NaHCO_3$ buffer + 2 mM $MgCl_2$with a 10 fold molar ratio of StarRed-NHS (Abberior, Germany, λ_{em} : 638 nm λ_{ex} : 655 nm) or QSY21-NHS (Thermo Fischer Scientific, USA, λ_{em} : 661 nm), respectively, for 12 h at RT. Purification of unreacted dye was conducted by size exclusion chromatography with illustra NAP-5 columns (GE healthcare, UK) using MilliQ water as mobile phase. Further purification of unlabeled DNA was conducted by HPLC with the C18 column (see Section 3.3.3) buffer A: 0.1 M Trietyhlammonium acetate (TEAA) and a gradient from 10 to 90 % of buffer B: acetonitrile.

Purified DNA strands were freeze dried and resuspended in a small volume of MilliQ water to obtain µM concentrations.

DNA-hairpin sensors were hybridized from the 3 single DNA strands with a final hairpin concentration of 300 nM (900 nM for experiments on hydrogels) in 1 M NaCl solution with 10 % excess of the bottom and top strand. They were heated up to 95 °C for 10 min and cooled down to 12 °C within 30 min in a thermal cycler (T100, Bio-Rad, Germany). Finally, additional bottom strands DNA were added in excess to obtain a final concentration of thiolated DNAstrands of 3 µM. This ensures the complete coverage of AuNPs, while keeping a low density of DNA-hairpin sensors on the surface, which limits the background fluorescence signal.

100 µl of this solution has been applied on a surface with immobilized AuNPs (see Section 3.3.1) and covered with another of these surfaces upside down to form a sandwich, which was incubated overnight at 4 °C. Unbound DNA was washed off in 100 mM phosphate buffer containing 150 mM NaCl and the coverglasses were carefully separated from each other. Substrates were further processed avoiding drying out of the tension probe-surface at any time.

3.3.5 *Titin-based Tension Probe*

Tension probes based on the I27 domain of titin were expressed in *E. coli* as previously described [51]. The plasmid pET22b-I27-RGD/E for the modified I27 domains containing an RGD or an RGE sequence for specific integrin adhesion or no specific adhesion, respectively, and the amber codon (TAG) was a kind gift from Dr. Korelia Galior (Prof. Khalid Salaita Lab, Emory University, Atlanta), as well as the pEVOL-pAzF plasmid for p-azidophenylalanine incorporation at the amber codon. The final amino acid sequence was as follows:

MTVYAVTGRG(D/E)SPASSAAHMGG(TAG)GGLIEVEKPLYGVEVF
VGETAHFEIESEPDVHGQWKLKGQPLAASPDCEIIEDGKKHILILH
NCQLGMTGEVSFQAANTKSAANLKVKELCCHHHHHH

3.3.5.1 *Preparation of Selective Agar Plates*

25 g LB Medium (Carl Roth, Germany) and 15 g Agar-Agar, Kobe I (Carl Roth) were dissolved in 1 l of water in an Erlenmeyer flask (2 l) and autoclaved. The medium was allowed to cool down to ~ 50 °C before the following antibiotics: 1:1000 chloramphenicol (AppliChem, Germany), c_{start} = 34 mg/ml in EtOH abs., 1:1000 kanamycin c_{start} = 30 mg/ml in H_2O, 1:2000 ampicillin c_{start} = 100 mg/ml in H_2O. The medium was carefully shaken to avoid bubble formation and poured in Petri dishes and left at RT to solidify before being stored at 4 °C until further use.

3.3.5.2 *Co-Transformation of Bacteria with Purified Plasmids*

45 µl of chemically competent *E. coli* (BL21(DE3), NEB, USA) are mixed with 5 µl of plasmid pET22b-I27-RGD or -RGE (50 or 42 ng/µl) and 5 µl of plasmid pEVOL-pAzF (40 ng/µl) and kept on ice for 5 min. Then, a heat-shock was performed for 45 s at 42 °C, followed by 2 min on ice again. 1 ml of LB medium was mixed with the 50 µl of bacteria solution and kept at 37 °C for 1 h while shaking with 750 rpm. The dispersion was spun down for 3 min at 14000 rpm to form a pellet and 750 µl of the supernatant was discarded while the remaining 250 µl were resuspended and distributed on the pre-warmed agar plates, which were incubated at 37 °C overnight.

3.3.5.3 *Initiation of a Starter Culture*

A single colony was picked and distributed in a falcon with 10 ml LB medium containing 50 µg/ml ampicillin, 34 µg/ml chloramphenicol and 0.2 % glucose (w/v) and incubated at 37 °C overnight in a shaker with holes in the lid for CO_2 exchange.

3.3.5.4 *Expression culture*

100 µl of the starter culture were used to inoculate 100 ml of growth medium in a 200 ml Erlenmeyer flask and the optical density (OD) was measured by UV-Vis spectroscopy (Lambda 25, Perkin-Elmer, USA). At an OD of 0.2, 1 mM of 4-azido-L-phenylalanine (Chem-Impex International, USA), at an OD of 0.4, 0.02 % (w/v) L-arabinose and at an OD of 0.8, isopropyl beta-D-1-thiogalactopyranoside (IPTG) was added to a final concentration of 1 mM. Cells were grown for 16 h at 30 °C while shaking (Excella E24 Incubator shaker series, New Brunswick Scientific, USA).

3.3.5.5 *Protein Purification*

The expression culture was transferred into 50 ml falcons and centrifuged for 10 min at 14000 rcf (Rotina 380R, Andreas Hettich, Germany). The supernatant was discarded and the bacteria pellet was resuspended in 10 ml 0.1 M KH_2PO_4 buffer (pH 7.4) with 1 mM Dithiothreitol (DTT) and 10 % Phenylmethylsulfonylfluorid (PMSF) (0.1 M in MeOH) and sonicated for 10 min by Omni Sonic Ruptor 400 (Omni International, USA, 40 % power purse, 50 % pulser frequency) to lyse the bacteria. The solution was centrifuged again for 30 min at 12000 rcf at 4 °C to get rid of the cellular debris and the supernatant was filtered with a Whatman syringe filter (cellulose acetate, 0.45 µm pore size). The I27 protein was purified by immobilized metal ion affinity chromatography with a 1 ml His-Trap column in the Äkta pure system (GE healthcare, UK) with buffer A: KH_2PO_4 buffer (pH 7.4) + 1 mM DTT + 30 mM imidazole and a gradient of 0 - 100 % buffer B: KH_2PO_4 buffer (pH 7.4) + 1 mM DTT + 500 mM imidazole. Protein

expression was checked by SDS page with NuPage 4-12 % bis-tris gel (Thermo Fischer Scientific, USA), MES buffer and a gel chamber with Powerpac basic supply (BioRad, Germany). Gels were stained with Coomassie plus protein assay reagent (Thermo Fischer Scientific, USA) and imaged in an Amersham Imager 600 (GE healthcare, UK).

3.3.5.6 *Protein Labeling*

Purified I27-RGD and I27-RGE proteins were desalted by gel filtration with Zeba spin columns (7000 MWCO, Thermo Fischer Scientific, USA) and subsequently randomly labeled with Alexa647-NHS (Thermo Fischer Scientific, USA) in 1:10 molar ratio in 0.1 mM KH_2PO_4 buffer at RT overnight. Unbound dye was removed again by gel filtration. Protein concentration and the labeling ratio was quantified by UV-Vis absorption in a NanoDrop ND-1000 (Peqlab, Germany). UV-Vis absorption and photo-counting of bleaching steps of single titin-based tension-sensors (in collaboration with Klaus Yserentant in the lab of Prof. Dirk-Peter Herten, Heidelberg University) revealed that the majority of titin sensors bear one or two fluorophores even though the I27 protein has multiple accessible lysins at its surface (cf. Figure A.1).

3.3.5.7 *Immobilization of Titin-based Tension Probes on Surfaces*

The I27-RGD or I27-RGE tension probe labeled with Alexa647 was typically diluted to a final concentration of 60 nM in 0.1 M KH_2PO_4 buffer (pH 7.4) for experiments on glass substrates and 12 nM for experiments on cTFM samples. A 6.4x molar excess (384 nM in this case) of COOH-$(CH_2$-CH_2-$O)_8$-SH was added to the solution and immediately 300 µl were applied on top of the surfaces with immobilized AuNPs and incubated for 1 h at RT. Samples with I27-RGD tension probes were used directly after washing in KH_2PO_4 buffer, while ligands for cellular interactions were attached to the samples with I27-RGE tension probes (see Section 3.3.6).

3.3.6 *Attachment of Ligands by CuAAC*

Different types of ligands can be linked to the azide-functionalized tension probes, which are immobilized on AuNPs (on glass or hydrogel substrates) by CuAAC. For the analysis of cell-generated traction forces via integrin receptors, cyclic Arg-Gly-Asp (cRGD)-alkyne (cyclo(Arg-Gly-Asp-D-Phe-Pra (see Figure 3.1 last row, custom-synthesized by Biotrend, Germany) was clicked on the tension probes following a protocol of Hong et al. [199]. Therefore, 100 mM phosphate buffer pH 7 equipped with 150 mM NaCl, 50 mM tris(3-hydroxypropyltriazolylmethyl)amine (THPTA), 20 mM $CuSO_4$and 100 mM aminoguanidine were prepared in MilliQ water

Table 3.4: Reaction mixture of CuAAC for covalent binding of cRGD-alkyne.

SUBSTANCE	c_{start} IN mM	c_{end} IN mM	V IN µL
phosphate buffer	100	~ 100	87
cRGD-alkyne	10	0.15	1.5
THPTA	50	0.5	1
$CuSO_4$	20	0.1	0.5
aminoguanidine	100	5	5
sodium ascorbate	100	5	5
			100

and stored at 4 °C until use and 100 mM (+) sodium L-ascorbate was always freshly prepared in MilliQ water. Substances were mixed according to table 3.4 and 100 µl of the reaction mixture were incubated on top of the surfaces immediately after washing off unbound tension probes for 2 h at RT in a humidity chamber in the dark.

4 VIRUS PARTICLE MODIFICATIONS

4.1 PURIFICATION OF REOVIRUS PARTICLES

Reovirus production and purification was performed by Marta Fratini in the lab of Dr. Steeve Boulant (Heidelberg University and DKFZ). Briefly, mammalian reovirus strain T3D (originally obtained from Bernard N. Fields (Harvard Medical School) was grown in L-cells as previously reported [200–202]. Frozen stocks of infected cells were thawed and disrupted by sonication (UP200Ht ultrasonic processor, 50 % of 200 W, 26 kHz, Hielscher Ultrasonics, Germany) for 40 s on ice. 1 % (v/v) of sodium desoxycholate (10 % w/v) was added, the mixture was stirred gently and incubated for 15 min on ice for cell lysis. 33 % (v/v) 1,1,2-trichlorotrifluoroethane were added and the sample was emulsified by sonication for 1 min avoiding the formation of bubbles. More trichlorotrifluoroethane was added to a final volume of 50 % (v/v) before sonicating again. To separate the two phases, the solution was centrifuged at 7000 rcf for 10 min (MF 48, awel international, France) and the top aqueous phase was transferred into a fresh falcon and emulsified again with trichlorotrifluoroethane, sonication and centrifugation. The top phase was subsequently layered over a CsCl gradient (1.25 - 1.45 g/cc) in virus buffer (VB) (150 mM NaCl, 10 mM $MgCl_2$, 10 mM tris(hydroxylmethyl) aminomethane (TRIS), pH 7.5) in a thin-wall polypropylene tube for use in SW 40 Ti ultracentrifuge rotor (Beckman Coulter, USA) and centrifuged at 23000 rpm in an ultracentrifuge at 4 °C overnight. Cell debris, empty capsids and intact virus particles were separated by their weight in different bands in the CsCl gradient. By piercing the bottom of the tube with a needle, drops of the band containing virus particles were collected into a 1 ml tube (Eppendorf, Germany). In order to get rid of the CsCl, virus particles were dialyzed against VB (3 ml Slide-A-Lyzer dialysis cassettes, 20000 MWCO, Thermo Fischer Scientific, USA) at 4 °C for 24 h.

The concentration of reovirus particles in solution was determined to be around $1.7 \cdot 10^{11}$ particles/ml by nanoparticle tracking analysis with the NanoSight 300 (Malvern, UK).

4.2 LABELING OF REOVIRUS PARTICLES

Reovirus particles were labeled randomly with fluorescent dyes and linker molecules for surface immobilization via NHS-amine coupling at the lysine side chains on the viral capsid as previously described

[169]. Therefore, reoviruses were first dialyzed against PBS to remove free amines from the buffer that would interfere with the NHS reaction in Slide-A-Lyzer MINI dialysis Devices, 3500 MWCO (Thermo Fischer Scientific, USA) at 4 °C overnight. Then 100 µl of the virus solution were mixed with the desired NHS-ligand and incubated for 1 h at RT. For experiments with covalently immobilized reovirus on single tension probes, propargyl-NHS at 33.2 µM final concentration and Alexa568-NHS (Thermo Fisher Scientific, USA) at 0.5 µM final concentration, and for experiments with non-covalently immobilized reovirus on NeutrAvidin surfaces, 8.4 µM EZ-link sulfo-NHS-biotin and Alexa647-NHS at 33.7 µM final concentration (both Thermo Fisher Scientific, USA) were used. The NHS reaction was quenched by addition of 10 % VB and unreacted dye was removed by gel filtration with Zeba spin columns (7000 MWCO, Thermo Fisher Scientific, USA).

4.3 PREPARATION OF VIRUS-LIKE PARTICLES FROM GOLD NANOPARTICLES

Biomimetic virus-like particles were composed from AuNPs with 100 nm diameter with differential surface coatings to fit the dimensions and chemical structure of reoviruses as follows: 3 ml of the gold nanoparticle solution (OD1, in citrate buffer) were incubated with final concentration of 25 µM SH-PEG-alkyne (MW ~ 3000 g/mol, Biochempeg, USA) and 2.5 µM SH-PEG-NH-StarRed (synthesis see Section 4.3.1) at RT overnight under constant shaking and exclusion of light. Subsequently, unbound thiol linkers were washed off by centrifuging the functionalized AuNPs three times (2600 rcf at 4 °C, for 10 min in 5417R centrifugee, Eppendorf, Germany) and discarding the supernatant. After the third washing step the pellet was resuspended in 50 µl MilliQ water and the concentration was determined by UV-Vis (Nanodrop) to be approximately $1 \cdot 10^{11}$ particles/ml.

For the non-covalent immobilization via biotin-NeutrAvidin (cf. Section 4.4.2), the AuNPs were further functionalized with azide-EG_3-biotin (Jena Bioscience, Germany), which was clicked at 15 µM final concentration to the alkyne functions of the AuNPs with $5 \cdot 10^{10}$ particles/ml in a total reaction volume of 150 µl (analogously to section 3.3.6). Further, the surface of these functionalized AuNPs can be modified to mimic ligands of viral capsids. Therefore, optionally cRGD-azide (cyclo[RGDfE]K(N3), Peptide Specialty Laboratories, Germany) was clicked in the same reaction at 300 µM final concentration. Modified AuNPs were purified from unbound ligands by size exclusion columns (Zeba Spin Desalting Columns, 7000 MWCO) and stored at 4 °C until further use for up to 2 weeks.

4.3.1 *Synthesis of SH-PEG-NH-StarRed*

20 µl of a 8 mM solution of SH-PEG-NH2 (MW ~ 3000 g/mol, Iris Biotech GmbH, Germany) and 18 µl of 0.8 mM StarRed-NHS(Abberior, Germany), both in DMSO, were mixed and supplemented with 2 µl triethylamine. The reaction was allowed to proceed at RT for two days under continuous stirring and exclusion of light. No purification steps were necessary, since unbound dye molecules cannot bind to the AuNPs and will be hence washed off after the coupling to gold. The product was stored at - 20 °C until further use and will be referred to as SH-PEG-NH-StarRed.

4.4 IMMOBILIZATION OF VIRUS PARTICLES

In order to study the initial phase of cell interaction with nanoparticles and initiation of endocytosis, in collaboration with Marta Fratini (Dr. Steeve Boulant lab, Heidelberg University and DKFZ) I developed a method to covalently immobilize reoviruses on modified substrates. In addition, I established a method to non-covalently immobilize reoviruses and virus-like particles on substrates with varying stiffness.

4.4.1 *Covalent Immobilization*

Covalent immobilization of virus particles allows to study the initiation of viral uptake, while the later stages of endocytosis and viral infection can be neglected. Therefore, I sought after a method that prevents the viral shape and infectivity in solution but allows to tether viral particles non-reversibly on biomimetic surfaces or tension probes. Here, I chose the highly selective CuAAC reaction, which was shown to be biocompatible for coupling of biological molecules with a copper-chelating agent such as THPTA [199, 203, 204]. Reoviruses were clicked directly to passivated glass coverslips with silane-PEG-azide (~ 3000 g/mol, Rapp Polymere, Germany) or on coverglasses modified for MTFM with molecular tension probes bearing an azide function (see Section 6.5).

To allow cell adhesion via integrin receptors, cRGD-alkyne or cRGD-azide was clicked to the silane-PEG-azide and silane-PEG-alkyne surfaces, respectively, analogously to section 3.3.6 at 150 µM end concentration each. Where virus particles were clicked via the same ligands to the surface, this reaction was conducted first for 1 h and subsequently cRGD was clicked on the sample for 1 h.

For combination of MTFM samples with virus particles as ligands, 10 % silane-PEG-alkyne (w/w) was mixed with the other PEGs for passivation of the glass coverslips (see Section 3.3.1 for details). Subsequently, cRGD-azide was reacted in a first step with the surface (just

like in section 3.3.6) and then AuNPs and tension probes were immobilized as described in section 3.3. The concentration of the DNA-hp-based and titin-based tension probes was adjusted to 300 pM and 3 nM, respectively, to limit the background fluorescence. Virus particles were reacted at a final concentration of ~ $5 \cdot 10^9$ particles/ml.

4.4.2 *Non-covalent Immobilization*

Biotinylated reoviruses or AuNPs (see Section 4.2 or 4.3) were non-covalently immobilized via NeutrAvidin, which is sandwiched on a biotin layer (see Figure 7.1).

Therefore, glass coverslips were passivated in a 0.3 mg/ml solution of silane-PEG-alkyne (~ 3000 g/mol, Biochempeg, USA) in toluene at 80 °C overnight analogously to section 3.3.1. After washing, azide-EG_3-biotin (Jena Bioscience, Germany) was immediately tethered to the PEGylated glasses by CuAAC. Further cRGD-azide was immobilized on the surface in the same reaction to allow cell adhesion via integrins. In detail 150 µM cRGDazide, 150 µM azide-EG_3-biotin, 500 µM THPTA, 100 µM $CuSO_4$, 5 mM aminoguanidine and 5 mM sodium-L-ascorbate (final concentrations) were mixed in 100 mM phosphate buffer (pH 7) and glass substrates were inverted on a 100 µl drop of this reaction solution for 2 h at RT. Samples are washed subsequently under a stream of MilliQ water and dried carefully over the edge with a tissue. NeutrAvidin (A2666, Thermo Fischer Scientific, USA) was reconstituted at 5 mg/ml in PBS and stored in 10 µl aliquots at -20 °C to avoid repeated freeze-thawing. Only clear solutions without visible precipitates were used and diluted 1:100 to a final concentration of 50 µg/ml in PBS and a drop of 150 µl was placed on top of the biotinylated glass surfaces at RT for 1 h in a humidity chamber. Afterwards, samples were immersed in a petridish with PBS for 5 min to wash off unbound NeutrAvidin with two exchanges of the washing solution. Successful binding of the protein was indicated by a change in hydrophility and a remaining layer of solution on top of the glass substrates after careful drying with a tissue over the edge. 100 µl of the biotinylated reovirus (see Section 4.2) or AuNPs with a final concentration of ~$1 \cdot 10^{10}$ particles/ml were added directly on the remaining liquid film and allowed to interact with the NeutrAvidin for 2 h at RT in the humidity chamber. Samples were glued onto 35 mm polystyrene petridishes with home-made 18 mm in diameter holes by TwinSil (Picodent, Germany) and washed with 50 ml sterile PBS avoiding to dry out the surface completely at any time.

5 PREPARATION OF CELL SAMPLES AND IMAGING

5.1 CELL CULTURE

All cells used in this study were cultured in Dulbecco´s modified eagle medium (DMEM) either with 4.5 g/l D-Glucose and L-Glutamine (#41965) or with 4.5 g/l D-Glucose, GlutaMAX and pyruvate (#31966), or Ham´s F12 medium (#21765-029, Thermo Fischer Scientific, USA), each equipped with 10 % (v/v) fetal bovine serum (FBS) and 1 % (v/v) Penicilin-Streptamycin, which was sterile filtered with Rotilabo syringe filters, cellulose mixed ester, 0.22 µm pore size (Carl Roth, Germany), in water saturated 5 % CO_2-atmosphere at 37 °C. Cells were subcultured at least once before usage in experiments by detaching them with StemPro Accutase (Thermo Fischer Scientific, USA) and diluting 1:5 in fresh growth medium. For MTFM experiments, cells were resuspended in their corresponding medium with reduced FBS concentration of 0.5 % (v/v). For experiments combining TFM with nanopatterned ligand presentation, culture medium without FBS and for all other experiments complete growth medium was used. Cells were count in Neubauer chamber and $1 - 5 \cdot 10^5$ cells were plated per sample. For the reference state in classical TFM experiments, cells were removed with 3 ml trypsin for 10 min followed by gentle pipetting up and down directly on the stage of the microscope. All culture media and complementary substances were purchased from Thermo Fischer Scientific, USA.

5.1.1 *Cell Lines*

Human breast myoepithelial cell lines were used as described in [40, 156, 205], cultured in Ham´s-F12 medium supplemented additionally with hydrocortisone (1 µg/ml), EGF (10 ng/ml) and insulin (5 µg/ml). They were employed for experiments with nano-spaced adhesion ligands on soft substrates in order to compare the results to previous studies.

Wildtype rat embryonic fibroblasts (REF) and REF stably expressing a fusion paxillin-yellow fluorescent protein (YFP) were originally obtained from the lab of Benny Geiger (Weizman Institute, Israel) and cultured in DMEM #31966. As fibroblasts, they have strong interactions with the extracellular matrix in vivo and are thus used for force transmission studies in this thesis.

Human osteosarcoma U2OS cells (HTB-96, ATCC, USA) originate from a 15 year old girl and were cultured in DMEM #31966. These

cells have been previously used in cell adhesion studies [206], but as epithelial cells, they are less strong than fibroblasts and were thus used for experiments on weaker tension probes in this study.

Wildtype BSC1 (CCL-26, ATCC, USA) derived from African green monkey kidney cells were cultured in DMEM #41965. BSC1 cells stably expressing AP2-enhanced green fluorescent protein (eGFP) were obtained from Dr. Steeve Boulant (Heidelberg University and DKFZ) [143]. These endothelial cells are a well-studied model for clathrin-mediated endocytosis and used in this context to study the origin of force during virus uptake.

U373-MG (referred to as U373 in the following) were originally obtained from Prof. Tomas Kirchhausen (Harvard Medical School, USA). This human glioblastoma astrocytoma cell line derived from a malignant tumor by explant technique and was cultured in DMEM #41965. U373 is another cell line to study coated plaques [207] and shows a high endocytic activity. Therefore, they were chosen for experiments on reovirus uptake and infection while inhibiting their actin cytoskeleton or endocytic proteins. U373 cells stably expressing AP2-eGFP were obtained from Dr. Steeve Boulant. U373 cells displaying a CRISPR/Cas9 induced double knockout of clathrin light chain (CLT) A and B were generated and kindly provided by Markus Mukenhirn. U373 cells with a transient overexpression of the dynamin mutant K44A were generated by Marta Fratini with the pEGFP-Dyn2-K44A plasmid [208] and co-expression of clathrin-tomato.

HeLa cells originating from human cervix adenocarcinoma of the 31 year old patient Henrietta Lacks in the United States in 1951 were purchased from ATCC (CCL2) and cultured in DMEM #41965. They are known to internalize mammalian reovirus in an integrin-dependent manner [157] and were thus chosen for experiments analyzing the receptor dependence of virus endocytosis.

CHO-K1 cells (CCL-61, ATCC, USA) are epithelial like Chinese hamster ovary cells cultured in Ham´s F12 medium. Since these cells do not express JAM-A, they were chosen as a control for reovirus uptake in the absence of JAM-A.

5.1.2 *Receptor Blocking*

Cellular receptors have been inhibited by incubating 10^5 cells in 200 µl FBS-free culture medium in solution for 1 h at RT with the following antibodies/ reagents: JAM-A antibody clone J10.4 (sc-53623, Santa Cruz Biotechnology, USA) at 10 µg/ml final concentration, human integrin β_1 (CD29) blocking antibody clone P5D2 (#MAB17781, R&D systems, USA) or clone 4B4 (#6603113, Beckman Coulter, USA) at 10 µg/ml final concentration, integrin $\alpha_5\beta_1$-selective ligand (FR248, obtained from the lab of Horst Kessler, TU Munich) at 2.5 µM final

concentration, sialic acids were digested by neuraminidase (N3786) diluted 1:10 with 50 mU/ml final concentration and matrix metalloproteinases (MMPs) were inhibited by GM6001 (#sc-203979, Santa Cruz Biotechnology, USA) at 25 µM.

5.1.3 *Protein Inhibition*

To disrupt the actin cytoskeleton or the endocytic machinery the following small molecules inhibitors have been applied to the cells in 3 ml growth medium during the experiments in the indicated final concentrations: actin polymerization was inhibited by cytochalasin D (#C8273) at 60 nM and actin filaments were disrupted by jasplakinolide (#J4580) at 100 nM, myosin II was blocked by blebbistatin (#B0560) at 10 µM, Rho-associated protein kinase (ROCK) was inhibited by Y-27632 (ALX-270-333, Enzo Life Sciences, USA) at 10 µM, Arp2/3 was inhibited by CK-666 (#SML0006) at 200 µM, formins were blocked by SMIFH2 (#S4826) at 30 µM, caveolin-dependent endocytosis was blocked with the tyrosine protein kinase-inhibitor genistein (#G6649) at 200 µM and membrane cholesterol was depleted with methyl-beta-cyclodextrin (#C4555) at 10 mM. Since most drugs were solved in dimethyl sulfoxide (DMSO) at 1000x of their final indicated concentration or higher, control cells were treated with 3 µl DMSO in 3 ml medium.

5.1.4 *Immunofluorescence*

Cells were fixed with 4 % (w/v) paraformaldehyde after washing once with PBS. For immunofluorescence (IF) of extracellular receptors only, fixation was quenched after 5 min with 0.1 M glycine in PBS and cells were directly blocked, otherwise fixation was continued for 20 min. Samples were washed twice in PBS and for membrane permeabilization cells were treated with Triton X-100 0.5 % (v/v) for 10 min. Subsequently, cells were blocked for 30 min in 1 % (w/v) bovine serum albumin (BSA) in PBS.

Antibodies against FA proteins, EEA1, CLT, the reovirus nonstructural protein µNS and reovirus T3D virion were diluted as indicated in table 5.1 in 1 % BSA solution and incubated on the samples for 1 h in a humidity chamber. Subsequently, samples were washed 3 times à 5 min in 1 % BSA while shaking. Secondary antibodies (see Table 5.2) and 1:500 WGA 488 (Thermo Fischer Scientific, USA), 1:100 Phalloidin-FITC, 1:100 Phalloidin-TRITC and 1:1000 DAPI, if applicable, were incubated on the samples for 1 h in the dark before washing again 3 times à 5 min in 1 % BSA and mounting the samples in mowiol 4-88.

Table 5.1: List of primary antibodies

EPITOPE	ORIGIN	SUPPLIER	CAT. NO.	DILUTION
vinculin	mouse	Sigma Aldrich	V9264	1:600
zyxin	mouse	Synaptic systems	307011	1:200
EEA1	mouse	BD Biosciences	610456	1:100
CLT	mouse	Sigma Aldrich	C1985	1:1000
µNS	rabbit	GenScript	custom-made	1:300
T3D-virion	rabbit	GenScript	costum-made	1:500

Table 5.2: List of secondary antibodies. All antibodies were purchased from Thermo Fischer Scientific, USA.

EPITOPE	ORIGIN	CONJUGATION	CAT. NO.	DILUTION
rabbit-IgG	goat	Alexa350	A-21068	1:200
rabbit-IgG	goat	Alexa488	A-11034	1:200
rabbit-IgG	goat	Alexa568	A-11036	1:500
mouse-IgG	goat	Alexa568	A-11031	1:1000
rabbit-IgG	goat	Alexa568	A-11011	1:500
mouse-IgG	donkey	Alexa647	A-31571	1:200
rabbit-IgG	goat	Alexa647	A-21244	1:200

5.2 CELL IMAGING

5.2.1 *Wide-field Microscopy*

Wide-field fluorescence and MTFM images were acquired on a DeltaVision system (GE healthcare, UK) based on an Olympus IX inverted microscope (Olympus, Japan) equipped with a cooled CCD camera (Coolsnap HQ, Roper Scientific, USA) and a home-build environmental chamber for temperature and CO_2 control. The 60x/1.4 NA PlanApo objective (Olympus, Japan) was used.

5.2.2 *Confocal Imaging*

Fixed and live cells interacting with single virus particles were imaged using the 405, 488, 561 and 633 nm laser lines of an inverted confocal microscope (LSM880, Zeiss, Germany). For live cell imaging, a stage-top incubator (PM 2000 RBT, PeCon, Germany) and the LD C-Apochromat 40x/1.1 NA water corrected immersion objective (Zeiss) was used. To limit the phototoxic effect of the laser light for living cells, images were recorded with 0.2 % laser intensity of the 561 or 633 nm laser and brightfield images were obtained from the

same scans with the transmitted light detector (T-PMT). To follow tearing of biotin-NeutrAvidin immobilized virus particles from glass surfaces, cells were seeded directly at the microscope and allowed to settle for 15 min. Up to 10 positions with adhering cells were chosen and imaged from 30 min post seeding on (t_0) with images taken every 5 - 10 min for up to 16 h.

5.2.3 *TIRF Imaging*

Single-molecule imaging of molecular tension probes in low density in combination with virus particles as ligands were performed on a total internal reflection fluorescence (TIRF) microscope in the group of Prof. Dirk-Peter Herten in collaboration with Klaus Yserentant. The microscope body Eclipse Ti (Nikon, Japan) was equipped with TIRF illumination and "Perfect Focus System 2". The 488 (4 % of 40 mW), 561 (5 % of 30 mW) and 640 nm (5 % of 50 mM) laser lines of the iChrome MLE-LFA (TOPTICA Photonics, Germany) were fiber-coupled to the TIRF illuminator and used in combination with 525/50 nm, 605/70 nm bandpass and 640 nm longpass filters. Excitation and emission wavelengths were split with a quadruple dichroic (R405/488/561/635, AHF Analysetechnik, Germany). The Apo TIRF 100x NA 1.49 oil objective was used with immersion oil n = 1.515 (both Nikon). As camera, the back-illuminated EMCCD iXon Ultra 897 (Andor, Ireland) was employed. Live-cell imaging was performed at 37 °C using a custom-built stage-top heating chamber and an objective heating collar. Time-laps movies were recorded 30 min post seeding of the cells for 10 min per cell with 0.25 Hz frame-rate.

TetraSpeck multi-color fluorescent microspheres (0.1 µm, blue/-green/orange/dark red, Thermo Fischer, USA) were used to correct the images for chromatic aberration with a custom-written software in Matlab (MathWorks, USA) by Dr. Kristin Grußmayer (formerly in the lab of Prof. Dirk-Peter Herten).

5.3 SCANNING ELECTRON MICROSCOPY

Scanning electron microscopy (SEM) is performed with a Zeiss LEO 1530 Gemini equipped with a Schottky-field-emission cathode at ~ 10 mm working distance and 5 kV acceleration voltage.

5.3.1 *Critical Point Drying of Cells*

To retain the structure of biological samples and making them accessible for the low pressure conditions during scanning electron microscopy, critical point drying is applied. Hereby, the transition between the liquid and the gas state occurs without any surface tension, which would damage the sample, at the specific temperature and

pressure of the critical point of the medium, typically CO_2 with 31 °C and 75 bar. Therefore, samples were fixed in 2 % glutaraldehyde in PBS for 15 min and the water in the biological samples was stepwise replaced with ethanol (25 %, 50 %, 75 %, two times 95 % and three times 100 %, each 10 min) and then transferred into the critical point dryer (CPD 030, Bal-Tec, Lichtenstein). Here, the dry ethanol was further replaced by liquid CO_2 without letting the sample run dry and then the solution was heated up to reach the critical point for CO_2 and the gas slowly released until the samples were completely dry. Finally, the glass samples were sputter-coated with a carbon layer (ACE 200, Leica, Germany) to be imaged by SEM.

5.3.2 *Cryo-SEM*

Transfer of AuNPs into polyacrylamide hydrogels (see Section 3.1.2) was analyzed by cryo-SEM. Therefore, samples were mounted in a liquid nitrogen-cooled stage and transferred to a freeze fracture system (EM BAF060, Leica, Germany). Here, samples were heated slowly to -90 °C, kept in vacuum for 45 min to sublimate the water at the interfaces, and coated with carbon. Samples were further shuttled via an evacuated liquid nitrogen-cooled shuttle (VLC 100, Bal-Tec, Lichtenstein) into the Cryo-SEM (Ultra 55 FE-SEM, Zeiss, Germany), where imaging was conducted at low-temperature conditions (T = -130 ± 5 °C) and low acceleration voltages of 1 - 1.5 kV because of the low conductivity of the samples with a working distance of 3 mm [156].

5.4 MALDI MASS SPECTROMETRY

For the matrix-assisted laser desorption/ionization (MALDI) matrix, a 10 mM solution of 2,5-dihydroxybenzoic acid (DHB) was prepared in tetrahydrofuran (THF) supplemented with 0.1 M NaCl as cationization agent. Products were dissolved in THF and mixed with an equal volume of the DHB matrix. 2 µl of this mixture were added to each well on the MALDI plate and allowed to dry for 20 min before being analyzed by a high performance MALDI time-of-flight mass spectrometer (Voyager-DE STR, Applied Biosystems, UK).

5.5 IMAGE PROCESSING AND DATA ANALYSIS

Fluorescent images were processed using Fiji software (Fiji is just ImageJ, version 1.51n, http://imgej.nih.gov/ij). Brightness, contrast and lookup tables (LUTs) of microscopy images were adjusted for the presentation. The software was furthermore used to determine nanoparticle distances in SEM images and measure the projected cell area in brightfield images. Distances between a gold nanoparticle and

its k-nearest neighbors ($k = 6$ for ordered nanostructures, $4 < k < 8$ for disordered nanostructures) for at least 300 particles of 2 individual nanostructures per condition have been evaluated.

5.5.1 *TFM Analysis*

Classical TFM images were processed in Fiji to register the bead images with and without cells with the plugin MultiStackReg [209]. PIV and FTTC were conducted with a custom written software in python by Dimitri Probst in the group of Prof. Ulrich Schwarz (Heidelberg University).

5.5.2 *MTFM Single-Molecule Analysis*

For the analysis of fluorescent signals from single molecular tension probes, TIRF images were analyzed with a custom written program in Matlab by Klaus Yserentant and Felix Braun the lab of Prof. Dirk-Peter Herten (Heidelberg University). First, a binary mask from the maximum projection of the virus particles was created by a particle tracking algorithm. Additionally a mask of the cells was manually created from background fluorescence in the AP2 channel. Underneath each particle the trace of the fluorescence intensity over time was corrected by the local background for each channel. Traces of the tension probe channel were manually evaluated for events with an increase in fluorescence corresponding to the opening of a tension sensor. Traces of the AP2 channel were analyzed for recurrent recruitment of AP2 with $n \geq 3$.

5.5.3 *Analysis of Tearing of Immobilized Viruses*

Confocal images of fluorescent viruses and nanoparticles were analyzed with a custom written particle tracking algorithm by Dr. Kota Miura (Network of European Bioimage Analysts, Heidelberg) in Fiji. Therefore time-laps image series were preprocessed with the plugins MultiStackReg, bleach correction and median filter with 1 pixel radius. All particles underneath the projected cell area 1 h post seeding were considered in the tracking. This underestimates the relative number of torn off viruses in the first frames, when the cell did not yet cover the whole area or in later frames, when cells are migrating outside the area. However, due to variability between the cells and the different conditions tested, this proved to be the most robust approach. The remaining particles in this area were normalized over time to those particles present in the first 2 frames. Thereby any tearing events, that happened during the first 40 min after cell seeding were neglected. Relative numbers of remaining particles underneath

each cell were plotted individually and fitted with a two-phase decay function as discussed in section 7.4.

5.5.4 *Statistics*

All data have been plotted and analyzed in Prism (GraphPad Software, USA). Column graphs are shown as the mean ± SD. Box plots are shown as min, max, 25th and 75th percentile and median. Significance was evaluated by unpaired t-test or one-way ANOVA, where more than two groups were compared. p-values less than 0.05 were considered as statistically significant.

Part III

RESULTS AND DISCUSSION

In the following, I will first present the results obtained for forces applied by single integrin receptors, and how this force load is instrumentalized by cells to sense extracellular ligand spacing. In the second part I will elucidate the forces exerted by cells on single viruses and nanoparticles.

6

FORCE LOAD ON SINGLE RECEPTORS

6.1 SENSING OF EXTRACELLULAR LIGAND DENSITY

In order to mimic the biophysical parameters of the extracellular matrix while accessing the traction forces exerted by cells, I created PAA substrates equipped with fluorescence marker beads for TFM and a gold nanoparticle array for differently spaced extracellular ligand presentation.

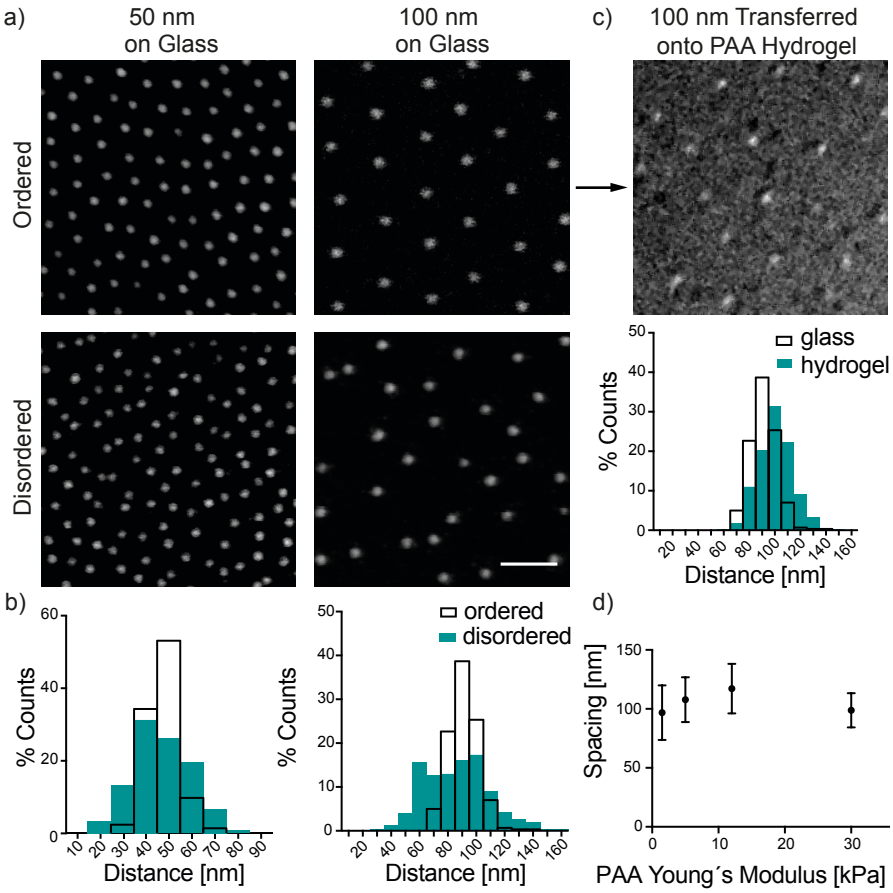

Figure 6.1: AuNP patterns for ordered and disordered nano-spaced ligand presentation. a) SEM images of BCML-derived AuNPs on glass were obtained at 100,000x magnification. Scale bar = 100 nm. b) Histograms of the distances to the nearest neighbors ($4 \leq k \leq 8$) as determined in ImageJ. c) Cryo-SEM analysis of the nanostructures after transfer onto hydrogels revealed an increase of the mean distances of ~15 %, which did not significantly differ among hydrogels with varying rigidities (d).

First, I produced the arrays of gold dots on glass, either in an ordered or in a disordered manner to dissect the effect of ligand density vs. nano-spacing for the clustering of cell adhesion receptors. Therefore, nanopatterns with an interparticle distance of ~ 50 nm or ~ 100 nm have been produced by BCML (see Section 3.1.1) and imaged via SEM (see Figure 6.1 a). Analysis of the ordered structures revealed mean distances of (47 ± 6) nm / (91 ± 11) nm and for disordered (47 ± 12) nm / (88 ± 32) nm, respectively (see Figure 6.1 b). After transfer of the gold nanoparticles onto PAA hydrogels via a bis-(acryloyl)cysteamine crosslinker, gels were allowed to swell for 72 h, which increased the interparticle distance by ~ 15 % to (100 ± 13) nm for the 100 nm ordered structures. The effective spacing was found to be independent from the rigidity of the substrate (Figure 6.1 d).

6.1.1 *Adhesion size depends on substrate rigidity and nano-patterned ligand presentation*

Next, thiolated ECM ligands, namely cRGDfK or GFOGER, have been immobilized on the AuNPs to achieve control over the distribution of ligands in the nanometer range. While more than one ligand can bind per AuNP, just one integrin receptor will be able to interact with each particle owing to steric hindrance [41, 43]. This results in an effective ligand spacing, which is dictated by the gold nanopattern. Different human and mouse cell lines or primary cells were used as model system to access their response to varying rigidity and differently spaced ligands by fluorescence microscopy in the lab of Prof. Pere-Roca Cusachs (IBEC, Barcelona) [156]. As expected, on very soft (1.5 kPa) substrates only small nascent adhesions formed (results not shown). On hydrogels above 5 kPa, focal adhesion formation was observed. However, unlike on stiff glass substrates, FAs formed for both: 50 nm and 100 nm spaced ligands. In contrary to previous studies [41, 102, 103], and reversed to the observation on glass, an increased receptor spacing even promoted the growth of FAs (see Figure 6.2). Interestingly, a disordered ligand distribution with the same average distances further increased adhesion growth.

An increase in the substrate rigidity also increased the FA size and total traction forces. However, adhesions seemed to collapse over a certain threshold rigidity where again only minor adhesions have been observed. This threshold rigidity was found to be 30 kPa for 100 nm and 150 kPa for 50 nm spaced ligands, respectively. For disordered ligand distribution this collapse occurs at lower rigidity thresholds but again an inverted behavior of focal adhesion size and ligand spacing was observed above 100 kPa compared to the lower rigidity regimes (Figure 6.2).

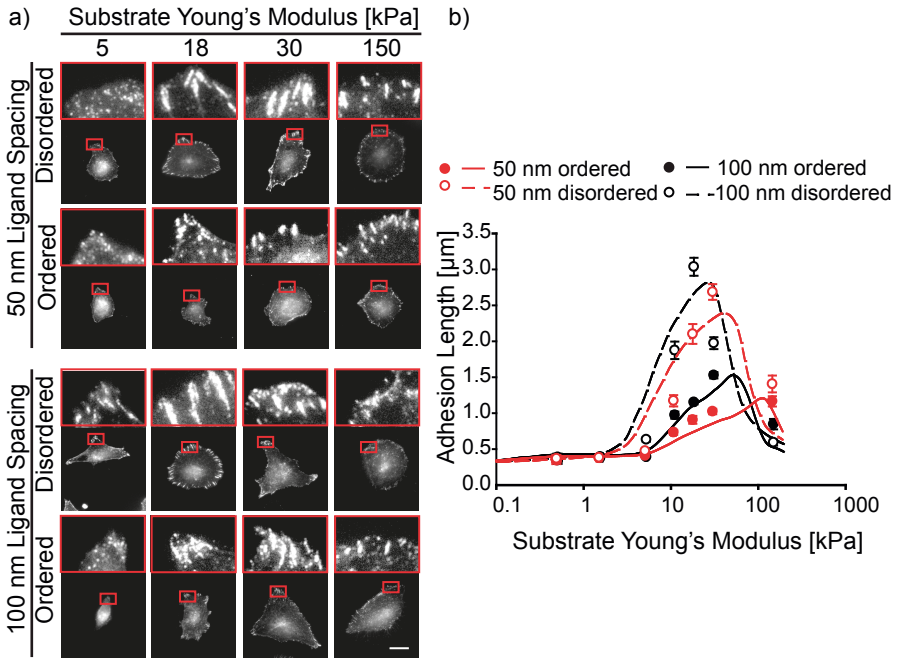

Figure 6.2: Fluorescence image analysis of FA length on nanopatterned ECM ligands on hydrogels. Human breast myoepithelial cells were seeded on PAA hydrogels ranging from 5 kPa to 150 kPa with 50 nm or 100 nm spaced cRGDfK ligands for 1 h. a) Staining of phospho-paxillin positive adhesions was analyzed for the length of FAs in $\geq$ 10 cells per condition. Scale bar = 20 µm. b) Experimental average values (data points $\pm$ SD) and corresponding model predictions (lines, cf. Section 6.1.3) for adhesion length. Differences between ordered and disordered conditions were significant ($p < 0.05$). Adapted from [156].

6.1.2 *Traction forces increase non-linearly with increasing substrate stiffness*

Total traction forces of myoepithelial cells on the nanopatterned hydrogels have been accessed by TFM in the lab of Prof. Pere-Roca Cusachs [156]. We found, as observed in previous studies [210–212], that tractions increase with increasing substrate rigidity (see Figure 6.3). However, this dependence is not linear. After an initial increase, traction forces reach a plateau or even slightly decrease at $\sim 5 - 10$ kPa, followed by another increase with increasing stiffness. At the threshold stiffness, where a collapse in adhesion size was observed, also traction forces level-off and are expected to collapse likewise. However, tractions on substrates with Young´s moduli higher than 30 kPa are not accessible by TFM since the deformations are too small to be resolved with standard fluorescence microscopy. Again, the increased ligand spacing promoted adhesion and thus higher traction forces have been observed at intermediate rigidities. Also an

increase of tractions can be noted with the disordered ligand distribution.

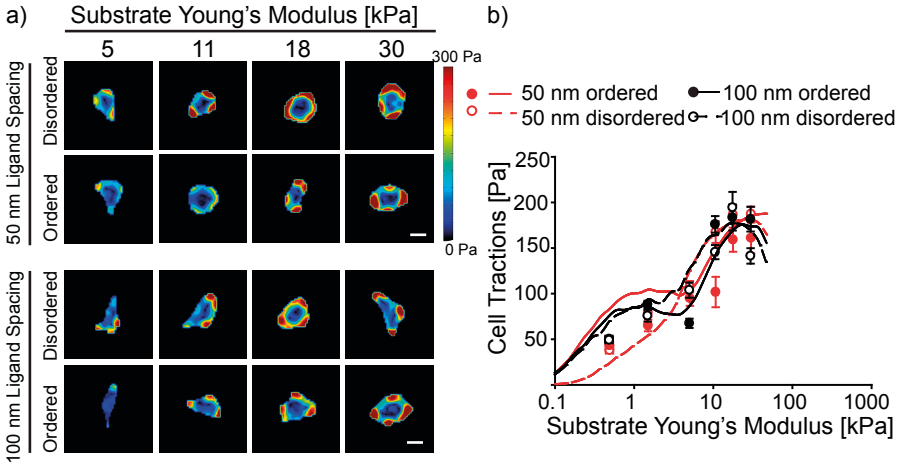

Figure 6.3: Traction forces of myoepithelial cells depending on ligand nanodistribution and substrate stiffness. a) TFM experiments on hydrogels ranging from 5 kPa to 150 kPa with 50 nm or 100 nm spaced cRGD ligands. Scale bar = 20 µm. b) Experimental average values (data points ± SD) and corresponding model predictions (lines) for cell tractions. Adapted from [156].

6.1.3 *Molecular Clutch Model Predicts Force Load on Individual Integrin Receptors*

These results are incompatible with the idea of a molecular ruler defining the optimal ligand density as suggested in previous studies [42]. Even considering the deformation of the elastic substrates and thus variety in the ligand spacing would not explain why FAs grow bigger on larger spaced ligands / on randomly spaced ligands with similar mean density on elastic substrates between 1 and 100 kPa. A regulation via the force load per integrin molecule as earlier suggested theoretically [213–215], on the other hand, can explain the observed behavior. Therefore, we extended and experimentally confirmed the molecular clutch model, which was first suggested 1988 by Mitchison and Kirschner [216]. Integrins couple extracellular proteins to the actomyosin-driven force generating machinery via molecular clutches. The more integrins bind, the less force is loaded per individual molecule, which influences the binding kinetics of integrins according to Bell´s model (see Section 1.3).

In my set-up the adhesion sites are the AuNPs with immobilized cRGD ligands that are coupled to the elastic substrate, which is modeled by springs with a force constant k_{sub} to the substrate and springs that couple the ECM ligands to each other with k_{link} (see Figure 6.4). The binding rates k_{on}/k_{off} between integrins and their ligands are further influenced by the catch bond behavior of integrins under ten-

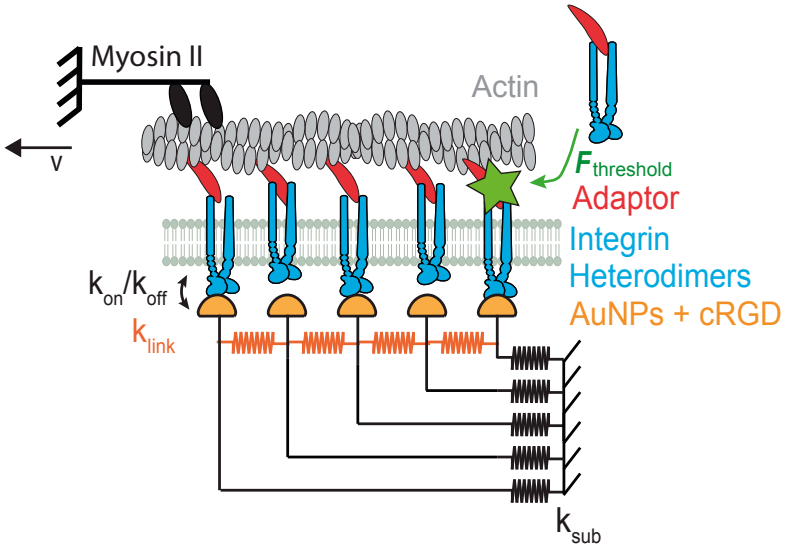

Figure 6.4: Schematic of the adjusted molecular clutch model. Myosin II motors (black) pull on actin filaments (gray) with a velocity v, which exerts a force on a set of parallel clutches formed by adaptor proteins (red) and integrins (blue). They dynamically bind and unbind cRGD ligands (yellow) with the corresponding binding rate k_{on}/k_{off}. Mechanosensitivity is introduced in the model by setting a force threshold $F_{threshold}$ in each clutch that triggers further integrin recruitment when surpassed (event symbolized by green star). The elastic substrate is represented by springs connecting ligands to the substrate (k_{sub}, black) and to each other (k_{link}, orange). Adapted from [156]. For details see table A.1.

sion. Above a certain threshold force $F_{threshold}$, which was adjusted to 87 pN in our model, the adaptor protein talin unfolds. In single molecule experiments talin was found to unfold at $29 - 51$ pN, which opens cryptic binding sites for vinculin [217, 218]. Vinculin binding in turn leads to further adhesion growth and YAP translocation (likely via vinculin-actin binding). Thus, the higher the force load on an individual integrin receptor induced by stiffer substrates and/or larger ligand spacings, the more likely talin unfolds resulting in adhesion growth. Mathematical details and model predictions were calculated by Jorge Escribano in the lab of Prof. José Manuel García-Aznar (University of Zaragoza) and the parameters are listed in the appendix A.1 [156]. For each ligand, its force F_i and the displacement from rest position x_i were calculated as follows:

$$F_i = k_{sub}x_i - k_{link}(x_i - x_{i-1}) + k_{inkl}(x_{i+1} - x_i) \tag{6.1}$$

This nicely predicts the observation of FA growth and traction forces on elastic substrates with differently spaced ECM ligands (Figure 6.2 and 6.3, lines represent modeling data). When the substrate gets too stiff or ligand spacing too high, the increased force load per molecule cannot be compensated by further integrin recruitment and

the adhesion collapses. This was considered in the model with a maximum integrin density $d_{int,max}$ based on the physical limit in integrin packing and size restriction to the radius of FAs a.

6.2 COMPARISON OF GLOBAL TRACTION FORCES AND LOCAL SINGLE RECEPTOR FORCE LOAD

The here developed molecular clutch model suggests that the distribution of forces amongst individual integrin heterodimers is important for the cell to sense extracellular ligand spacing as well as the rigidity of the substrate. By classical TFM, however, the force load per single receptor can only be estimated from the ensemble measurement. I therefore combined classical as well as reference-free TFM with MTFM, which is capable of measuring forces transduced by individual receptors. This allows further to cross-validate the results obtained from these two state-of-the-art techniques in mechanobiology and I could show, for the first time, the force distribution on individual integrin heterodimers in cells growing on soft substrates.

6.2.1 *Molecular Tension Fluorescence Microscopy*

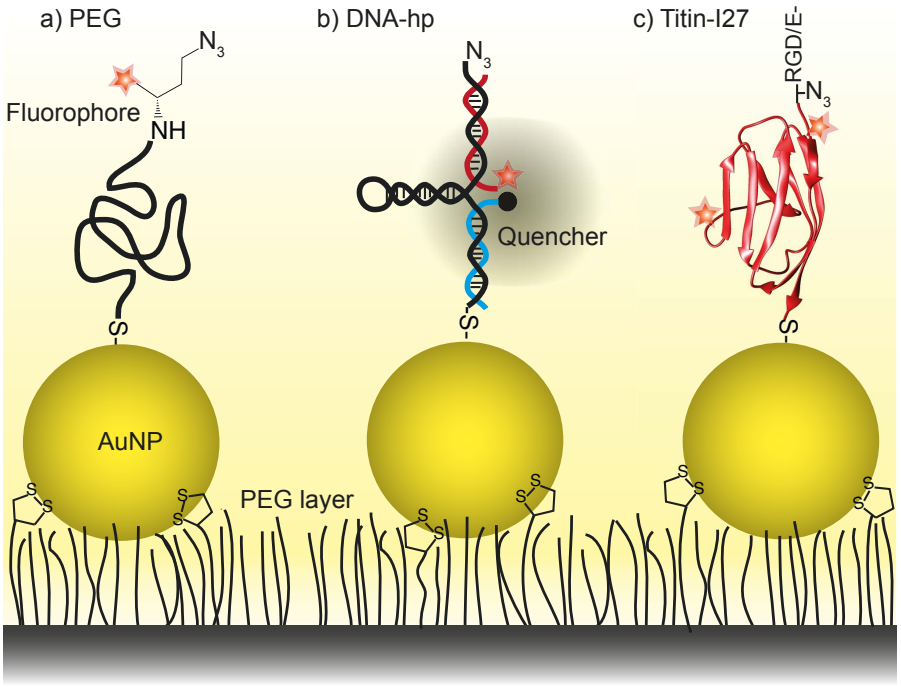

Figure 6.5: Schematic of the molecular tension probes used in this thesis. A self-assembled PEG layer presenting thiol functions was formed on glass substrates. 9 nm AuNPs (yellow) were trapped on top and a) PEG-based, b) DNA-hp-based or c) Titin-based tension probes were immobilized via their thiol-functions. Ligands bearing an alkyne function have been clicked to the top via CuAAC.

In this study, I employed molecular tension probes based on either PEG [79], DNA-hairpins [97] or titin-linkers [51] as depicted in figure 6.5. I changed the design of the molecules compared to these previous studies towards modular tension probes, capable of bearing different types of ligands. Therefore, I introduced an azide-function at the upper end of the tension probes, which can be addressed in a bio-orthogonal CuAAC. This allows to access forces transduced by integrins and other cellular receptors on single binding motives (such as RGD) as well as whole virus particles (see Chapter 7) that have been modified with alkyne functions. First, I characterized the functionality of the newly developed molecular tension probes on glass substrates, before transferring them on PAA hydrogels.

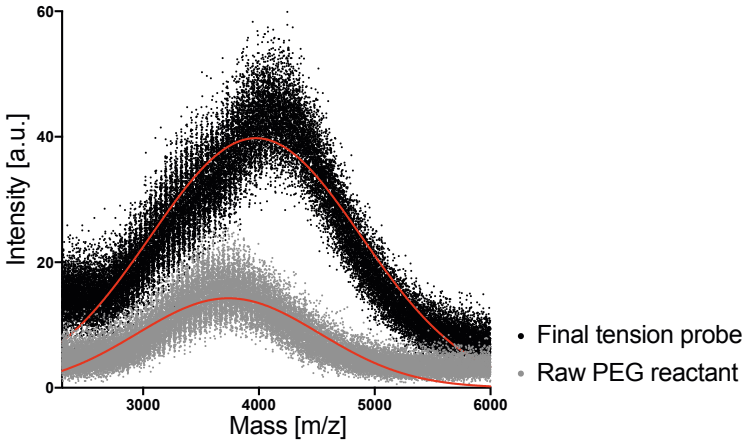

Figure 6.6: MALDI-TOF analysis of PEG-based tension molecule. The shift in the mass spectra from the raw PEG reactant (grey) to the final PEG-based tension probes (black) was quantified by gaussian fits (red).

The PEG-based tension probe was synthesized according to section 3.3.3 and analyzed by MALDI-TOF (see Figure 6.6). The long PEG species thiol-PEG(3000)-NHS, which was used for the synthesis, has a mean mass distribution of $m/z = 3737 \pm 788\,g/mol$. After coupling of the intermediate tension probe product (L-Aha-butan-1-Cy3B), the mass spectra shifted to $m/z = 3979 \pm 910\,g/mol$. Although the fitted gaussian curves are not significantly different from each other because of the broad distribution of molecular weights of the PEG species, a successful coupling was proven by their functionality. PEG-based tension probes were mixed with AuNPs and immobilized on a glass substrate and subsequently cRGD-alkyne was clicked on top. However, binding to the AuNPs as well as coupling of the adhesive ligand via click reaction was sterically impaired due to their mushroom confirmation in rest state. This resulted in a low binding efficiency and thus low signal-to-noise ratios in experiments with BSC1 cells growing on the substrates (see Figure 6.7 a).

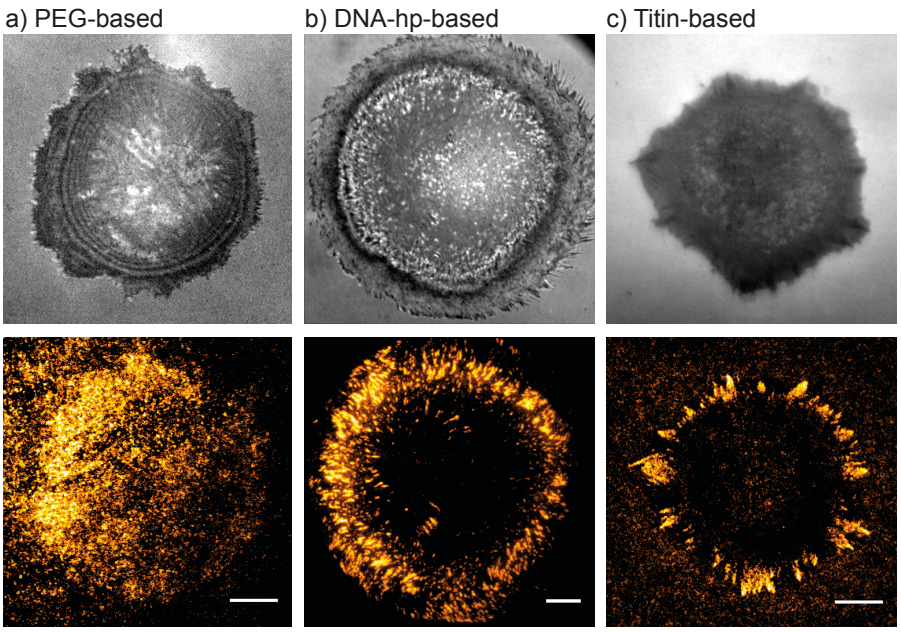

Figure 6.7: Characterization of molecular tension probes on glass substrates. Representative interference reflection images (upper row) and fluorescence wide-field images (lower row) of BSC1 cells on a) PEG-based and b) DNA-hairpin-based (12 pN) tension probes and REF cells on c) titin-based tension probes. The sensor molecules were incubated on glass substrates with randomly immobilized AuNPs as anchor points and fluorescence quencher. cRGD-alkyne was clicked on a) and b) and RGD was co-presented on titin in c) as ligand for integrin binding. Images were recorded 1 h post seeding in culture medium containing 0.5 % FBS. Scale bars = 10 µm.

DNA-hairpin based tension sensors are available with discrete opening forces between $4 - 19$ pN. Here, "19 pN hairpins" have been used, which provide a fluorescence tension map of the adherent cells at 37 °C, where integrins have exceeded the opening force of 19 pN (see Figure 6.7 b). Again cRGD-alkyne was clicked directly to the force transmitting strand by CuAAC. The signal-to-noise ratio of these tension probes was the best compared over the other tension molecules possibly due to this digital behavior and good accessibility of the azide-function on top of the protruding DNA-probe for ligand binding. Further, I applied a double quenching mechanism, which was achieved by (i) an organic dark quencher molecule (QSY21), which acts as FRET acceptor of the StarRed fluorophore and (ii) by the gold nanoparticle via NSET (cf. Section 1.4.2).

The titin-tension probe was expressed such that it contains a RGD sequence for integrin binding. Thus no further step is necessary for the coupling of a ligand. The I27 domain of titin is mechanically more stable than the entropic PEG- or digital DNA- probe. Hence, only strong cells such as fibroblasts are capable of opening the probe within the time-course of a typical experiment (< 2 h), where non-

specific opening events can be neglected. The quenching efficiency is limited by the random labeling of titin with Alexa647-NHS. By photocounting of the bleaching steps of single titin-based tension sensors in fluorescence imaging I quantified the number of dyes per sensor to be mainly one or two (see Figure A.1). Attached to the upper end, the fluorophore might be already too far away ($\geq$ 7 nm) from the quenching gold nanoparticle in resting state, or, when attached to the lower part of the I27 molecule, no strong increase in fluorescence is expected upon opening. However, a clear fluorescence signal was observed at focal adhesion sites in REF cells (see Figure 6.7c).

To conclude, for applications where low forces are expected, such as on soft hydrogels, DNA-based tension probes are preferred for their bright and specific signal. For cells exerting higher forces titin-based tension probes were chosen, while the PEG-based tension probes were omitted for further experiments due to their low signal-to-noise ratio.

6.2.2 *Combination of Molecular Tension Fluorescence Microscopy and Traction Force Microscopy*

For the combination of MTFM with TFM, AuNPs were transferred onto PAA hydrogels as described before (see Section 3.1.2 and 6.1). However, I observed a very low binding efficiency of the molecular tension probes, which might be related to buried AuNPs or oxidation of the gold in the hydrogels during the swelling process. To improve the binding affinity, I therefore applied electroless deposition of gold(III)chloride trihydrate, which grows the existing gold particles and increases their reactivity towards thiols. A visual change from colorless-translucent hydrogels to purple-red was observed due to an increase in plasmon absorption (see Figure 6.8 b). Structural analysis by SEM revealed a mean diameter of (11 ± 1) nm for AuNPs on glass, which were transferred and grown to (16 ± 4) nm diameter. Notably, not all AuNPs on the hydrogel were increased in size. Potentially, the remaining originally-sized particles were shielded by the swollen hydrogel and thus did not respond to the electroless deposition. However, the resulting density of ~500 grown particles/µm² proved to be sufficient for MTFM.

Next, molecular tension probes have been incubated on the hydrogels (see Section 3.3). Because of their high signal-to-noise ratio and low force regime, DNA-hp probes up to 19 pN have been used. An increased concentration of DNA-hairpins of 900 nM was used compared to the control experiments on glass substrates (300 nM), to increase the fluorescence signal on the hydrogels.

REF cells seeded on the samples for 2 h exerted clearly visible forces on the hydrogels as observed by 1.) the deformation of the hydrogel visualized by fluorescent beads and 2.) an increase in fluorescence

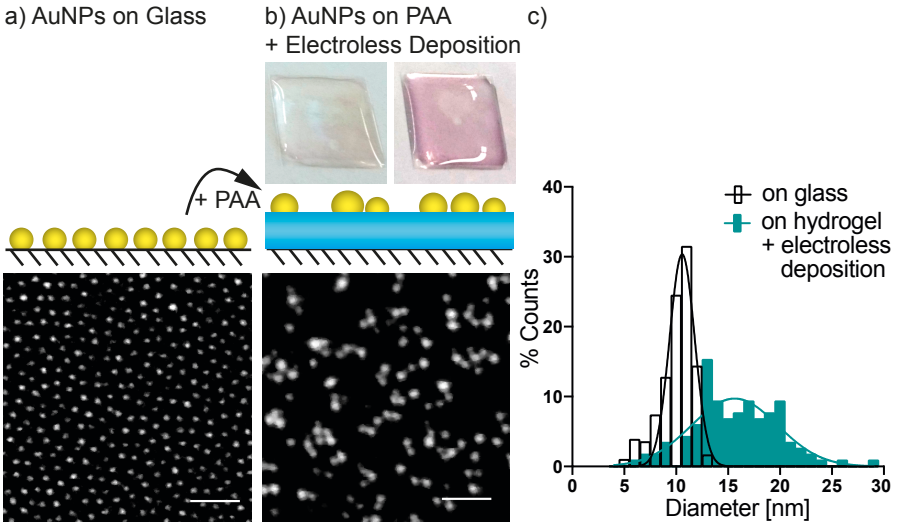

Figure 6.8: Transfer and growth of AuNPs on PAA. A visible change in absorption of the hydrogels from colorless to pink occurred upon increasing the size of the AuNPs (b, $2x2\,cm^2$hydrogels). SEM images of AuNPs on a) glass and b) on PAA hydrogels with electroless deposition of gold to enlarge the particles. Scale bars = 100 nm. c) Histogram of the size distribution of AuNPs with gaussian fits resulted in mean particle diameter of (11 ± 1) nm on glass and (16 ± 4) nm after transfer and electroless deposition on PAA.

underneath the cell from opening of the 12 pN tension probes (see Figure 6.9). After taking an image cells were removed by trypsination, the gel relaxed and a reference image was acquired. Tractions were reconstructed from the deformation of the hydrogel by PIV and FTTC algorithm (see Section 5.5.1). The results are displayed as a heat map distribution of tractions (see Figure 6.9), clearly depicting peripheral tractions with absolute stress values up to 2.7 kPa.

Analysis of the fluorescence intensity signal of the DNA-hp sensors, on the other hand, was conducted by subtraction of the background signal obtained from the reference image. The result is displayed in figure 6.9 g. In contrast to the tractions reconstructed by TFM, a relatively homogeneous increase in fluorescence was observed underneath the cell. This evenly distributed forces exceed the opening force of 12 pN for the DNA-hp probe. This resembles the behavior of integrins outside focal adhesions, which Wang et al. observed with the use of $12 - 54$ pN TGT-DNA sensors on glass substrates [50]. Interestingly, after trypsinization of the cell, empty spots remain in the image at sites of cell-surface interactions, presumably FAs (see Figure 6.9 f). Integrins within FAs have been reported to exert forces as high as 110 pN [51], which may have led to DNA rupture and thus removal of the DNA-bound fluorophore in these areas. The global distribution of integrins underneath the adhesion area of the cell bearing at least 19 pN suggests that this force is not high enough to initiate the

reinforcement through adhesion growth which is leading to focal adhesion formation. In fact, the threshold force that was defined in our molecular clutch model is 87 pN (cf. Section 6.1.3). Hence, unless this threshold force is reached, no FA formation is expected.

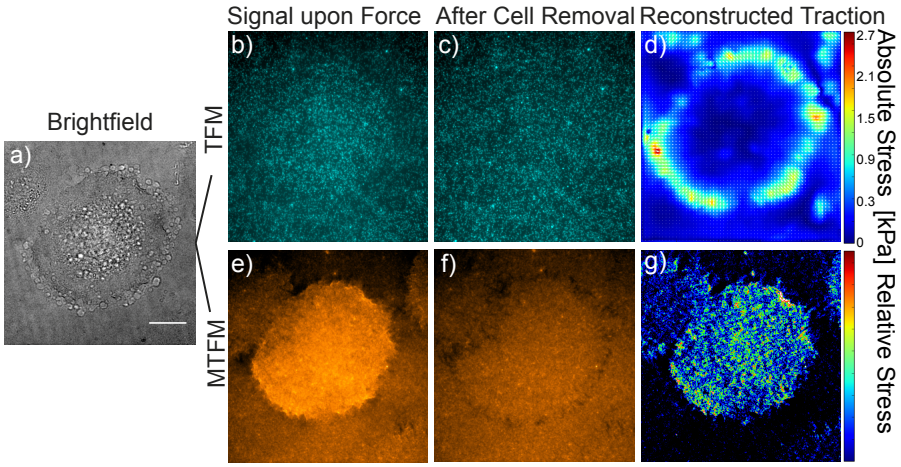

Figure 6.9: Molecular tensions probes differ from TFM in force. DNA-hp tension probes with an opening force of 12 pN (e and f, for MTFM) were attached via an array of AuNPs on top of 12 kPa PAA hydrogels with embedded fluorescent marker beads (b and c, for TFM). REF cells were seeded in culture medium containing 0.5 % FBS for 2 h and removed by trypsinization. Images were recorded with an inverted wide-field fluorescence microscope, analyzed in ImageJ (g) and with a FTTC algorithm in Python (d). Scale bar = 20 µm.

When comparing the tractions obtained by classical TFM to the molecular force data from MTFM, one has to consider the directionality of the force. A two-dimensional analysis of the bead displacements only takes the projection of forces in the xy-plane into account, while the direction of the force with currently available tension sensors cannot be determined. The difference in the distribution of the observed forces is thus very likely linked to different directionalities and hence, a well resolved three-dimensional analysis of bead displacement becomes indispensable for future studies. Further, the possibility should be excluded, that the increase in the fluorescence signal of force sensors underneath the cell might stem from local enrichment of background fluorescence due to the deformation of the substrate. In an ongoing work, I therefore restricted the tension probes to particularly small sites, which cannot be deformed. As described in the outlook (cf. Chapter 8), I applied molecular tension probes on substrates with micropatterned gold arrays in order to combine MTFM with confocal reference-free TFM.

7

FORCES DURING VIRUS PARTICLE UPTAKE

Forces transduced via integrin receptors are not limited to cell adhesion but they play a role in mechanosensing and possibly also during virus particle uptake, where integrins serve as specific receptors [219]. To highlight the role of forces during endocytosis I applied, for the first time, whole infectious reovirus particles as ligands on molecular tension probes (Section 7.2). Therefore, I established a method to covalently and non-covalently bind reovirus particles to glass substrates allowing to characterize the early steps of endocytosis by fluorescence microscopy in unprecedented detail (see Section 4.4 and 7.1).

7.1 IMMOBILIZATION OF REOVIRUS PARTICLES

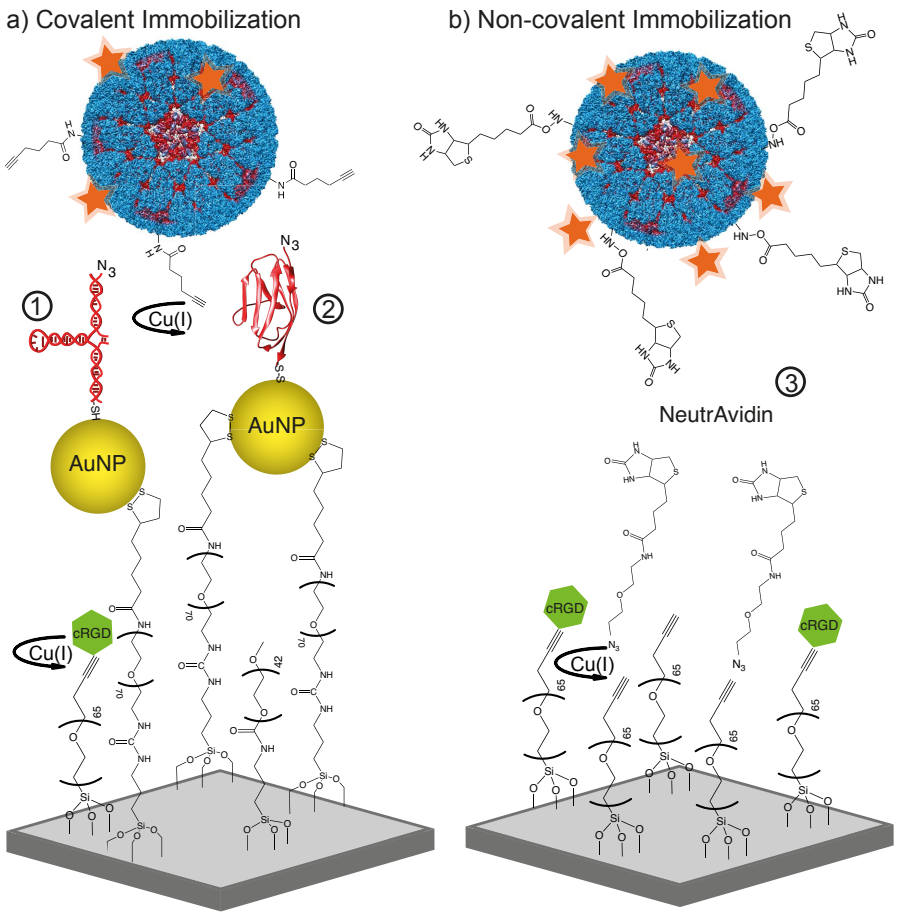

Figure 7.1: Schematic of covalent and non-covalent immobilization strategies for virus particles (not to scale). Blue: reovirus, orange: fluorophores, (1): DNA-hp probe, (2): titin probe, (3): NeutrAvidin.

As depicted in figure 7.1 a, covalent immobilization of reovirus on molecular tension probes was achieved via passivating glass surfaces with silane-PEG-methoxy, silane-PEG-alkyne and silane-PEG-lipoic acid, the latter binding AuNPs. DNA-hairpin-based or titin-based tension probes were attached to the AuNPs via thiol functions and alkyne-modified reoviruses were clicked by CuAAC to the azide function of the tension probes. Non-covalent immobilization (b) was achieved via passivation of glass surfaces with silane-PEG-alkyne and CuAAC of a biotin-azide linker. NeutrAvidin, which is the deglycosylated version of avidin, was incubated on the surfaces and unbound molecules were washed off before applying the biotinylated reoviruses. On both types of surfaces cRGD-azide ligands were clicked to the silane-PEG-alkyne to allow cell adhesion.

For detection and immobilization of the virus particles functional linkers were covalently bound to the viral capsid via NHS-amine reaction, namely Alexa568- or Alexa647-NHS for life fluorescence imaging, alkyne-NHS for covalent immobilization (cf. Figure 7.1a) and biotin-NHS for non-covalent immobilization (cf. Figure 7.1b). At

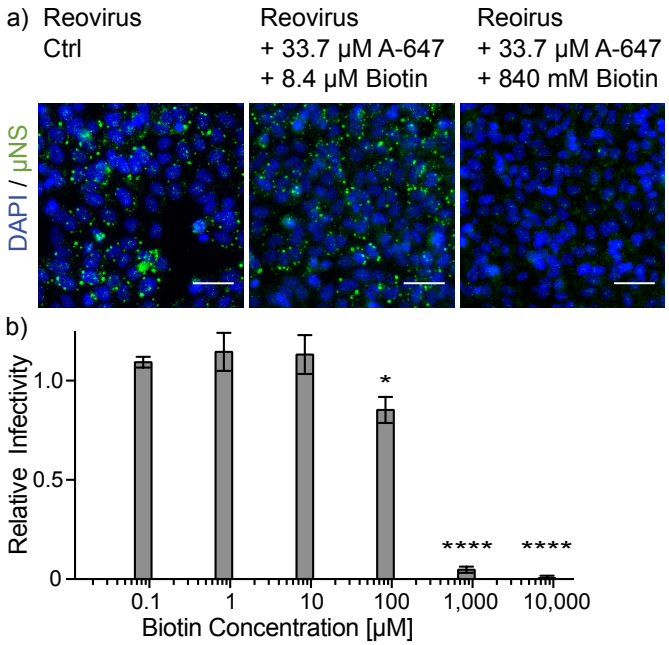

Figure 7.2: Infectivity of modified reovirus particles. Reovirus particles were labeled with Alexa647-NHS (A-647) at $c_{final} = 33.7\,\mu M$ and biotin-NHS (biotin) between 0 and 10 mM. a) HeLa cells infected with the indicated virus solutions were stained for reovirus infection with an antibody against the non structural reovirus protein µNS (green) and for cell nuclei with DAPI (blue) and imaged with wide-field fluorescence microscopy. Scale bar = 50 µm. Percentage of infected cells was normalized to the percentage of cells infected with non-modified virus (b). *, $P < 0.0376$ and ****, $P < 0.0001$ in comparison to non-modified virus infected cells.

moderate concentrations these modifications had no or a limited effect on the infectivity of the reovirus particles (see Figure 7.2). Reovirus infectivity was checked by application of $5 \cdot 10^5$ virus particles per cell on a layer of HeLa or BSC1 cells, incubation overnight, fixation and staining for reovirus infection. The number of infected cells was quantified for 3 individual cover glasses per condition in ImageJ and normalized to the percentage of cells infected with non-modified viruses. Above 42 µM final NHS concentration (33.7 µM Alexa dye + 8.4 µM biotin linker) a significant drop in the relative infectivity was observed. The indicated concentrations were therefore chosen for further experiments since they proved to be sufficient for imaging and stable immobilization but they did not significantly decrease the infectivity. Further, as shown by Fratini et al. [220] the conditions during CuAAC have only a limited effect on the integrity and thus infectivity of reovirus particles. Therefore, BSC-1 cells were incubated with Alexa647/alkyne-virus, which were pre-incubated for 2 h at RT with 1 mM $CuSO_4$ and checked for infectivity as described above (see Figure A.2).

7.2 MOLECULAR TENSION FLUORESCENCE MICROSCOPY ON SINGLE VIRUS PARTICLES

Until now, MTFM was used with a homogeneous layer of adhesion sites probing an array of integrins or other cellular receptors [76, 92]. Here, I utilized single reovirus particles as ligands on DNA-hp-based and titin-based tension probes. Since the concentration of virus particles produced with the described method (cf. Section 4.1) is much lower than the concentration of cRGD, only some of the tension probes will bear a virus particle. However, theoretically one virus can bind to several tension sensors on one or even different AuNPs because of the virus´ diameter of ~ 84 nm and its icosahedral structure. To prove the binding of individual virus particles to the tension probes on randomly immobilized AuNPs and their interactions with cells, I performed scanning electron microscopy. As clearly depicted in figure 7.3 b, covalent binding of reovirus particles to surface bound tension probes resulted in the presentation of individual virus particles. To allow integrin mediated cell adhesion, cRGD was covalently immobilized on the silane-PEG-alkyne in the AuNPs interspace. The snapshot of a cell in figure 7.3 a) proves the successful spreading and interaction with the surface. Further, the retracting plasma membrane that was captured in Figure 7.3 c) indicates interactions between cells and the immobilized reovirus particles (see arrow). The apparent connection on the marked virus might has been a linkage towards the cell, which was broken upon preparation of the samples for SEM. Since such connections have been observed for few virus particles only, it can be excluded that they are a result of the preparation process itself.

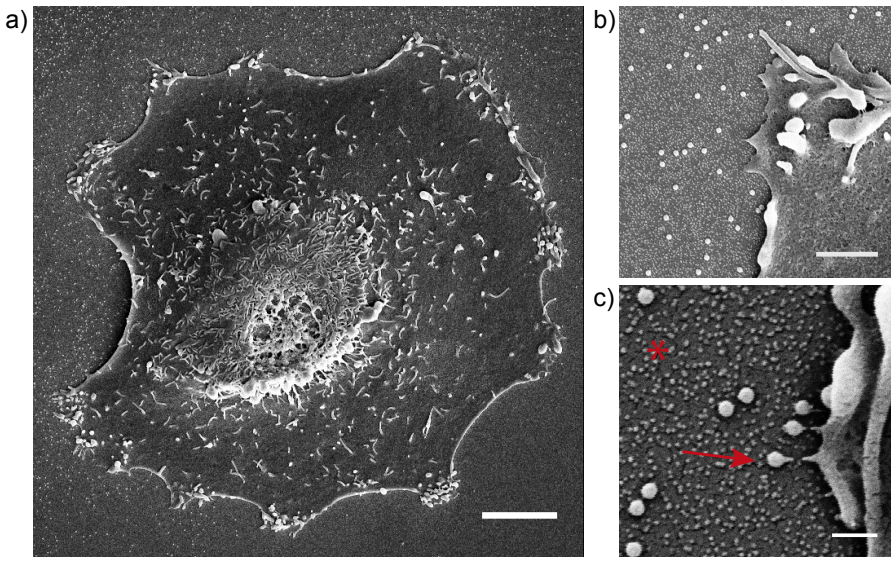

Figure 7.3: SEM images of cells on an array of tension sensors on gold nanoparticles, interacting with single virus particles. 9 nm AuNPs (c, asterisk) were covalently immobilized on glass as shown in figure 7.6. Surface-modified reovirus particles (c, arrow) were clicked and BSC1 cells were seeded on top for 1 h. Scale bars: a) 5 µm, b) 1 µm, c) 200 nm.

To be able to detect single fluorophores from the individual force sensors, TIRF microscopy was performed (see Section 5.2.3 for details). Further, the concentration of molecular tension probes had to be reduced compared to the ensemble measurements (see Section 3.3) to improve the signal-to-noise ratio. The reason for modifying the established protocol was the high background signal, consisting of not fully quenched or stochastically opened tension probes. To estimate the background fluorescence intensity, I quantified the number of AuNPs per diffraction limited area of ~3800 nm² (with $\lambda_{em} = 655$ nm for the StarRed dye and NA = 1.49) from SEM images to be ~ 20. For bulk MTFM experiments I further assumed values for the binding rate of ~ 8 tension probes per AuNPs and a quenching efficiency of ~ 95 % from literature [79, 97]. This results in a background fluorescence equalling ~ 8 activated tension probes, which makes it impossible to detect single tension probe signals.

Hence, for a successful combination of single virus particles with live cell imaging, I reduced the concentration of the tension probes to 300 pM for DNA-hp-based and to 3 nM for titin-based tension probes compared to the ensemble measurements. BSC1 and U373 cells stably expressing AP2-eGFP were seeded on the surfaces for 30 min. This allowed to follow clathrin-coated pit formation with respect to pulling events on single virus particles. Fluorescence time-lapse movies were recorded for 10 min per cell with a frame rate of 3 s of DNA-hp-sensor-StarRed or titin-sensor-Alexa647, reovirus-Alexa568 and AP2-eGFP (see Figure 7.4 a and 7.5 a).

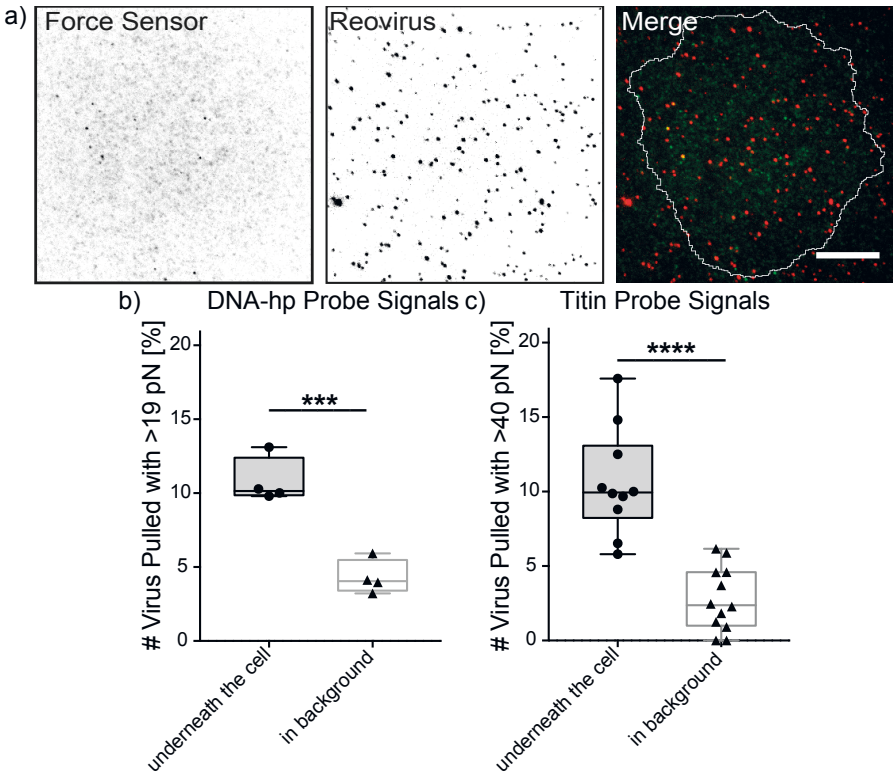

Figure 7.4: MTFM on single reovirus particles reported forces exceeding 40 pN. Single molecule MTFM with reovirus as ligands was performed on a TIRF microscope. a) Maximum projections of a 10 min time-lapse movie of a BSC1 cell spreading on the sensor surface. In the merged image the force sensor is depicted in green and reovirus in red. Scale bar = 10 µm. Quantitative analysis of the virus particles colocalizing with characteristic increase in the fluorescence of the force sensors. As control non-specific events in the background were quantified. b) Fluorescence signal of DNA-hp based tension probes corresponds to a force of 19 pN and c) of the titin-based force probe >40 pN, respectively. ***, $P = 0.0005$; **** $P < 0.0001$.

For the DNA-hp-based tension sensors with 19 pN opening force 11 ± 2 % of the virus particles underneath the cells ($100 - 500$ total particles per cell) were found to colocalize with fluorescent signal of the tension probes (see Figure 7.4 b). This suggests that ~ 10 % of the viruses are actively pulled by the cell with a force exceeding 19 pN within a 10 min time window. Interestingly, for the mechanically stronger titin-based tension probe, which takes $40 - 150$ pN to unfold, likewise 11 ± 4 % of the reovirus particles were pulled by the cell on average (see Figure 7.2 c). However, during these highly sensitive single-molecule experiments, some tension-sensors reported non-specific signals e.g. induced by misfolding, missing quencher-strands or non-specific opening from thermal fluctuations. Especially DNA-hps with lower opening force than 10 pN are unstable since the thermal energy at 37 °C is sufficient to induce unfolding and these tension

probes were thus excluded from the analysis (data not shown). To prove the specificity of the signal measured, I analyzed the colocalization of force signals with virus particles in the background without cells. Indeed, underneath the cells the force signal on virus particles was significantly higher (see Figure 7.2 b and c). These results suggest that cells can exert major forces of at least 40 pN on single reovirus particles from their basal side. Further, the higher mechanical resistance of immobilized virus particles with differently stiff tension probes does not impede with the frequency of pulling events. This indicates, that the forces measured are an inherent part of the uptake of virus particles and not induced by the immobilization and thus hindered uptake.

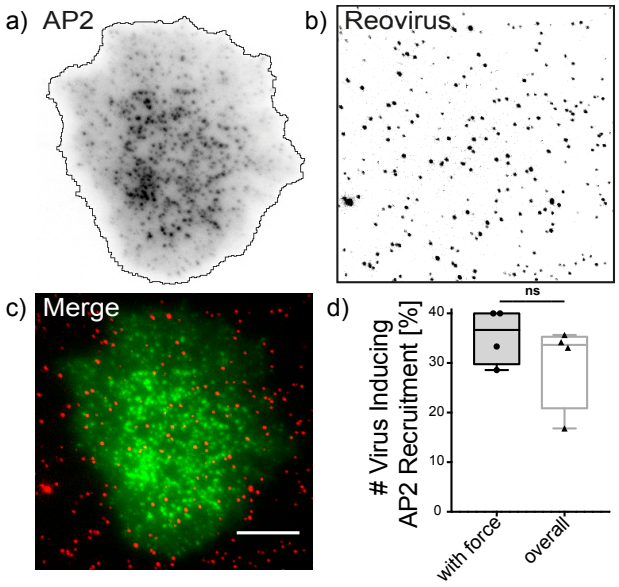

Figure 7.5: Colocalization of virus with AP2 and forces signals. Single molecule MTFM with reovirus as ligands was performed as shown in figure 7.4. a-c) Maximum projections of a 10 min time-lapse movie of a BSC1 cell spreading on the sensor surface. In the merge the clathrin adaptor AP2 is depicted in green and reovirus in red. Scale bar = 10 µm. d) Colocalization of viruses with AP2 was analyzed for recurrent recruitment of AP2 with regards to the signal coming from the force probes.

Next, I analyzed the colocalization and temporal consistency with clathrin-mediated endocytosis followed by AP2 clustering. Based on Fratini et al., covalent immobilization of reovirus induces a recurrent recruitment of the clathrin machinery above the virus particle. While clathrin coated pits form continuously on random spots all over the cellular membrane, CCPs on immobilized reovirus particles last on average 59 s and are recurrently recruited every 75 s [220]. Here, 30 ± 5 % of the virus particles underneath the cell induced such a recurrent colocalization with AP2, which is within the range that was determined for directly immobilized reovirus particles to glass

substrates without tension sensing molecules. However, no significant increase was observed for reoviruses that induced a force signal (35 ± 6 %, see Figure 7.5 d). Neither a temporal correlation between the force event and the first AP2 clustering could have been distinguished. These findings suggest that the observed forces do not induce neither are a result of CME, which is in line with the knowledge that CME is the main but not the only pathway for reovirus uptake [160, 169].

7.3 TEARING OF IMMOBILIZED REOVIRUS PARTICLES FROM GLASS SUBSTRATES

To follow the actual uptake of reovirus particles from the basolateral side, where cell-matrix interactions are established, reoviruses were simply deposited or non-covalently attached via biotin-NeutrAvidin to glass substrates (cf. 7.1). The latter immobilization method proved to be very specific since virus particles were exclusively observed on surfaces treated with NeutrAvidin, while passivated surfaces presenting only biotin and cRGD did not bear viruses. Further biotinylation of virus particles did not harm their infectivity (see Figure 7.2 a). This allowed me to study the dependence of particle uptake on specific receptors (cf. Section 7.5), the cytoskeleton (cf. Section 7.6) or different proteins of the endocytic machinery (cf. Section 7.7).

Intriguingly, I observed that BSC1, U373, HeLa and CHO cells, which were seeded on these surfaces, were strong enough to brake the NeutrAvidin-biotin bonds, rip off the viruses from the surface and internalize them resulting in viral infection of these cells (see Figure 7.6 c and d). To exclude the possibility that the biotin-NeutAvidin bond is destroyed by proteases rather than by force-induced dissociation, the matrix metalloprotease inhibitor GM6001 was added to the cells which did not prevent virus uptake (see Figure 7.6 e).

In contrast, covalently immobilized virus particles could not be removed by cells and thus did not cause viral infection (see Figure 7.6 a and b). Here, I passivated glass substrates with silane-PEG-azide and reovirus particles bearing alkyne functions were clicked in the lab of Dr. Steeve Boulant (Heidelberg University and DKFZ) analogously to experiments on tension probes (cf. 4.4.1).

This was a surprising observation since biotin-NeutrAvidin is a widely used immobilization technique for biological molecules and there has been only one report of unbinding upon cellular forces [52]. In single-molecule force spectroscopy experiments in literature rupture forces between 100 and 250 pN have been reported for the biotin-NeutrAvidin interaction [221]. However, it is of note, that the exact force depends on the loading rate and thus on the time cells are actually pulling on viral particles.

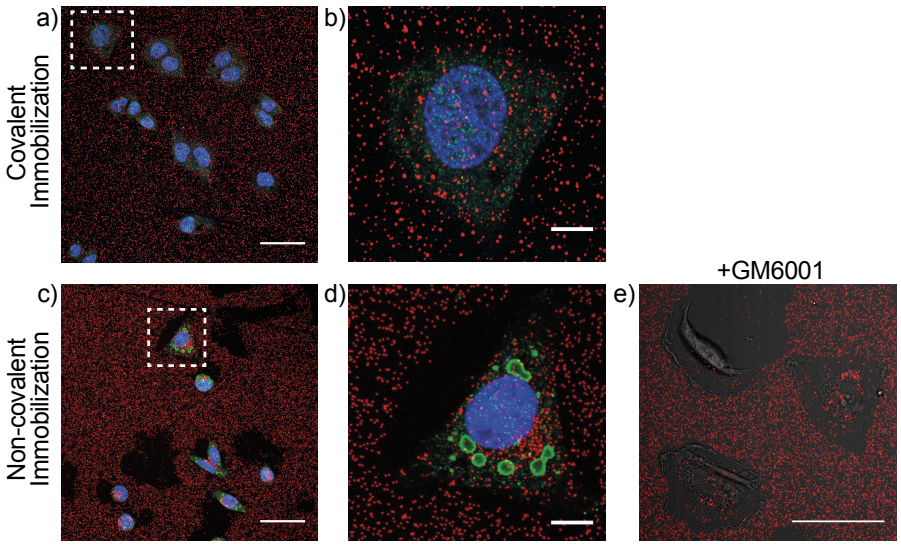

Figure 7.6: Cell interaction with viruses either covalently or non-covalently immobilized reoviruses on surfaces. a and b) Covalent immobilization of alkyne-modified reovirus particles (red) was achieved via CuAAC. c-e) Non-covalent immobilization of biotin-modified reoviruses (red) was mediated by NeutrAvidin. a-d) HeLa cells seeded on the surfaces for 16 h were stained for µNS indicating viral infection (green) and DAPI (blue). e) U373 cells (in brightfield, grey) pre-treated with 25 µM of the protease inhibitor GM6001 were imaged after 4 h. Scale bar = 50 µm and 10 µm in the zoom-in.

Since the cells are spreading and migrating on the samples, I estimated a minimum force using the interaction time between the cell and the particles, which was in the order of $\Delta t \approx 5$ min before virus tear off events were observed underneath the cell. Since the thermal energy is stochastically distributed among individual molecules, I further assumed that rupture of an individual bond occurs at 50 % probability (P) of unfolding and estimated the rate of unfolding k for a first order decay as follows:

$$P = 1 - e^{-k_{off} \cdot \Delta t} \Rightarrow k_{off} \approx 2.31 \cdot 10^{-3}\, s^{-1} \tag{7.1}$$

Applying now the Bell´s function (see Section 1.3, Equation 1.2):

$$k_{off} = k^0_{off} \cdot e^{\frac{F \Delta x}{k_B T}}$$

with the distance to the transition state $\Delta x \approx 0.5$ nm [55, 222], the temperature $T = 310.15$ K and the dissociation rate for single biotins from NeutrAvidin at zero force $k^0_{off} \approx 3.8 \cdot 10^{-4}\, s^{-1}$ [223], this corresponds to a force exceeding 15 pN. However, the real desorption rate constants for the biotinylated virus particles may vary dramatically from the values for dissociation rates found in literature. Depending on the analysis method used, dissociation rates for avidin and strep-

tavidin, which showed lower affinities to biotin compared to NeutrAvidin [53], are reported two orders of magnitude smaller [224, 225].

The sandwich-like targeting of a NeutrAvidin protein from 2 sides, which I applied here, might have a mutual influence on the respective desorption rates. Further, multivalent binding of up to 4 biotins per NeutrAvidin or even multiple NeutrAvidin adaptors per virus particle could significantly increase the immobilization stability. Hence, to obtain conclusive force values, the kinetics of virus uptake from the biotin-NeutrAvidin surfaces were analyzed by live fluorescence microscopy.

7.4 KINETICS OF TEARING VIRUSES FROM BIOTIN-NEUTRAVIDIN SURFACES

The herein presented method of analyzing the removal of non-covalently immobilized viral particles from a surface serves as direct force measurement for endocytosis by itself. This circumvents the difficulties of single molecule fluorescence imaging. Therefore, U373 and HeLa cells were recorded by live confocal microscopy 30 min after seeding on the surface with a frame rate of 5 or 10 min for up to 16 h. However, a strong phototoxic effect inhibiting endocytosis was observed in the first place. While most cells on the substrate teared off almost all viruses underneath their spreading area, those cells imaged overnight on the same substrate did not uptake any virus particles. However, their spreading and migrating behavior remained normal. To limit the photoxicity of live-cell imaging, reoviruses were labeled with Alexa647 instead of Alexa568 since the red excitation light is less harmful to cells. Therefore, imaging was conducted with the HeNe 633 nm laser only, omitting the GFP-signal for clathrin coated pits. A small percentage of the laser light was split and recorded with a transmitted light detector for bright field images of the cells (see Figure 7.7 a). The relative number of teared off virus particles underneath the full spread area of the cells (defined at 1 h post seeding) was analyzed with a particle-tracking algorithm developed by Dr. Kota Miura (Network of European Bioimage Analysts, Heidelberg) in Fiji.

Similar to the frequency of force events measured with the molecular tension probes, $10 \pm 5\,\%$ of viruses underneath U373 and $9 \pm 4\,\%$ underneath HeLa cells were teared off within 10 min (see Figure 7.7 b). Conveniently, due to the high stability of the biotin-NeutrAvidin bond very low percentage ($1.3 \pm 0.7\,\%$) of cell-independent unbinding events of reovirus from the surface have been observed during the 10 min movie in the background.

Since the concentration of viruses underneath the cells was reduced upon tearing and internalization, the data resembles a first order decay. This becomes obvious by plotting the relative number of viruses

remaining surface-bound over time (see Figure 7.7 c). However, the efficiency of tearing off viruses was not constant over time. This is likely due to the different phases cells are undergoing during spreading [226, 227]. During initial attachment cell-matrix interactions are established via integrins, which activates cell spreading. During this phase when cells have not reached their maximal spreading area yet, the observed tearing of virus particles was highest. Next, fast actin polymerization initiates the increasing contact area between the cell and the surface and the cell is spreading and polarizing upon external cues. Later, the membrane tension rises, Rho GTPases are activated and the cell is actively pulling and retracting the substrate to test the environment [228].

To account for the different behavior of the cells and the change in the cell-surface interaction area due to cell spreading and migration, I fitted a two-phase decay function with normalized initial concentration of virus particles $c^0_{virus} = 1$ and final concentration $Plateau = 0$, since complete uptake was observed after overnight incubation (see Figure 7.6):

$$c_{virus} = c^0_{virus} \cdot \left(\frac{Percent(I)}{100} \cdot e^{-k_I \cdot t} + \frac{Percent(II)}{100} \cdot e^{-k_{II} \cdot t}\right) \qquad (7.2)$$

The percentage of the phases I and II were optimized by the fitting algorithm, which allowed to take the individual spreading behavior of cells into account and their respective rates of tearing off viruses k_I and k_{II}. I further analyzed the rates for k_I, since the variation in the rates for k_{II} between the cells have been high due to the migration of cells outside of the detection area.

Surprisingly, the rate of uptake of biotin-NeutrAvidin immobilized virus particles on silane-PEG-alkyne-biotin/cRGD surfaces by HeLa cells was, with $k_{I,Biotin} = (1.3 \pm 0.7) \cdot 10^{-3} s^{-1}$, even higher than the rate of uptake of physisorbed reovirus particles, which were deposited on untreated coverglasses $k_{I,deposited} = (0.6 \pm 0.2) \cdot 10^{-3} s^{-1}$ (see Figure 7.7 c). It should be noted that the van-der-Waals and electrostatic interactions between the virus particles and the glass can also be considerably strong [128] since only a little number of particles were observed to dissociate cell-independently. Further, the biophysical properties of these two surfaces differ from each other regarding stiffness and specific ligand presentation for the cells and the observed differences in cell behavior might arise from this fact. However, it proves that the uptake of biotin-NeutrAvidin immobilized viruses is comparable to the uptake of non-specifically trapped viruses. In literature, there is a growing evidence that interactions between viruses and the ECM can also contribute to virus entry [229–231]. Moreover, I found that the number of reovirus particles internalized upon tearing from the basolateral side was similar to the percentage of reoviruses internalized from those adhering to the apical side when particles were applied in solution (see Figure A.4).

From the biotin-NeutrAvidin immobilized virus particles that dissociated cell-independently in areas without cells (background) during an overnight time-lapse experiment I derived the dissociation rate at zero-force $k^0_{virus} = (1.060 \pm 0.007) \cdot 10^{-5}\, s^{-1}$ by fitting a one-phase decay function with $Plateau = 0$. Taking these values into consideration for Bell´s function (cf. Section 7.3) one obtains a mean force of 41.2 ± 4.6 pN. The accuracy of the mean force strongly depends on the quality of the value for the distance to the transition state ($\Delta x \approx 0.5$ nm [222]) and on the assumption, that the force is applied along this direction. Further the kinetics of individual cells and the dissociation at zero force varied largely between single experiments. To account for this different behavior I analyzed all cells in the following experiments with respect to an internal control.

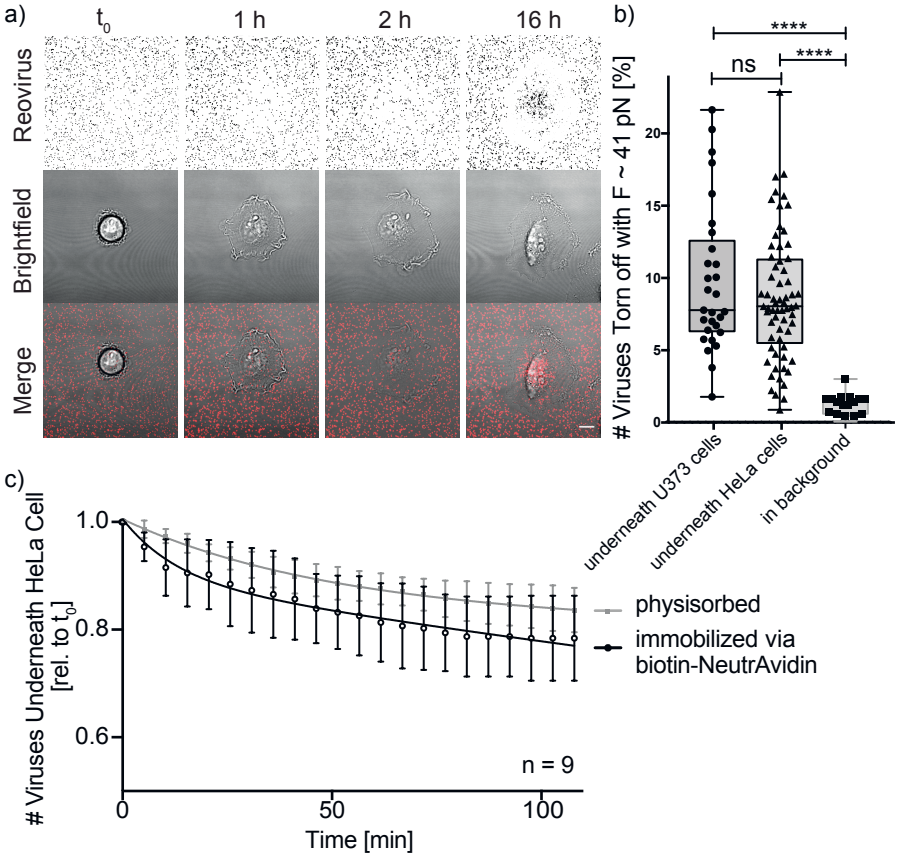

Figure 7.7: Tearing of non-covalently immobilized reovirus particles. U373 and HeLa cells were seeded on biotin-NeutrAvidin immobilized virus particles a) Confocal snap-shots of a HeLa cell (grey) spreading and tearing biotin-viruses-A647 (red) off the surface. Scale bar = 10 µm. b) The number of viruses torn off between 40 and 50 min after seeding. ****, $P < 0.0001$. c) Relative number of virus particles, either physisorbed on glass (grey) or immobilized via biotin-NeutrAvidin (black), underneath HeLa cells. Data are shown as mean ± SD and two-phase exponential fits (lines).

This is the first time such high forces have been observed for endocytic events at the basal side of cells. For the uptake of EGF and notch endocytosis 4 and 10 pN, respectively, were reported in literature [92, 184]. The herein obtained force might be higher due the larger size of virus particles, which lowers the energetic cost for membrane bending and their multivalency allowing multiple receptors to bind (cf. Section 2.2 and 2.3.1, respectively). Studies on the interaction between virus particles and the apical side of cells revealed values between $10 - 44$ pN [174, 181, 183] (cf. Section 2.5). However, these studies are limited to measure unbinding forces only and thus characterizing adhesion strength from viruses being externally pulled away from cells. Forces exerted by a cell itself on $4 - 20$ nm sized nanoparticles were reported to range from 39 up to 126 pN by means of AFM trace peak analysis [175–177]. Unfortunately, no studies on the forces applied on bigger particles that are comparable to reoviruses exist to date. Following the proportional relationship, much higher values would be expected for viruses of ~ 85 nm than the values derived from molecular tension probes and biotin-NeutrAvidin rupture analysis in the here presented work. One reason for the comparatively small forces observed during reovirus uptake could be the lower adhesion energy, which is gained from specific receptor binding compared to van-der-Waals forces all over the smooth nanoparticle surface (cf. Section 2.2). Further, the tracing and retracing speed in the above mentioned studies could have been of influence. In contrast, the method I established here allows to detect the force between living cells and single virus particles without externally probing their interaction. This method can be further extended to the use with inanimate nanoparticles as will be seen in section 7.5.4.

To test the contribution of 1) adhesion forces generated upon receptor binding, 2) pulling forces by the cytoskeleton and cell contractility, and 3) forces through an assembly of the endocytic machinery, cells have been treated with blocking antibodies and small molecule inhibitors during adhesion, spreading and migrating on these surfaces.

7.5 CONTRIBUTION OF CELLULAR RECEPTORS TO FORCES DURING ENDOCYTOSIS

Through the specific interactions between binding motifs at the surfaces of viruses and cell surface receptors, viruses gain adhesion energy, which was speculated to be sufficient to overcome the membrane tension during endocytosis (see Section 2.3.1). In the following experiments I controlled the interaction between reoviruses and their specific receptors by inhibiting sialic acids, JAM-A and integrins with either the protease neuraminidase cleaving sialic acids or blocking antibodies against JAM-A and/or against integrin $\beta 1$. This allowed me to investigate the contribution of cellular receptors on the two initial

phases of virus infection: 1) viral adhesion (cf. Section 7.5.1) and 2) virus internalization (cf. Section 7.5.3 and 7.5.2). Further, I studied the uptake of nanoparticles lacking any specific interaction site (cf. Section 7.5.4).

7.5.1 *Effect of Receptor Blocking on Reovirus Infectivity*

To prove the effect of receptor binding on virus infectivity, reoviruses were added in solution and allowed to adhere on the cells on ice for 1 h, before unbound viruses were removed by washing. Cells were further incubated overnight, fixed and stained to quantify viral infection in collaboration with Marta Fratini (lab of Dr. Steeve Boulant, Heidelberg University and DKFZ, see Figure 7.8 a). Thus, here only the initial phase of virus binding is considered, since endocytic processes are stalled at low temperatures during the first hour whereas later the effect of antibody (Ab) blocking is reduced by receptor homeostasis. Indeed infectivity in HeLa cells treated with either neuraminidase or JAM-A Ab was significantly reduced, proving that the treatment is affecting cell-virus interaction. Further, the blocking Ab against integrin $\beta 1$ (clone P5D2) has been applied. However, blocking $\beta 1$ integrin did not significantly inhibit viral infection (see Figure 7.8 b).

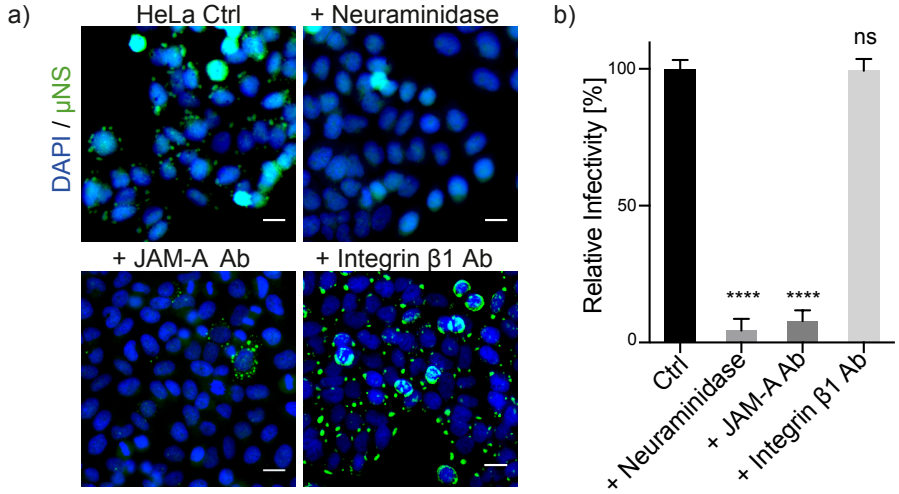

Figure 7.8: Reovirus infectivity upon receptor blocking. Reovirus receptors in HeLa cells were blocked. a) Adherent HeLa cells, pre-treated with neuraminidase and blocking antibodies against JAM-A or integrin $\beta 1$ at RT for 1 h, were incubated with soluble reovirus particles, fixed and stained for virus factories (green) and DAPI (blue). Scale bar = 10 µm. Images acquired by Marta Fratini. b) Quantification of infected cells normalized to untreated control cells. ****, $P < 0.0001$.

While the results for neuraminidase and JAM-A blocking are in line with the reduced infection rate observed in literature [166, 232],

knockout as well as blocking of integrin $\beta 1$ was previously shown to also decrease the infectivity with soluble viruses [157]. Although I proved that the blocking integrin $\beta 1$ Ab (clone P5D2) was successfully inhibiting HeLa cell spreading on $\alpha 5\beta 1$-selective surfaces (results not shown), it could be that the reovirus binding site on integrin $\beta 1$ was not addressed with this antibody. Unfortunately, the antibody used by Maginnis et al. was not commercially available.

To conclude: reovirus binding was found to depend on sialic acids and JAM-A but not on integrin $\beta 1$. However, $\beta 1$ integrins might be involved in the next phase of viral infection, namely the internalization.

7.5.2 *Effect of Receptor Blocking on Reovirus Internalization*

To better distinguish between virus binding and internalization, I conducted experiments with the same receptor blocking procedure as described above and reovirus particles in solution but fixed the cells after 1 h without permeabilizing the plasma membrane. This allows to specifically stain virus particles that are not internalized. 3D stacks were recorded with a confocal microscope (see Figure 7.9 a) and the absolute number of reoviruses interacting with the cell (b) as well as the relative number of internalized particles over the total number of particles (c) was quantified.

As expected, blocking of JAM-A dramatically reduced the number of virus particles attached to the cell (see Figure 7.9 b). Out of ~ 500 particles applied per cell in solution, 41 particles (median value) attached to untreated cells while almost none particles adhered on JAM-A blocked cells. However, out of these particles a similar amount got internalized into blocked cells, 61 %, compared to 49 % under control conditions. Note, that due to the low number of total viruses attached to the JAM-A Ab treated cells the distribution is rather digital with one reovirus particle being either inside or outside the cell (see Figure 7.9 c). Since receptor blocking through Abs is targeting membrane recruited receptors only, the intracellular pool is still active and can replace the blocked receptors. The low amount of viruses bound and internalized could have been thus engaged by single JAM-A receptors that are not blocked.

To exclude this effect, CHO cells have been employed, which do not express JAM-A and are thus poorly permissive for reovirus infection [157, 233, 234]. Just like for blocking of JAM-A in HeLa cells, I found only a very small number of reovirus particles interacting with CHO cells after 1 h of incubation. Surprisingly, CHO cells that did bind a few reovirus particles, 50 % of those got internalized.

These findings are in line with the observations of Marta Fratini that induction of CME is JAM-A independent [220]. And to conclude, JAM-A might be dispensable for mediating endocytosis of reoviruses.

Further, HeLa cells treated with integrin $\beta 1$ blocking Abs have been analyzed for virus binding from solution. To exclude that the Ab clone P5D2 does not block the reovirus binding site on integrin $\beta 1$ as discussed above, another clone (4B4) was employed, which has been previously reported to reduce integrin $\beta 1$ mediated adhesion [235, 236]. Like for the tearing of surface bound reovirus particles, I observed no effect on adhesion of reovirus (median of 44 reoviruses for both integrin $\beta 1$ blocking Abs) neither on their internalization (52 % and 45 % of attached viruses were internalized after treatment with integrin $\beta 1$ blocking Ab P5D2 and 4B4, respectively; see Figure 7.9 c).

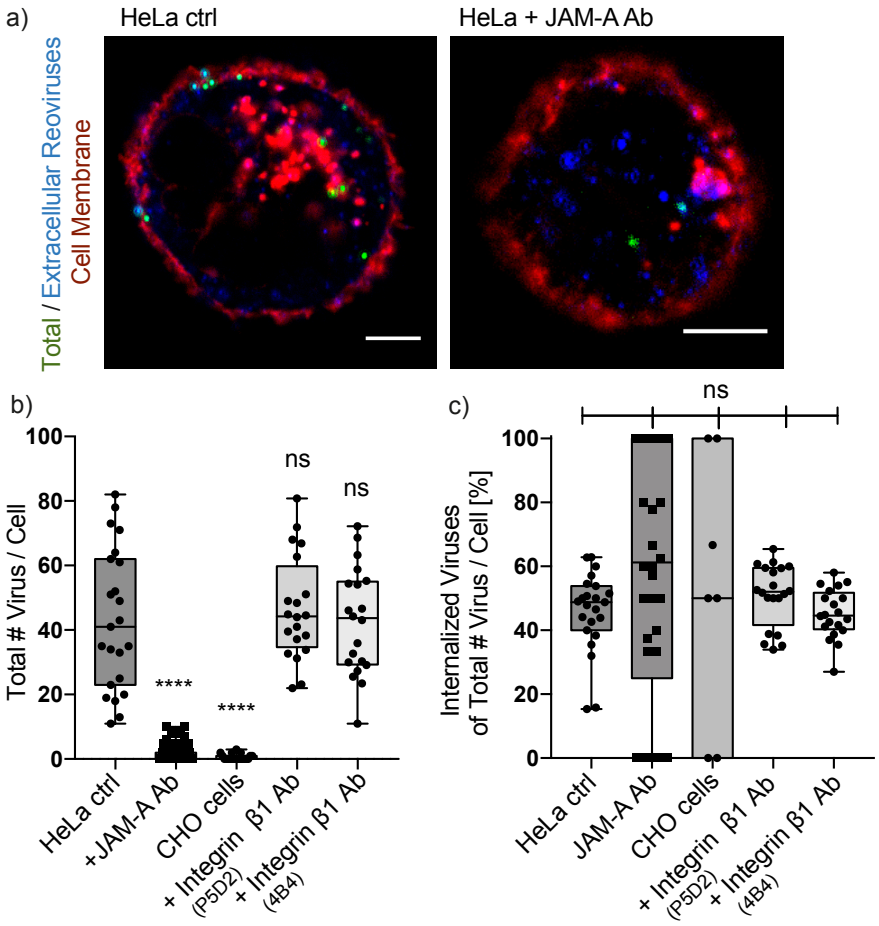

Figure 7.9: Virus internalization from the apical side upon receptor blocking. Adherent HeLa and CHO cells were incubated for 1 h at RT with the indicated blocking antibodies against reovirus receptors and subsequently reovirus particles (green) were added in solution for 1 h under physiological conditions. Afterwards unbound viruses were removed by washing and the cells were fixed and stained by IF selectively for extracellular reovirus particles (blue) and the cellular membrane (red) and imaged by confocal fluorescence microscopy. Scale bars = 5 µm. b) Quantification of the absolute number of virus particles attached/internalized per cell. c) Relative number of virus particles internalized of the total number of viruses attached per cell. ****, $P < 0.0001$.

7.5.3 *Effect of Receptor Blocking on Tearing of Biotin-NeutrAvidin Immobilized Reoviruses*

In the following I elucidated the role of reovirus receptors on the uptake of virus particles at the basal side. Here, not only membrane tension and receptor presentation differs from the apical side but the virus particles are already trapped in close contact to the cell. Therefore, I pre-treated HeLa cells with neuraminidase, JAM-A Ab, integrin $\beta 1$ Ab or both antibodies at a time for 1 h at room temperature in

suspension, before seeding them on surfaces with non-covalently immobilized reoviruses and followed the tearing of viruses by confocal imaging as described before (Section 7.3). The initial rate of tear off was calculated from two-phase exponential fits for each individual cell (see Figure A.3). Untreated cells were prepared in parallel and seeded on the same surfaces separated by partition walls. The median of the rate of initial virus tear off $\tilde{k}_{I,ctrl}$ from untreated cells of each experiment served as control for the respectively treated cells. Their difference was calculated by $\Delta k_I = k_I - \tilde{k}_{I,ctrl}$.

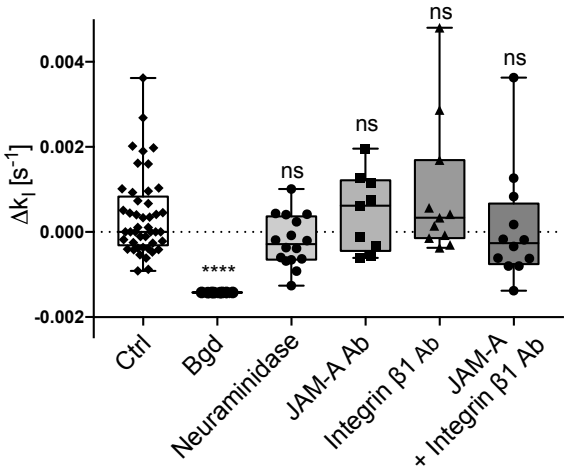

Figure 7.10: Tearing of biotin-NeutrAvidin immobilized reoviruses upon receptor blocking. Difference in the kinetic rate constants of initial virus tear off by HeLa cells, which were incubated with neuraminidase or blocking antibodies against JAM-A and/or integrin β1 at RT for 1 h in solution to their corresponding control cells. The dotted line indicates the median of all untreated cells (ctrl). Cell-independent virus unbinding was quantified from the background (bgd). ****, $P < 0.0001$.

Although neuraminidase and JAM-A blocking Ab treatments showed strong inhibitory effects on the cells with respect to virus binding and thus prevention of viral infection, they did not significantly alter the rupturing behavior of biotin-NeutrAvidin immobilized virus particles (see Figure 7.10). Remarkably, also the rate of viral uptake was not significantly reduced by blocking integrin β1. In addition, I co-treated the cells with antibodies against JAM-A and integrin β1. Similarly, this co-blocking did not significantly reduce the rate of virus uptake.

Sialic acids are mediating the primary attachment of reoviruses to cells [151]. Thus it can be easily understood that neuraminidase treatment had a strong effect on infectivity upon addition of soluble viruses, while the tearing of reoviruses, which are already immobilized in close contact to the cells, did not significantly change. In contrast, JAM-A and integrin β1 have been suggested to mediate endocytosis [168, 237]. However, my results revealed that the role of

JAM-A for reovirus uptake is, similarly to sialic acids, limited to the initial step of viral adhesion and not for mediation of the uptake itself. Once the virus-cell contact is established, by receptor binding or as purely physical contact between the immobilized viruses and adhesive cells, they seem to become obsolete for endocytosis. Unlike observed by Maginnis et al. [157, 168], blocking of integrin $\beta 1$ had neither an effect on virus binding (as checked in the infectivity assay with soluble reoviruses) nor on the rupturing and uptake from biotin-NeutrAvidin surfaces. This could be explained by the redundancy of the different receptors for virus binding. Especially among integrins many subunits are known to recognize the RGD binding sites and they are performing similar functions [25, 27]. Also further ligands like Nogo receptor 1 (NgR1), which has been identified to serve as reovirus receptor in neurons [238], could be utilized if the main receptors are lacking.

To conclude, I could show that specific receptor types might be dispensable for tearing off trapped viruses and their endocytosis. This might be due to blocking-induced recruitment of the same receptor species from intracellular pools. The complete lack of a specific receptor type can also lead to engagement of different receptors.

7.5.4 *Tearing of Biotin-NeutrAvidin Immobilized Nanoparticles*

To analyze if specific receptors are not required in general, inanimate nanoparticles of the same size as reovirus particles have been presented to the cells in a similar way. Therefore, AuNPs of 100 nm in diameter were coated with a protein-repellent PEG layer disabling any cellular interactions. Further, Abberior StarRed dye and biotin-moieties were linked to the particles´ PEG layer allowing for analogous immobilization as virus particles on the silane-PEG-alkyne-biotin/cRGD surfaces via NeutrAvidin.

Surprisingly, HeLa cells seeded on these substrates were capable of ripping off the nanoparticles from the surface and internalizing them even without specific adhesion sites. However, they did so at a slightly lower rate $k_{I,\,AuNPs} = (0.7 \pm 0.4) \cdot 10^{-3}\,s^{-1}$ than they teared off biotinylated reovirus particles, which were prepared in parallel $(1.0 \pm 0.5) \cdot 10^{-3}\,s^{-1}$. On the contrary, AuNPs coated additionally with cRGD, allowing for specific interactions with integrin receptors on the cells, showed a significant increase in their uptake rate with $(1.8 \pm 1.5) \cdot 10^{-3}\,s^{-1}$ (see Figure 7.11 a). Since cRGD also promotes integrin mediated adhesion to the substrate, I investigated the adhesion capability of HeLa cells on these surfaces. As can be seen in figure 7.11 b, HeLa cells adhered to a similar extent and speed on both substrates. Thus, the increased uptake behavior is not due to a better adhesion or faster spreading on the surfaces.

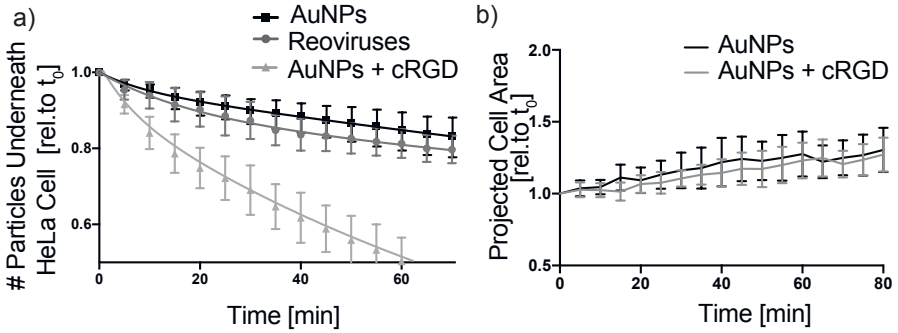

Figure 7.11: Tearing of biotin-NeutrAvidin immobilized nanoparticles with and without specific ligands. 100 nm PEGylated AuNPs functionalized with Abberior StarRed, biotin and optionally with cRGD were immobilize analogously to reovirus particles via NeutrAvidin on glass. HeLa cell induced tearing was followed by live confocal imaging. a) Relative number of AuNPs (black), AuNPs with cRGD (light grey) and reoviruses (black) underneath the cells over time. b) Projected cell area of HeLa cells spreading on substrates with immobilized AuNPs with (black) and without cRGD (grey).

This challenges also the hypothesis, that specific receptor-interactions are responsible for the energy that is needed to oppose the energetic cost for membrane bending. However, for smaller particles or viruses this energetic cost is higher and the chemical recognition thus might become more dominant. To conclude, I could show with these experiments that endocytosis of viruses and nanoparticles can happen receptor independent via non-specific adhesion forces (such as discussed in Section 2.4). However, specific ligands, such as cRGD that was used here, can significantly increase the speed of uptake and thus the forces applied. These differences in the kinetics certainly play a major role in biological systems and hence can have been of evolutionary advantage for virus particles. But the major part of the observed forces of approximately 41 pN during endocytosis of viruses and nanoparticles from the basolateral side of cells are most likely not receptors-mediated. Thus, these forces must have another origin, likely connected to the cytoskeleton.

7.6 CONTRIBUTION OF THE CYTOSKELETON TO FORCES DURING ENDOCYTOSIS

The actomyosin cytoskeleton can generate large scale forces that are transmitted to the extracellular matrix and neighboring cells via specific adhesion sites. In order to dissect the origin of the forces during virus particle uptake, I focused on the different force generating processes including actin polymerization, actin branching mediated by Arp2/3, initiated polymerization by formins as well as contractility of the actin cytoskeleton caused by myosin II.

7.6.1 *Effect of Cytoskeleton on Tearing of Biotin-NeutrAvidin Immobilized Reoviruses*

Here, I used small molecule inhibitors to diminish specific force generating mechanisms and analyzed their effect on the tearing and uptake of biotin-NeutrAvidin immobilized reoviruses. To account for the variability among individual cells, each cell was imaged for 30 min before drug addition, which served as internal control. The change in the virus uptake was determined as ratio from the number of particles torn off 20 min after addition of a cytoskeletal drug for 20 min, relative to the 20 min directly before drug addition (see Figure 7.12 a).

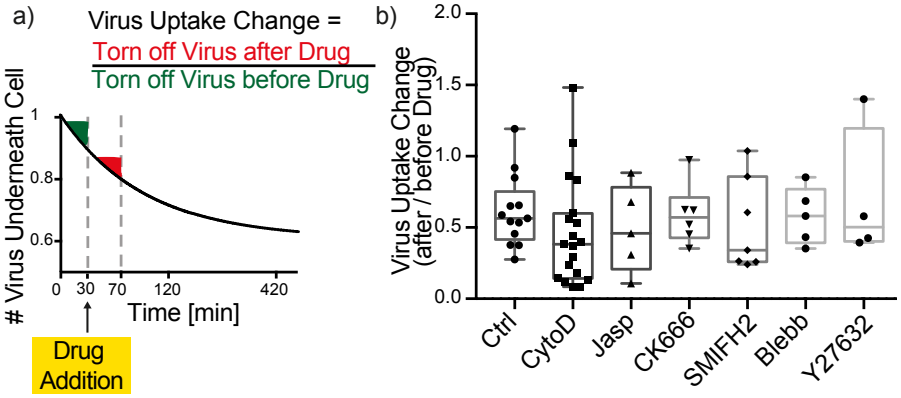

Figure 7.12: Virus tearing upon inhibition of the actin cytoskeleton. U373 cells were seeded on the biotin-NeutrAvidin immobilized reovirus particles and imaged starting 30 min after seeding. After another 30 min cells were treated with small molecule inhibitors cytochalasin (CytoD), jasplakinolide (Jasp), CK666, SMIFH2, blebbistatin (Blebb) and Y27632 or DMSO as a control (ctrl). a) Schematic of the analysis of virus uptake change after addition of cytoskeletal drugs. (b) Virus uptake change for cells treated with the indicated drugs.

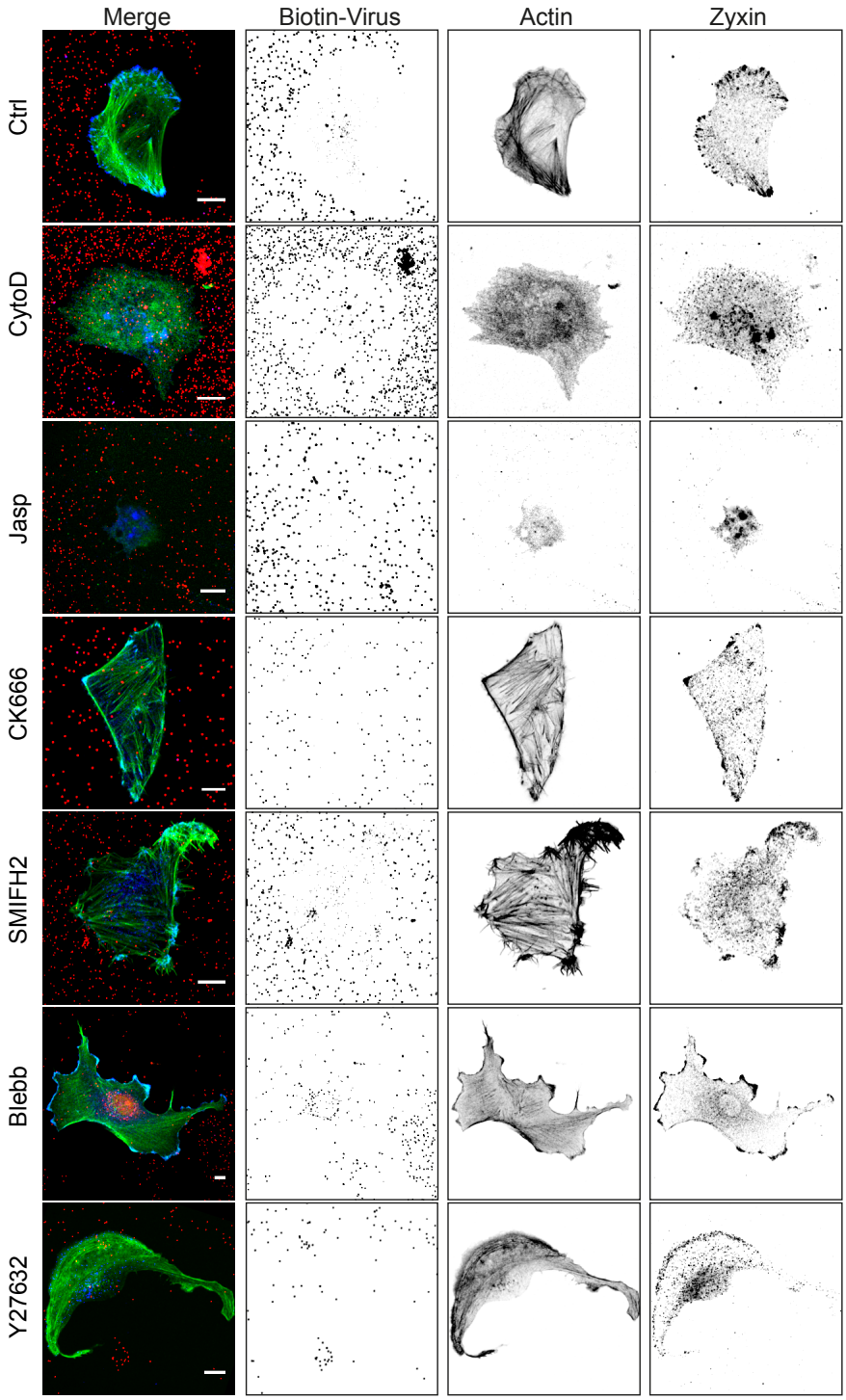

Figure 7.13: Fluorescence images of U373 cells on biotinylated virus particles upon inhibition of the actin cytoskeleton. After overnight incubation of U373 cells on the biotin-NeutrAvidin immobilized reovirus particles (red), cells were fixed and stained for F-actin (green) and zyxin (blue) to confirm the effect of the drugs on the cytoskeleton. Scale bar = 10 µm.

Actin polymerization was inhibited by cytochalasin D in U373 cells. Since actin is crucial for many vital processes in the cell, the concentration was adjusted in a dose-response assay to $c_{final} = 625\,\text{nM}$ (data not shown) to break down most of the actin stressfibers while maintaining cellular attachment and survival for at least 1 h. Likewise, jasplakinolide was applied at $c_{final} = 100\,\text{nM}$ to destabilize actin. Commonly it is known to stabilize F-actin but was also found to destabilize the actin cytoskeleton [239], arresting CCPs [124] and, in yeast, inhibiting endocytosis [137]. Surprisingly, even with a completely disrupted actin cytoskeleton (see Figure 7.13), cells continued to rip off biotinylated reovirus particles from the surfaces with no significant difference in the uptake before and after drug addition compared to the control group (see Figure 7.12 b). After overnight incubation cells were fixed and stained for F-actin and zyxin proving the disassembly of the F-actin stress fibers. Consequently a lack of focal adhesions as well as the uptake of virus particles have been shown by confocal z-stacks (see Figure 7.13).

Actin assembly into branched networks was disrupted by the Arp2/3 inhibitor CK666 at $c_{final} = 200\,\mu\text{M}$ and actin nucleation by the formin FH2 domain inhibitor SMIFH2 ($c_{final} = 30\,\mu\text{M}$). These proteins are essential for membrane shaping in lamellipodia and filopodia, respectively and especially Arp2/3 was reported to aid in CME and other dynamin-dependent endocytic pathways [134, 139]. Inhibition of Arp2/3 disrupted lamellipodia formation completely resulting in tri- or rectangularly shaped cells, while the inhibition of formin disrupted filopodia and generally reduced membrane tension visible by membrane ruffling (see Figure 7.13). However, neither of these drugs reduced the virus uptake behavior of U373 cells indicating a Arp2/3 and formin independent pathway.

Large forces such as those observed during virus particle uptake are associated with contraction of the cytoskeleton. This is mediated by myosin II activity, which was inhibited by blebbistatin ($c_{final} = 10\,\mu\text{M}$) and ROCK inhibitor (Y-27632, $c_{final} = 10\,\mu\text{M}$). Both drugs induced strong morphological changes and increased the migratory behavior as can be seen in Figure 7.13. However, they did not decrease the rip-off efficiency (see Figure 7.12 b). On the contrary, the amount of total virus uptake after overnight incubation was even increased due to their enhanced mobility.

To conclude, the tearing of biotin-NeutrAvidin immobilized virus particles did not depend on F-actin, actin branching and contractility of the actin cytoskeleton. However, cortical actin polymerization was not addressed with the above mentioned drugs and thus might be the origin of the forces observed. So unlike the endocytosis of notch, which is clathrin-dependent and was found to require actin [184], endocytosis of reovirus does not seem to depend on actin. Difficulties here are the numerous processes in cells, which involve actin making

it difficult to totally knock out the cytoskeleton. This could also explain the varying literature on the importance of actin for endocytosis [127, 143, 240, 241].

7.6.2 *Effect of Soft Substrates on Tearing of Biotin-NeutrAvidin Immobilized Reoviruses*

Likewise, the reduction of cellular tractions by growing cells on soft hydrogels with biotinylated fibronectin and NeutrAvidin immobilized reovirus did not obviously change the uptake behavior. On PAA hydrogels ranging from 1.5 to 30 kPa a substantial uptake of reovirus particles was observed between 2 h post seeding and 18 h (see Figure 7.14). Quantitative analysis of these substrates was not possible with the current methods since the custom-made tracking software would account displaced particles on the deformed substrates as torn off particles resulting in a lot of false positive counts. Further the spreading and migration behavior of the cells changed between the substrates with different stiffnesses and a consistent comparison between the cells is thus hampered.

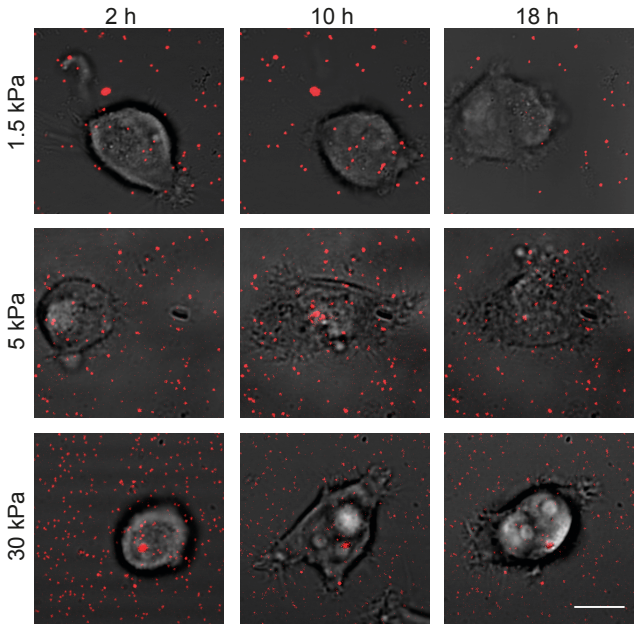

Figure 7.14: Tearing of biotin-NeutrAvidin immobilized reovirus particles from PAA hydrogels. U373 cells were seeded on PAA hydrogels of 1.5, 5 or 30 kPa stiffness coated with biotinylated fibronectin and biotinylated reovirus particles (red dots) immobilized via NeutrAvidin and imaged with confocal microscopy overnight. Scale bar = 10 µm.

To summarize, the reduction of total traction forces induced by tuning the physical parameters of the substrates as well as small molecule inhibitors did not reduce the uptake efficiency of substrate-bound virus particles.

I further used these soft substrates to analyze the reverse effect: can the presence of immobilized / non-immobilized reoviruses alter cellular traction forces applied to the ECM? I therefore conducted TFM with U373 cells seeded on PAA hydrogels with biotinylated fibronectin and either NeutrAvidin immobilized reovirus or reoviruses added in solution compared to cells without virus exposure. Analysis via PIV and FTTC algorithms revealed that the total strain energy applied by the cells were neither significantly altered by viruses added in solution nor by biotin-NeutrAvidin immobilized reoviruses after 4 h incubation time each (see Figure 7.15). While cells experiencing virus interaction from their apical side showed increased tractions, cells interacting with reovirus particles from their basolateral side did not behave differently from cells without viral contact. This goes along with my finding that tearing of reoviruses and uptake from the basolateral side does not depend on actomyosin contraction, which is responsible for generation of traction forces.

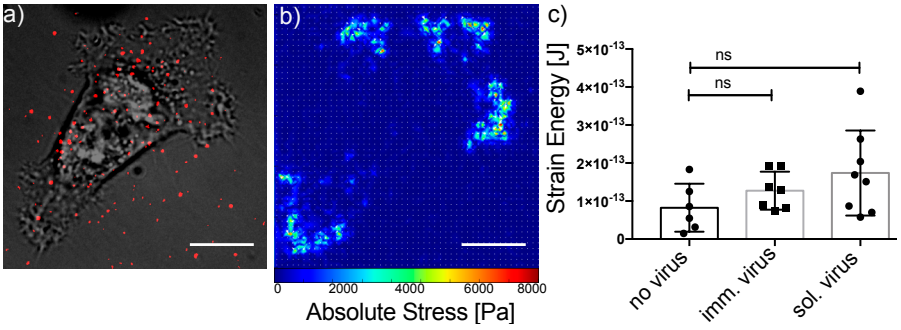

Figure 7.15: Traction force microscopy on cells interacting with virus particles. a) Merge of U373 cell (brightfield) spreading on TFM substrate with a stiffness of 12 kPa coated with fibronectin and fluorescent reovirus particles (red) immobilized on biotinylated fibronectin via NeutrAvidin. Scale bar = 10 µm. b) Traction forces with absolute stress values between 0 and 6000 Pa according to color code. c) Quantification of total strain energy per cell interacting with bare fibronectin, immobilized viruses or soluble viruses.

7.7 CONTRIBUTION OF THE ENDOCYTIC MACHINERY

Clathrin-mediated endocytosis (CME) is a major but not the only uptake route for reoviruses [160, 169]. As I presented earlier (cf. Figure 7.5), around 30 % of immobilized viruses induce a recurrent recruitment of the clathrin machinery. Thereby, formation of clathrin coated pits (CCP) stabilizes the bent plasma membrane, which lowers the bending energy and enables the GTPase dynamin to bind and to actively constrict the membrane neck, thus helping budding off from the membrane (cf. Section 2.2).

To investigate whether the observed forces leading to tearing of viruses from biotin-NeutrAvidin surfaces are induced by CCP formation and growth, U373 cells with a double knockout (KO) for CLT a and b (cf. Section 5.1.1 and Figure A.5) were seeded on the surfaces. While the general tearing of virus particles underneath the cells persisted and thus U373 with CLT KO showed significant amount of internalized particles and viral infection, the rate of virus tearing was significantly reduced (see Figure 7.16 a and b and Figure A.6 for individual fits).

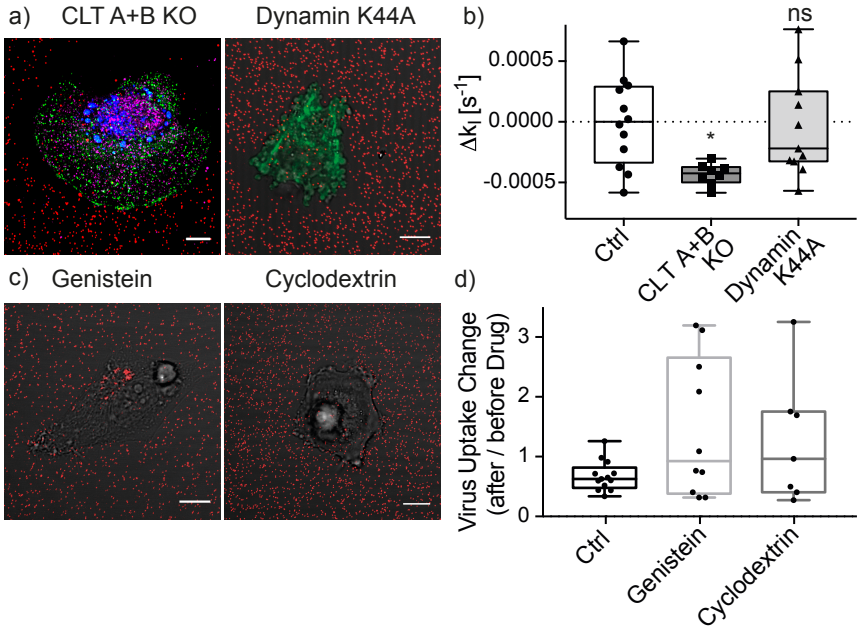

Figure 7.16: Contribution of components of the endocytic machineries to virus tearing from biotin-NeutrAvidin. a) U373 cells with a double knockout of clathrin light chain (CLT) A and B (CLT Ab in purple, AP2 in green, viral factories in blue) and cells overexpressing the dynamin mutant K44A (clathrin in green) were seeded on biotin-NeutrAvidin immobilized reovirus particles (red). Difference in the uptake rate Δk_I with respect to the median of the control cells, *,P =0.018. c) U373 cells treated with 200 µM genistein or 10 mM methyl-β-cylodextrin. d) Change in virus tearing before and after addition of the drugs. Scale bars in a and c = 10 µm.

Further, dynamin was inhibited by transient overexpression of the dynamin mutant K44A (with an eGFP tag, cf. Section 5.1.1), which is deficient in GTP binding and therefore not functional. The efficiency of CCV release was determined during live cell imaging in U373 cells co-transfected with clathrin-tomato. Cells with reduced dynamin activity did not show a reduced number of internalized viruses neither a decreased rate of virus particle uptake (see Figure 7.16 b). However, these results should be treated cautiously since overexpression of the dynamin mutant has been discussed critically in literature because at

high dosage it induces apoptosis due to failure of mitosis while being inefficient at low dosage [242]. Indeed, most transfected cells showed a damaged morphology as can be seen in figure 7.16 a. Alternative tools including RNAi, knockout cell lines or small molecule inhibitors should be applied in order to validate the results.

Taking into account that CME is only one of the possible pathways for reovirus to enter cells, these results indicate that the clathrin machinery can contribute to the forces, however, it is not the main determinant for tearing of particles from the biotin-NeurAvidin surfaces.

Caveolin-Dependent endocytosis was proposed as alternative pathway for reovirus uptake since it is known to be used by other viruses such as avian reoviruses [160, 243, 244]. Inhibition of the caveolin pathway was conducted by adding the drugs genistein or methyl-β-cylodextrin 1 h after seeding U373 cells on biotin-NeutrAvidin immobilized virus surfaces. Genistein is a broad-spectrum tyrosine kinase inhibitor, so its target is not limited to caveolin-mediated endocytosis. In fact, genistein was shown to diminish reovirus infectivity [245]. However, the authors focused on the effect of genistein on the Src pathway inhibiting the targeting of incoming virions to lysosomes for viral disassembly and thus functional entry into host cells.

Here, I found that cells showed strong morphological response to the drugs since they are affecting membrane composition by depleting cholesterol. However, virus tearing was not reduced compared to untreated cells (see Figure 7.16 c and d). On the contrary, some cells showed even an increased virus tearing after drug addition, which might be associated with the morphological changes.

Inhibition of caveolin-dependent endocytosis can reduce reovirus infection to 30 % as reported by Schulz et al. [160]. To better estimate the effect of caveolin on virus tearing and internalization in future studies, KO cells or cells expressing a dominant-negative form of caveolin should be employed.

To summarize, inhibition of specific endocytic molecules and pathways did not prevent virus particle tearing and internalization. This is possibly linked to the redundancy of different pathways. Blocking one pathway does not completely stop virus entry, because other pathways can be upregulated and thus compensating this depletion.

The herein presented methods allow to study the forces during particle uptake from the basolateral side in unprecedented detail. Furthermore, I conducted functional assays revealing the importance of individual proteins and ligands for virus particle uptake. Since reoviruses display a promiscuous uptake behavior, no single receptor or pathway could be identified that would explain the total force of ~ 40 pN. However, there is evidence that actin polymerization and connection to the clathrin-machinery contribute to the mechanics of reovirus uptake.

Part IV

CONCLUSION AND OUTLOOK

8

MOLECULAR FORCE LOAD AND RIGIDITY SENSING

The first objective of this work was to investigate the force load on single cellular receptor proteins while adjusting the stiffness and ligand spacing of the surrounding substrate. For this purpose, I engineered elastic hydrogels with fluorescent marker beads and nanopatterned gold particles bearing extracellular ligands for defined cell adhesion. This setup allowed to study adhesion growth as well as cellular traction forces depending on the nano-distribution of cellular receptors and the rigidity of the substrate in unprecedented detail.

In contrast to earlier experiments on glass [41, 102, 155], cellular adhesions on medium-soft substrates (between $\sim 5 - 30\,\mathrm{kPa}$) grew bigger and displayed higher traction forces on bigger ligand spacings (100 nm) than on smaller spacings (50 nm). However, above a certain threshold stiffness adhesions collapsed. Next, I produced substrates with disordered ligand presentation with the same mean spacing as the ordered substrates. The disordering resulted in larger spacings for individual integrin receptors, which in turn were experiencing higher traction forces and thus engaged more integrin receptors, leading to adhesion growth. The results were in-line with the molecular clutch model suggesting a minimal force load per integrin receptor that needs to be surpassed for further integrin recruitment. By feeding the molecular clutch model with new experimental data and educated assumptions it was even possible to correctly predict the observed adhesion lengths and traction forces. A limit that was set for adhesion growth allowed to model the collapse of adhesions when the traction forces get too high to compensate the increased force load per integrin by further integrin recruitment.

This model helps to understand the basic biophysical process of how cells are sensing both, substrate rigidity and extracellular ligand density. Furthermore the hypothesis of a molecular ruler measuring receptor distances [42] becomes obsolete since the optimal spacing was found to be dependent on the stiffness of the substrate.

While the global traction forces nicely resembled the model predictions, it was not possible to confirm the predicted local force loads per individual integrin molecule with the current methods. I therefore successfully developed molecular tension probes based on PEG, DNA-hp and the I27-titin domain capable of reporting forces applied to various ligands which can be tethered to the tension molecules via CuAAC reactions. Their functionality was confirmed with RGD ligands reporting on integrin-mediated forces on glass substrates with randomly immobilized AuNPs.

Next, I applied these molecular tension probes on PAA hydrogels with fluorescent marker beads which allowed, for the first time, to access the forces on individual integrin receptors on soft substrates. Unlike the traction forces reported by TFM analysis originating exclusively at focal adhesions, integrin molecules all over the adhesion area of the cells showed a force load of > 19 pN indicated by an increase in fluorescence signal of the DNA-hp tension probes. While such a behavior of integrins outside FAs was observed before on glass substrates [50], no measurements exist proving these global forces under physiological, soft conditions. TFM is mainly in-sensitive to depict out-of-plane forces because tracking and traction reconstruction algorithms of randomly incorporated marker beads get more complicated in 3D and the optical resolution in z is limited. Therefore, I combined MTFM with cTFM, which can detect z-components of traction forces in high precision while being computationally less complicated than classical TFM analysis [74, 246].

In an ongoing study, cTFM samples (see Section 3.2.2 and [75]) were applied, which exhibit fluorescent nanodisc arrays of Qdots and AuNPs. Here, individual nanodiscs were 200 nm in diameter and spaced 3 µm from each other. On one hand, they were used to immobilize molecular tension probes via their thiol functions and, on the other hand, they served as reference sites for the deformation of the silicon hydrogels. The Qdots used for tracing the deformation of the substrate were composed from CdS/ZnS core/shells and applied on the silicon hydrogels by electro-hydrodynamic printing (see Section 3.2.2). To avoid a bleed-through from the strong-emitting Qdots into the channel of molecular tension probes, blue Qdots ($\lambda_{em} = 457$ nm) in combination with red-emitting tension probes ($\lambda_{em} = 655$ nm) have been chosen. Unfortunately, the blue Qdots used in this study were very sensitive to oxidation in liquids and thus could not been used to trace the deformations. However, their reflection visible in interference reflection microscopy proved to be sufficient for detection of the arrays (see Figure 8.1 b). For future studies, oxidation could be limited by the use of reducing agents such as ascorbic acid, or other types of Qdots exhibiting more stable shells might be employed. Here, 2D tractions were reconstructed from the reflection images of the nanodisc array compared to the optimal pattern with a nonlinear finite element analysis by Tobias Lendenmann (in the group of Dr. Aldo Ferrari, ETH Zürich). This algorithm does not require any regularization and thus circumvents subjective parameterization as used in PIV-based TFM analysis, which are prone to underestimation of tractions [75].

First results proved a successful immobilization of molecular tension probes (DNA-hairpins as well as titin sensors) to the nanodisc arrays without further modification. However, closer analysis revealed that mainly the Qdots in the nanodiscs are responsible for binding the

molecular tension probes owing to their thiolated shell. In samples with printed AuNPs only, I did not observe binding of the molecular tension probes (data not shown). Since the 457 nm-Qdots are not capable of quenching the red fluorescence signal from the molecular tension probes, only sensors with internal quencher, such as DNA-hairpins, might be used. For future experiments the concentration of the tension probes has to be optimized, since the background fluorescence on the arrays was very high even without cell induced forces (see Figure 8.1 d and e).

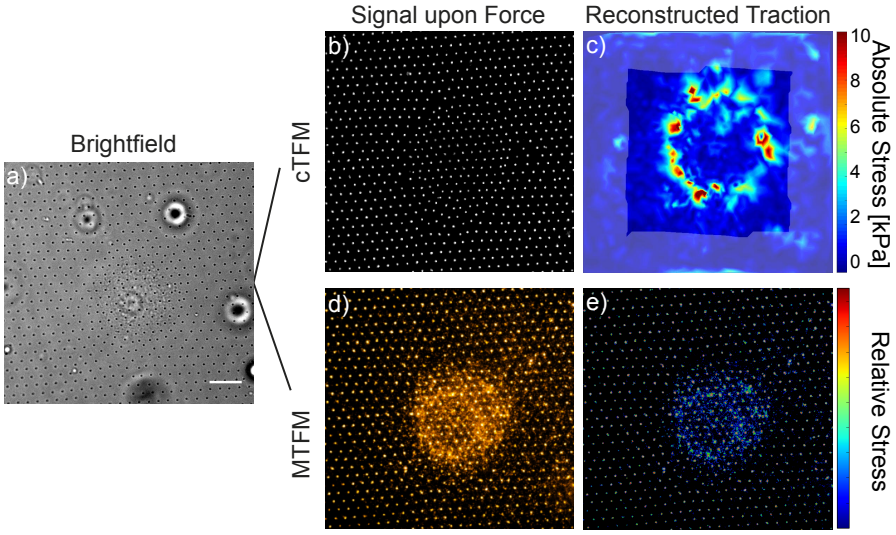

Figure 8.1: Tension probes on cTFM samples readily bind to arrays of Qdots. DNA-hp tension probes with an opening force of 19 pN (d, for MTFM) were coupled to an array of 457 nm-Qdots on 12.6 kPa silane substrates (b, for cTFM). REF cells were seeded in culture medium supplemented with 0.5 % FBS for 1 h and removed by trypsinization. Images were recorded on an inverted wide-field fluorescence microscope, analyzed in ImageJ and with a finite element algorithm in Matlab. Scale bar = 10 µm.

Concluding, the combination of TFM with MTFM can help to get a more complete image of the mechanical interactions between cells and their surrounding. To further investigate the force load on individual integrins for testing the molecular clutch model, tension probes with higher threshold forces such as TGT sensors or titin probes have to be used. Furthermore, this method will help to cross-validate the results for cellular traction forces obtained by the two state-of-the-art techniques TFM and MTFM with regard to the localization and direction of the forces as well as the absolute values for the force load on individual receptors.

9 VIRUS UPTAKE

In the second part of this thesis I applied the modular tension probes, which were successfully generated and tested with integrin ligands in the first part, to measure the forces during virus particle uptake in an adhesive environment. I therefore developed a non-invasive technique for covalent and non-covalent immobilization of non-enveloped virus particles, which preserves their infectivity in an unbound state. Cells interacting with surface-bound reovirus particles on molecular tension probes generated forces exceeding ~40 pN as measured with DNA-hp and titin-based tension probes in single molecule fluorescence experiments.

Cells growing on surfaces with non-covalently bound reovirus particles were able to tear them off the surface, internalize them and eventually get infected. This is the first time that cellular uptake of particles immobilized via biotin/NeutrAvidin from an adhesive surface has been observed, which is surprising since it is a widely used immobilization technique for biological substances.

Kinetic analysis of the cell-induced unbinding and unbinding at zero force revealed a mean force of ~41 pN, which is in line with the results I achieved by single-MTFM. Interestingly, the range of forces I obtained from these measurements at the basal side of cells resembles those forces that have been measured for virus-cell interactions at the apical side in literature. This hints towards a general mechanism of force generation during virus internalization.

To unravel this mechanism, I first tested the contribution of receptor-binding. Therefore, I blocked cells for sialic acids, JAM-A and integrins. While sialic acids are thought to mediate the initial attachment of viruses only, JAM-A and $\beta 1$ integrins are regarded as genuine receptors, important for the endocytosis of reovirus. However, none of the blockings significantly reduced the uptake rate from immobilized virus particles and thus the generated forces. Neither did it change the percentage of internalized particles from reoviruses attached to the apical side of cells. Since antibody blockings do not lead to a complete silencing, it is advisable for future experiments to better control the inhibition of cellular receptors with knockout cells or to work with RNAi to suppress their translation. In the end, the results suggest that either the remaining or a different type of receptors are sufficient, or that the tearing and endocytosis of virus particles can take place receptor independent. Indeed, passivated AuNPs of 100 nm in diameter were torn off the biotin-NeutrAvidin surface without specific ligands for cells at a similar rate as reoviruses. Hence, pure receptor-binding cannot explain the origin of the pulling forces

during virus particle uptake. However, increasing the adhesion force on the AuNPs by presenting integrin ligands (cRGD) on their surface significantly increased their uptake rate.

Next, I quantified the contribution of the actin cytoskeleton on the observed forces with small molecule inhibitors and by altering traction forces via changing the stiffness of the substrate. Lowering the tractions with blebbistatin, ROCK-inhibitor or by soft substrates did not significantly affect the uptake behavior. This indicates, that contractility of the actomyosin cytoskeleton is not responsible for the observed forces. While I could observe a reduced virus uptake upon inhibition of actin polymerization by cytochalasin D in many cells, the results were not statistically significant. Cellular behavior regarding spreading kinetics and migration differed a lot between individual cells and experimental conditions. Therefore, increasing the data pool can help to compensate for this variability and will allow to draw a more precise image of the role of actin during particle internalization.

Finally, CME and caveolin-dependent endocytosis were addressed with mutant cells and small molecule inhibitors, respectively. Knock out of the clathrin light chains significantly slowed down virus particle uptake while overexpression of the dynamin mutant K44A had a limited effect on the uptake kinetics. Inhibition of the caveolin pathway by genistein and methyl-β-cylodextrin rather accelerated than slowed down the uptake. For future studies more controls including KO cells or cells expressing a dominant-negative form of e.g. caveolin should be employed to better target specific proteins. To conclude, endocytic pathways of reovirus are manifold and, depending on the chosen route, different adaptor proteins and the cytoskeleton might be important to a greater or lesser extent.

The herein presented method to couple intact virus particles via biotin/NeutrAvidin to an adhesive surface and observing cell induced virus tear off by fluorescence microscopy provides a novel tool to study the forces during endocytosis. Together with my experiments utilizing molecular tension probes, this is the first time the mechanics between virus particles and the basal side of cells have been recorded. In order to compare these forces to those, cells are applying from the apical side lacking nearby adhesions, AFM studies on reovirus particles could be conducted in a similar manner to the studies on rhinovirus, influenza and virus-like particles [174, 179, 181]. The comparison with biotin/NeutrAvidin immobilized reovirus particles on bigger beads or flakes applied from the apical side would bear even more resemblance. However, this approach did not result in virus tearing events in previous tests. To further improve the presented method, one could micropattern the cell adhesion ligands, which would standardize cellular shapes and polarization. This would allow to track hotspots in virus uptake and correlate them to e.g. focal adhesions.

Part V

APPENDIX

A

ADDITIONAL DATA

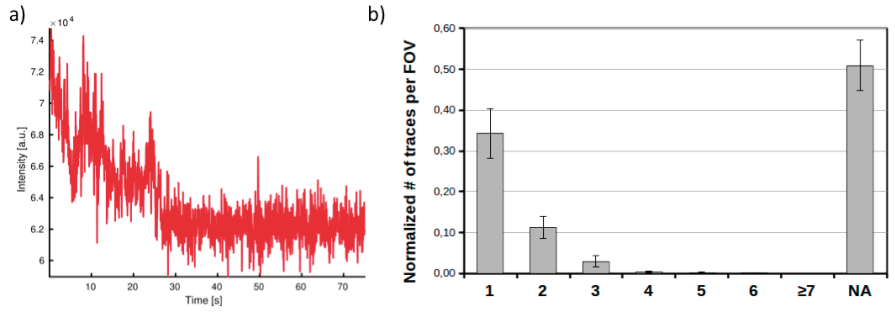

Figure A.1: Bleaching-step analysis of titin-based tension molecules. a) Single-molecule trace with two bleaching steps, indicating two fluorophores bound on one titin-based tension probe. b) Normalized abundance of titin-based tension molecules with 1-7 or not analyzable (NA) bleaching steps per field of view (FOV) as analyzed by Klaus Yserentant (lab of Prof. Dirk-Peter Herten, Heidelberg University).

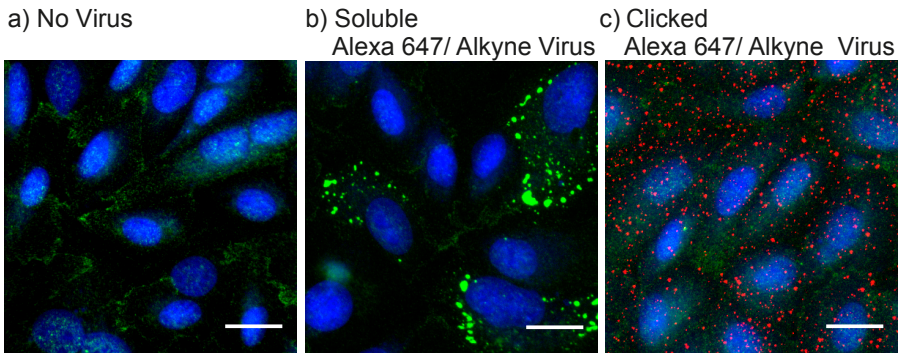

Figure A.2: Effect of conditions during CuAAC on reovirus infectivity. BSC1 cells were incubated (a) without virus, (b) with soluble Alexa647/Alkyne-virus, which was pre-incubated with 1 mM $CuSO_4$ for 2 h at RT or (c) seeded on covalently (via CuAAC in absence of THPTA) immobilized reoviruses (red). After overnight incubation cells were fixed and stained for virus factories (green) and DAPI (blue). Scale bar = 25 µm. Images provided by Marta Fratini (lab of Dr. Steeve Boulant, Heidelberg University and DKFZ).

Table A.1: Parameters for the molecular clutch model. Adapted from [156].

PARAMETER	MEANING	VALUE	ORIGIN
n_m	Number of myosin motors	190	Adjusted
F_m	Myosin motor stall force	$2\,pN$	[247]
v_u	Unloaded myosin motor velocity	$90\,nm/s$	Values measured here and [213]
n_l	Number of ligands (cRGD-functionalized nano-dots)	$180\,(50\,nm)$ $130\,(100\,nm)$ $5\,(200\,nm)$	Adjusted
d_{int}	Initial integrin density on the membrane	$300/\mu m^2$	[40]
$d_{int,max}$	Maximum integrin density on the membrane	$2200/\mu m^2$	Adjusted
k_{on}	True binding rate	$2.3x10^{-4}\,\frac{\mu m^2}{s}$	Adjusted, of the order of values reported for $\alpha IIB\beta 3$ [248]
k_{off}	Unbinding rate, scaling factor applied to force curve reported in [47]	0.5	Adjusted, catch bond dependency from [47]
$F_{threshold}$	Threshold reinforcement force	$87\,pN$	Adjusted, of the order of reported values [218]
d_{add}	Integrins added after each reinforcement event	$120/\mu m^2$	Does not affect model output
a	Radius of adhesion	$750\,nm$	Adjusted
k_{link}/k_{sub}	Elastic coupling between ligands	$10\,(50\,nm)$ $5\,(100\,nm)$ $1x10^{-19}\,(200\,nm)$	Adjusted

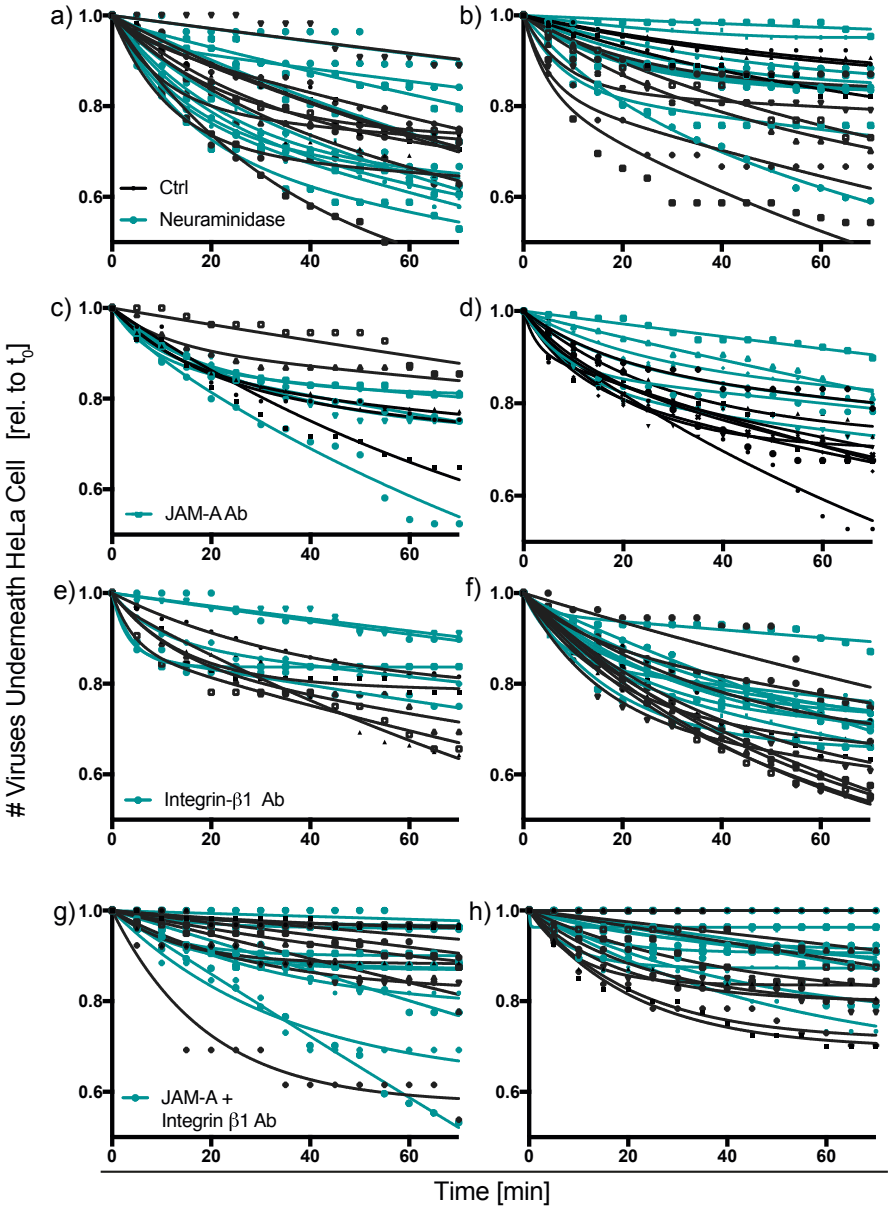

Figure A.3: Individual two phase decay-fits of virus uptake upon receptor inhibition. HeLa cells have been treated with Neuraminidase (a and b) or Abs against JAM-A (c and d) or/and integrin $\beta 1$ (e and f and g and h, respectively) or incubated without treatment (Ctrl). Cell induced tearing of biotin-NeutrAvidin immobilized reoviruses is plotted for each cell for eight individual experiments.

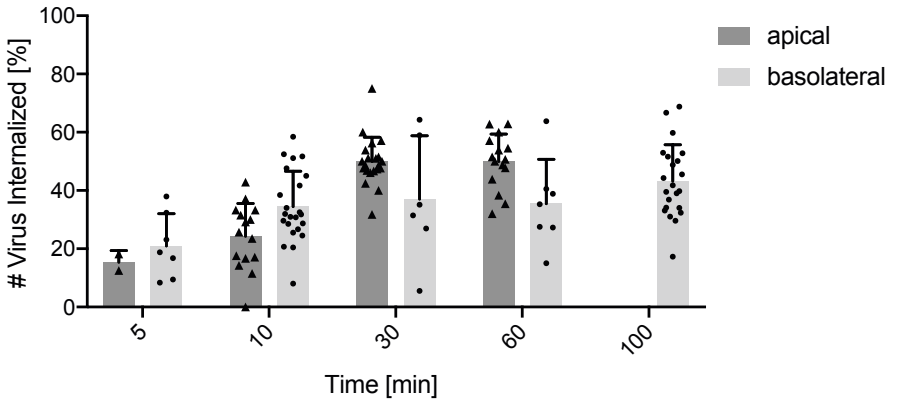

Figure A.4: Uptake of reovirus particles from the apical versus basolateral side. Percentage of reoviruses internalized into HeLa cells from the apical side were analyzed by confocal microscopy 5, 10, 30 and 60 min after addition of soluble reoviruses (see Section 7.5.2). Internalization from the basolateral cell-side of biotin-NeutrAvidin immobilized reoviruses was determined at the indicated time points after initial cell spreading with respect to the local concentration of reoviruses in the background (see Section 7.4).

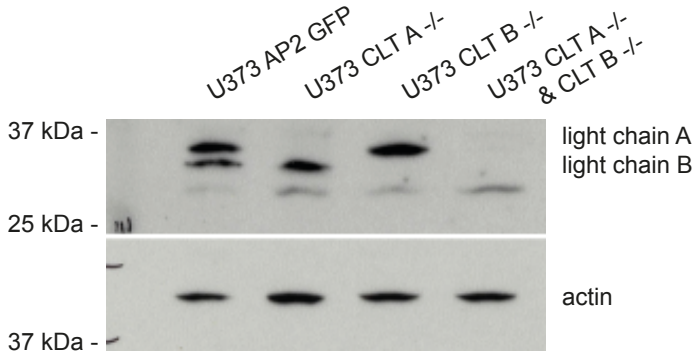

Figure A.5: Western blot of U373 CLT KO cells. U373 cells were transformed by CRISPR/CAS9 and checked for deletion of CLT A and B by Markus Mukenhirn (lab of Dr. Steeve Boulant, Heidelberg University and DKFZ).

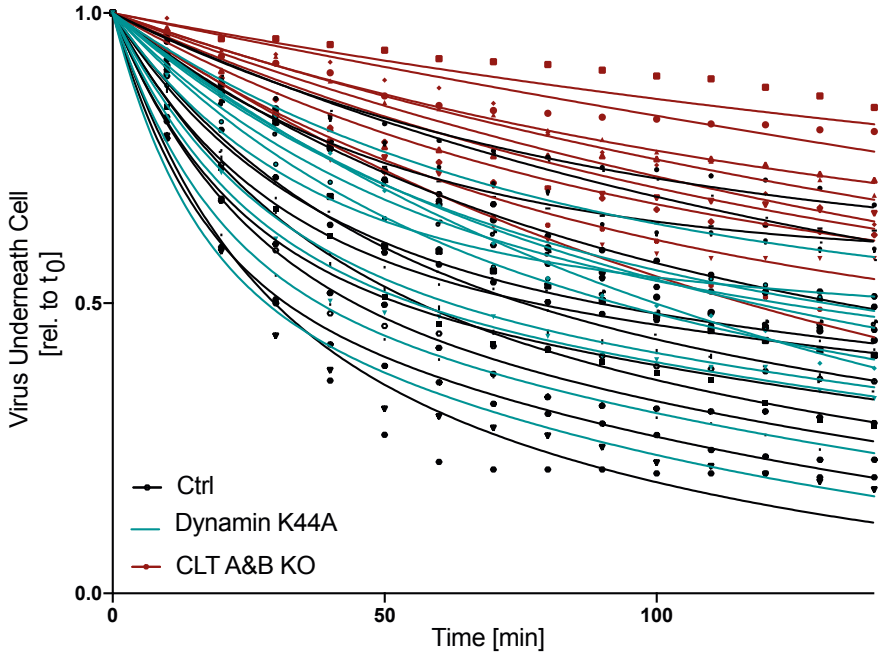

Figure A.6: Virus uptake kinetics upon inhibition of dynamin or clathrin light chain. U373 wildtype cells (Ctrl, black), or cells overexpressing the dynamin mutant K44A (turquoise), or with a double knockout of clathrin light chain (CLT A&B KO, red) were seeded on biotin-NeutrAvidin immobilized reovirus particles. Relative number of reoviruses underneath the cells over time with individual two phase decay-fits.

BIBLIOGRAPHY

[1] Adam J Engler, Shamik Sen, H Lee Sweeney, and Dennis E Discher. "Matrix elasticity directs stem cell lineage specification." In: *Cell* 126.4 (Aug. 2006), pp. 677–89. DOI: 10.1016/j.cell.2006.06.044 (cit. on p. 3).

[2] Wayne A Orr, Brian P Helmke, Brett R Blackman, and Martin A Schwartz. "Mechanisms of mechanotransduction." In: *Developmental cell* 10.1 (Jan. 2006), pp. 11–20. DOI: 10.1016/j.devcel.2005.12.006 (cit. on p. 3).

[3] Ulrich S Schwarz and Margaret L Gardel. "United we stand - integrating the actin cytoskeleton and cell-matrix adhesions in cellular mechanotransduction." In: *Journal of cell science* 125.Pt 13 (July 2012), pp. 3051–60. DOI: 10.1242/jcs.093716 (cit. on pp. 3, 4).

[4] Brenton D Hoffman, Carsten Grashoff, and Martin A Schwartz. "Dynamic molecular processes mediate cellular mechanotransduction." In: *Nature* 475.7356 (July 2011), pp. 316–23. DOI: 10.1038/nature10316 (cit. on p. 3).

[5] Bruce Alberts, Alexander Johnson, Julian Lewis, Martin Raff, Keith Roberts, and Peter Walter. *Molecular Biology of the Cell*. 5th ed. New York: Garland Science, 2008 (cit. on pp. 3, 4, 11).

[6] Thomas Iskratsch, Haguy Wolfenson, and Michael P. Sheetz. "Appreciating force and shape — the rise of mechanotransduction in cell biology." In: *Nature Reviews Molecular Cell Biology* 15.12 (2014), pp. 825–833. DOI: 10.1038/nrm3903 (cit. on p. 3).

[7] Daniel A Fletcher and R Dyche Mullins. "Cell mechanics and the cytoskeleton." In: *Nature* 463.7280 (2010), pp. 485–492. DOI: 10.1038/nature08908 (cit. on p. 3).

[8] Ulrich S. Schwarz and Samuel a. Safran. "Physics of adherent cells." In: *Reviews of Modern Physics* 85.3 (2013), pp. 1327–1381. DOI: 10.1103/RevModPhys.85.1327. arXiv: 1309.2817 (cit. on p. 4).

[9] M. Footer, J. Kerssemakers, J. Theriot, and Marileen Dogterom. "Direct measurement of force generation by actin filament polymerization using an optical trap." In: *Proceedings of the National Academy of Sciences* 104.7 (2007), pp. 2181–2186. DOI: 10.1073/pnas.0607052104 (cit. on p. 4).

[10] Martin Streichfuss, Friedrich Erbs, Kai Uhrig, Rainer Kurre, Anabel E M Clemen, Christian H J Böhm, Tamás Haraszti, and Joachim P Spatz. "Measuring forces between two single actin filaments during bundle formation." In: *Nano Letters* 11.9 (2011), pp. 3676–3680. DOI: 10.1021/nl201630y (cit. on p. 4).

[11] Scot C Kuo and Michael P Sheetz. "Force of single kinesin molecules measured with optical tweezers." In: *Science* 260.5105 (1993), pp. 232–234. DOI: 10.1126/science.8469975 (cit. on p. 4).

[12] Jeffrey T. Finer, Robert M. Simmons, and James A. Spudich. "Single myosin molecule mechanics: piconewton forces and nanometre steps." In: *Nature* 368.6467 (1994), pp. 113–119. DOI: 10.1038/368113a0 (cit. on p. 4).

[13] Gretchen Baneyx, Loren Baugh, and Viola Vogel. "Fibronectin extension and unfolding within cell matrix fibrils controlled by cytoskeletal tension." In: *Proceedings of the National Academy of Sciences of the United States of America* 99.8 (2002), pp. 5139–5143. DOI: 10.1073/pnas.072650799 (cit. on p. 4).

[14] Elaine P S Gee, Donald E Ingber, and Collin M Stultz. "Fibronectin unfolding revisited: Modeling cell traction-mediated unfolding of the tenth type-III repeat." In: *PLoS ONE* 3.6 (2008), e2373. DOI: 10.1371/journal.pone.0002373 (cit. on p. 4).

[15] Pirta Hotulainen and Pekka Lappalainen. "Stress fibers are generated by two distinct actin assembly mechanisms in motile cells." In: *The Journal of cell biology* 173.3 (May 2006), pp. 383–94. DOI: 10.1083/jcb.200511093 (cit. on p. 4).

[16] Anne J. Ridley, Martin A Schwartz, Keith Burridge, Richard A Firtel, Mark H Ginsberg, Gary Borisy, J Thomas Parsons, and Alan Rick Horwitz. "Cell migration: integrating signals from front to back." In: *Science (New York, N.Y.)* 302.5651 (Dec. 2003), pp. 1704–9. DOI: 10.1126/science.1092053 (cit. on p. 4).

[17] M Fritzsche, D Li, H Colin-York, V T Chang, E Moeendarbary, J H Felce, E Sezgin, G Charras, E Betzig, and C Eggeling. "Self-organizing actin patterns shape membrane architecture but not cell mechanics." In: *Nature Communications* 8 (2017), p. 14347. DOI: 10.1038/ncomms14347 (cit. on p. 4).

[18] Marcus Prass, Ken Jacobson, Alex Mogilner, and Manfred Radmacher. "Direct measurement of the lamellipodial protrusive force in a migrating cell." In: *The Journal of cell biology* 174.6 (Sept. 2006), pp. 767–72. DOI: 10.1083/jcb.200601159 (cit. on p. 4).

[19] David R Kovar and Thomas D Pollard. "Insertional assembly of actin filament barbed ends in association with formins produces piconewton forces." In: *Proceedings of the National Academy of Sciences of the United States of America* 101.41 (Oct. 2004), pp. 14725–30. DOI: 10.1073/pnas.0405902101 (cit. on p. 4).

[20] M. Bindschadler and J. L. McGrath. "Formin' new ideas about actin filament generation." In: *Proceedings of the National Academy of Sciences* 101.41 (2004), pp. 14685–14686. DOI: 10.1073/pnas.0406317101 (cit. on p. 4).

[21] A Mogilner and B Rubinstein. "The physics of filopodial protrusion." In: *Biophysical journal* 89.2 (Aug. 2005), pp. 782–95. DOI: 10.1529/biophysj.104.056515 (cit. on p. 4).

[22] Serge Dmitrieff and François Nédélec. "Amplification of actin polymerization forces." In: *The Journal of cell biology* 212.7 (Mar. 2016), pp. 763–6. DOI: 10.1083/jcb.201512019 (cit. on p. 4).

[23] Herbert B Schiller et al. "β1- and αv-class integrins cooperate to regulate myosin II during rigidity sensing of fibronectin-based microenvironments." In: *Nature cell biology* 15.6 (June 2013), pp. 625–36. DOI: 10.1038/ncb2747 (cit. on pp. 4, 6, 11).

[24] Carlos Mas-Moruno, Florian Rechenmacher, and Horst Kessler. "Cilengitide: The First Anti-Angiogenic Small Molecule Drug Candidate. Design, Synthesis and Clinical Evaluation." In: *Anti-Cancer Agents in Medicinal Chemistry* 10.10 (Dec. 2010), pp. 753–768. DOI: 10.2174/187152010794728639 (cit. on p. 5).

[25] Sanford J Shattil, Chungho Kim, and Mark H Ginsberg. "The final steps of integrin activation: the end game." In: *Nature reviews. Molecular cell biology* 11.4 (Apr. 2010), pp. 288–300. DOI: 10.1038/nrm2871 (cit. on pp. 5, 84).

[26] C G Knight, Laurence F Morton, Anthony R Peachey, Danny S Tuckwell, Richard W Farndale, and M J Barnes. "The collagen-binding A-domains of integrins alpha(1)beta(1) and alpha(2)beta(1) recognize the same specific amino acid sequence, GFOGER, in native (triple-helical) collagens." In: *The Journal of biological chemistry* 275.1 (2000), pp. 35–40. DOI: 10.1074/jbc.275.1.35 (cit. on p. 5).

[27] Jonathan D Humphries, Adam Byron, and Martin J Humphries. "Integrin ligands at a glance." In: *Journal of cell science* 119.Pt 19 (Oct. 2006), pp. 3901–3. DOI: 10.1242/jcs.03098 (cit. on pp. 5, 84).

[28] Benjamin Geiger, Joachim P Spatz, and Alexander D Bershadsky. "Environmental sensing through focal adhesions." In: *Nature reviews. Molecular cell biology* 10.1 (Jan. 2009), pp. 21–33. DOI: 10.1038/nrm2593 (cit. on pp. 5, 6).

[29] Patrick W Oakes, Yvonne Beckham, Jonathan Stricker, and Margaret L Gardel. "Tension is required but not sufficient for focal adhesion maturation without a stress fiber template." In: *The Journal of cell biology* 196.3 (Feb. 2012), pp. 363–74. DOI: 10.1083/jcb.201107042 (cit. on p. 5).

[30] Sirio Dupont et al. "Role of YAP/TAZ in mechanotransduction." In: *Nature* 474.7350 (June 2011), pp. 179–83. DOI: 10.1038/nature10137. arXiv: NIHMS150003 (cit. on p. 5).

[31] Boon Chuan Low, Catherine Qiurong Pan, G V Shivashankar, Alexander Bershadsky, Marius Sudol, and Michael Sheetz. "YAP/TAZ as mechanosensors and mechanotransducers in regulating organ size and tumor growth." In: *FEBS letters* 588.16 (Aug. 2014), pp. 2663–70. DOI: 10.1016/j.febslet.2014.04.012 (cit. on p. 5).

[32] Alberto Elosegui-Artola, Roger Oria, Yunfeng Chen, Anita Kosmalska, Carlos Pérez-González, Natalia Castro, Cheng Zhu, Xavier Trepat, and Pere Roca-Cusachs. "Mechanical regulation of a molecular clutch defines force transmission and transduction in response to matrix rigidity." In: *Nature cell biology* 18.5 (2016), pp. 540–548. DOI: 10.1038/ncb3336 (cit. on pp. 5, 6, 11).

[33] Antonio Totaro, Martina Castellan, Giusy Battilana, Francesca Zanconato, Luca Azzolin, Stefano Giulitti, Michelangelo Cordenonsi, and Stefano Piccolo. "YAP/TAZ link cell mechanics to Notch signalling to control epidermal stem cell fate." In: *Nature communications* 8 (May 2017), p. 15206. DOI: 10.1038/ncomms15206 (cit. on p. 5).

[34] Tito Panciera, Luca Azzolin, Michelangelo Cordenonsi, and Stefano Piccolo. "Mechanobiology of YAP and TAZ in physiology and disease." In: *Nature reviews. Molecular cell biology* (Sept. 2017). DOI: 10.1038/nrm.2017.87 (cit. on p. 5).

[35] Dimitris Missirlis, Tamás Haraszti, Catharina v. C. Scheele, Tina Wiegand, Carolina Diaz, Stefanie Neubauer, Florian Rechenmacher, Horst Kessler, and Joachim P Spatz. "Substrate engagement of integrins $\alpha 5\beta 1$ and $\alpha v\beta 3$ is necessary, but not sufficient, for high directional persistence in migration on fibronectin." In: *Scientific Reports* 6.November 2015 (2016), p. 23258. DOI: 10.1038/srep23258 (cit. on p. 6).

[36] Jay D. Humphrey, Eric R. Dufresne, and Martin a. Schwartz. "Mechanotransduction and extracellular matrix homeostasis." In: *Nature Reviews Molecular Cell Biology* 15.12 (Oct. 2014), pp. 802–812. DOI: 10.1038/nrm3896 (cit. on p. 6).

[37] Ingmar Schoen, Beth L. Pruitt, and Viola Vogel. "The Yin-Yang of Rigidity Sensing: How Forces and Mechanical Properties Regulate the Cellular Response to Materials." In: *Annual Review of Materials Research* 43.1 (2013), pp. 589–618. DOI: 10.1146/annurev-matsci-062910-100407 (cit. on pp. 6, 11).

[38] Margaret L Gardel, Benedikt Sabass, Lin Ji, Gaudenz Danuser, Ulrich S Schwarz, and Clare M Waterman. "Traction stress in focal adhesions correlates biphasically with actin retrograde flow speed." In: *The Journal of cell biology* 183.6 (Dec. 2008), pp. 999–1005. DOI: 10.1083/jcb.200810060 (cit. on p. 6).

[39] E. C. Yusko and C. L. Asbury. "Force is a signal that cells cannot ignore." In: *Molecular Biology of the Cell* 25.23 (2014), pp. 3717–3725. DOI: 10.1091/mbc.E13-12-0707 (cit. on pp. 6, 7).

[40] Alberto Elosegui-Artola et al. "Rigidity sensing and adaptation through regulation of integrin types." In: *Nature materials* May (2014). DOI: 10.1038/NMAT3960 (cit. on pp. 6, 11, 30, 45, 104).

[41] Marco Arnold, Elisabetta Ada Cavalcanti-Adam, Roman Glass, Jacques Blümmel, Wolfgang Eck, Martin Kantlehner, Horst Kessler, and Joachim P Spatz. "Activation of integrin function by nanopatterned adhesive interfaces." In: *Chemphyschem : a European journal of chemical physics and physical chemistry* 5.3 (Mar. 2004), pp. 383–8. DOI: 10.1002/cphc.200301014 (cit. on pp. 6, 12, 29, 56, 95).

[42] Elisabetta Ada Cavalcanti-Adam, Tova Volberg, Alexandre Micoulet, Horst Kessler, Benjamin Geiger, and Joachim P Spatz. "Cell spreading and focal adhesion dynamics are regulated by spacing of integrin ligands." In: *Biophysical journal* 92.8 (Apr. 2007), pp. 2964–74. DOI: 10.1529/biophysj.106.089730 (cit. on pp. 6, 29, 58, 95).

[43] Jinghuan Huang, Stefan V Gräter, Francesca Corbellini, Sabine Rinck-jahnke, Ralf Kemkemer, Horst Kessler, Jiandong Ding, and Joachim P Spatz. "Impact of Order and Disorder in RGD Nanopatterns on Cell Adhesion." In: *Nano letters* 9.3 (2009), pp. 1111–1116. DOI: 10.1021/nl803548b.Impact (cit. on pp. 6, 12, 29, 56).

[44] Israel Patla, Tova Volberg, Nadav Elad, Vera Hirschfeld-Warneken, Carsten Grashoff, Reinhard Fässler, Joachim P Spatz, Benjamin Geiger, and Ohad Medalia. "Dissecting the

molecular architecture of integrin adhesion sites by cryo-electron tomography." In: *Nature cell biology* 12.9 (Sept. 2010), pp. 909–15. DOI: 10.1038/ncb2095 (cit. on p. 6).

[45] Mark Schvartzman, Matteo Palma, Julia Sable, Justin Abramson, Xian Hu, Michael P Sheetz, and Shalom J Wind. "Nanolithographic control of the spatial organization of cellular adhesion receptors at the single-molecule level." In: *Nano letters* 11.3 (Mar. 2011), pp. 1306–12. DOI: 10.1021/nl104378f (cit. on p. 6).

[46] Ulrich S Schwarz, N Q Balaban, D Riveline, A Bershadsky, Benjamin Geiger, and S a Safran. "Calculation of forces at focal adhesions from elastic substrate data: the effect of localized force and the need for regularization." In: *Biophysical journal* 83.3 (Sept. 2002), pp. 1380–94. DOI: 10.1016/S0006-3495(02)73909-X (cit. on pp. 6, 9, 12).

[47] Fang Kong, Andrés J García, A. Paul Mould, Martin J Humphries, and Cheng Zhu. "Demonstration of catch bonds between an integrin and its ligand." In: *The Journal of cell biology* 185.7 (June 2009), pp. 1275–84. DOI: 10.1083/jcb.200810002 (cit. on pp. 6, 104).

[48] Fang Kong, Zhenhai Li, William M Parks, David W Dumbauld, Andrés J García, a Paul Mould, Martin J Humphries, and Cheng Zhu. "Cyclic mechanical reinforcement of integrin-ligand interactions." In: *Molecular cell* 49.6 (Mar. 2013), pp. 1060–8. DOI: 10.1016/j.molcel.2013.01.015 (cit. on p. 6).

[49] Xuefeng Wang and Taekjip Ha. "Defining Single Molecular Forces Required to Activate Integrin and Notch Signaling." In: *Science* 7219.May (2013), pp. 991–994 (cit. on pp. 6, 10–12).

[50] Yongliang Wang and Xuefeng Wang. "Integrins outside focal adhesions transmit tensions during stable cell adhesion." In: *Scientific reports* 6.July (Nov. 2016), p. 36959. DOI: 10.1038/srep36959 (cit. on pp. 6, 64, 96).

[51] Kornelia Galior, Yang Liu, Kevin Yehl, Skanda Vivek, and Khalid Salaita. "Titin-Based Nanoparticle Tension Sensors Map High-Magnitude Integrin Forces within Focal Adhesions." In: *Nano Letters* 16.1 (Jan. 2016), pp. 341–348. DOI: 10.1021/acs.nanolett.5b03888 (cit. on pp. 6, 11, 12, 37, 61, 64).

[52] Carol Jurchenko, Yuan Chang, Yoshie Narui, Yun Zhang, and Khalid Salaita. "Integrin-generated forces lead to streptavidin-biotin unbinding in cellular adhesions." In: *Biophysical journal* 106.7 (Apr. 2014), pp. 1436–46. DOI: 10.1016/j.bpj.2014.01.049 (cit. on pp. 6, 12, 73).

[53] Trang T Nguyen, Krystal L Sly, and John C Conboy. "Comparison of the energetics of avidin, streptavidin, neutrAvidin, and anti-biotin antibody binding to biotinylated lipid bilayer examined by second-harmonic generation." In: *Analytical Chemistry* 84.1 (2012), pp. 201–208. DOI: 10.1021/ac202375n (cit. on pp. 6, 75).

[54] Vincent T Moy, Ernst-Ludwig Florin, and Hermann E Gaub. "Intermolecular forces and energies between ligands and receptors." In: *Science* 266.5183 (Oct. 1994), pp. 257–259. DOI: 10.1126/science.7939660 (cit. on p. 6).

[55] Rudolf Merkel, P. Nassoy, A. Leung, K. Ritchie, and Evan Evans. "Energy landscapes of receptor–ligand bonds explored with dynamic force spectroscopy." In: *Nature* 397.6714 (Jan. 1999), pp. 50–53. DOI: 10.1038/16219 (cit. on pp. 6, 8, 74).

[56] Chunbo Yuan, Aileen Chen, Pamela Kolb, and Vincent T Moy. "Energy Landscape of Streptavidin-Biotin Complexes Measured by Atomic Force Microscopy." In: *Biochemistry* 39.33 (Aug. 2000), pp. 10219–10223. DOI: 10.1021/bi992715o (cit. on p. 6).

[57] Mark C Leake. *Biophysics: Tools and Techniques*. CRC Press, 2016, pp. 42–46 (cit. on p. 6).

[58] Charles S Peskin, Garrett M Odell, and George F Oster. "Cellular motions and thermal fluctuations: the Brownian ratchet." In: *Biophysical journal* 65.1 (July 1993), pp. 316–24. DOI: 10.1016/S0006-3495(93)81035-X (cit. on p. 7).

[59] K D Sattler. *Handbook of Nanophysics: Nanomedicine and Nanorobotics*. Vol. 9. 1. May 2010, pp. 94–96 (cit. on pp. 7, 8).

[60] Evan Evans and Ken Ritchie. "Dynamic strength of molecular adhesion bonds." In: *Biophysical Journal* 72.4 (Apr. 1997), pp. 1541–1555. DOI: 10.1016/S0006-3495(97)78802-7 (cit. on pp. 7, 8).

[61] David Alsteens, Moritz Pfreundschuh, Cheng Zhang, Patrizia M Spoerri, Shaun R Coughlin, Brian K Kobilka, and Daniel J Müller. "Imaging G protein-coupled receptors while quantifying their ligand-binding free-energy landscape." In: *Nature methods* 12.9 (Sept. 2015), pp. 845–851. DOI: 10.1038/nmeth.3479 (cit. on p. 8).

[62] G Bell. "Models for the specific adhesion of cells to cells." In: *Science* 200.4342 (May 1978), pp. 618–627. DOI: 10.1126/science.347575 (cit. on p. 7).

[63] Evan A Evans and David A Calderwood. "Forces and Bond Dynamics in Cell Adhesion." In: *Science* 316.5828 (May 2007), pp. 1148–1153. DOI: 10.1126/science.1137592 (cit. on p. 8).

[64] Emily B Walton, Sunyoung Lee, and Krystyn J Van Vliet. "Extending Bell's model: how force transducer stiffness alters measured unbinding forces and kinetics of molecular complexes." In: *Biophysical journal* 94.7 (2008), pp. 2621–2630. DOI: 10.1529/biophysj.107.114454 (cit. on p. 8).

[65] William J Polacheck and Christopher S Chen. "Measuring cell-generated forces: a guide to the available tools." In: *Nature Methods* 13.5 (2016), pp. 415–423. DOI: 10.1038/nmeth.3834 (cit. on pp. 8, 9).

[66] AK Harris, P Wild, and D Stopak. "Silicone rubber substrata: a new wrinkle in the study of cell locomotion." In: *Science* 208.4440 (1980), pp. 177–179 (cit. on p. 8).

[67] John L Tan, Joe Tien, Dana M Pirone, Darren S Gray, Kiran Bhadriraju, and Christopher S Chen. "Cells lying on a bed of microneedles: an approach to isolate mechanical force." In: *Proceedings of the National Academy of Sciences of the United States of America* 100.4 (Feb. 2003), pp. 1484–9. DOI: 10.1073/pnas.0235407100 (cit. on pp. 9, 12).

[68] Pere Roca-Cusachs, Vito Conte, and Xavier Trepat. "Quantifying forces in cell biology." In: *Nature Cell Biology* 19.7 (2017), pp. 742–751. DOI: 10.1038/ncb3564 (cit. on p. 9).

[69] James H-C Wang and Jeen-Shang Lin. "Cell traction force and measurement methods." In: *Biomechanics and modeling in mechanobiology* 6.6 (Nov. 2007), pp. 361–71. DOI: 10.1007/s10237-006-0068-4 (cit. on p. 9).

[70] James P Butler, Iva Marija Tolić-Nørrelykke, Ben Fabry, and Jeffrey J Fredberg. "Traction fields, moments, and strain energy that cells exert on their surroundings." In: *American journal of physiology. Cell physiology* 282.3 (Mar. 2002), pp. C595–605. DOI: 10.1152/ajpcell.00270.2001 (cit. on p. 9).

[71] Benedikt Sabass, Margaret L Gardel, Clare M Waterman, and Ulrich S Schwarz. "High resolution traction force microscopy based on experimental and computational advances." In: *Biophysical journal* 94.1 (Jan. 2008), pp. 207–20. DOI: 10.1529/biophysj.107.113670 (cit. on p. 9).

[72] N Q Balaban et al. "Force and focal adhesion assembly: a close relationship studied using elastic micropatterned substrates." In: *Nature cell biology* 3.5 (May 2001), pp. 466–72. DOI: 10.1038/35074532 (cit. on p. 9).

[73] Huw Colin-York, Dilip Shrestha, James H. Felce, Dominic Waithe, Emad Moeendarbary, Simon J. Davis, Christian Eggeling, and Marco Fritzsche. "Super-Resolved Traction Force Microscopy (STFM)." In: *Nano Letters* 16.4 (2016),

pp. 2633–2638. DOI: 10.1021/acs.nanolett.6b00273 (cit. on p. 9).

[74] Wesley R Legant, Jordan S Miller, Brandon L Blakely, Daniel M Cohen, Guy M Genin, and Christopher S Chen. "Measurement of mechanical tractions exerted by cells in three-dimensional matrices." In: *Nature methods* 7.12 (Dec. 2010), pp. 969–71. DOI: 10.1038/nmeth.1531 (cit. on pp. 9, 96).

[75] Martin Bergert et al. "Confocal reference free traction force microscopy." In: *Nature communications* 7 (Sept. 2016), p. 12814. DOI: 10.1038/ncomms12814 (cit. on pp. 10, 32, 96).

[76] Carol Jurchenko and Khalid Salaita. "Lighting up the Force: Investigating Mechanisms of Mechanotransduction Using Fluorescent Tension Probes." In: *Molecular and Cellular Biology* 35:15.August (2015), pp. 2570–2582. DOI: 10.1128/MCB.00195-15 (cit. on pp. 10, 69).

[77] Anna-Lena Cost, Pia Ringer, Anna Chrostek-Grashoff, and Carsten Grashoff. "How to Measure Molecular Forces in Cells: A Guide to Evaluating Genetically-Encoded FRET-Based Tension Sensors." In: *Cellular and Molecular Bioengineering* 8.1 (Mar. 2015), pp. 96–105. DOI: 10.1007/s12195-014-0368-1 (cit. on p. 10).

[78] Thomas Pons. "On the Quenching of Semiconductor Quantum Dot Photoluminescence by Proximal Gold Nanoparticles." In: *Nano Letters* 7.10 (2007), pp. 3157–3164 (cit. on p. 10).

[79] Yang Liu, Kevin Yehl, Yoshie Narui, and Khalid Salaita. "Tension sensing nanoparticles for mechano-imaging at the living/nonliving interface." In: *Journal of the American Chemical Society* 135.14 (Apr. 2013), pp. 5320–3. DOI: 10.1021/ja401494e (cit. on pp. 10–12, 25, 34, 35, 61, 70).

[80] Rahul Chhabra, Jaswinder Sharma, Haining Wang, Shengli Zou, Su Lin, Hao Yan, Stuart Lindsay, and Yan Liu. "Distance-dependent interactions between gold nanoparticles and fluorescent molecules with DNA as tunable spacers." In: *Nanotechnology* 20.48 (Dec. 2009), p. 485201. DOI: 10.1088/0957-4484/20/48/485201 (cit. on p. 10).

[81] C S Yun, A Javier, T Jennings, M Fisher, S Hira, S Peterson, B Hopkins, N O Reich, and G F Strouse. "Nanometal surface energy transfer in optical rulers, breaking the FRET barrier." In: *Journal of the American Chemical Society* 127.9 (Mar. 2005), pp. 3115–9. DOI: 10.1021/ja043940i (cit. on p. 10).

[82] Yang Liu, Rebecca Medda, Zheng Liu, Kornelia Galior, Kevin Yehl, Joachim P Spatz, Elisabetta Ada Cavalcanti-adam, and Khalid Salaita. "Nanoparticle Tension Probes Patterned at the

Nanoscale: Impact of Integrin Clustering on Force Transmission." In: *Nano letters* 14 (2014), pp. 5539–5546 (cit. on pp. 10, 11, 25, 34, 35).

[83] Sosuke Iwai and Taro Q P Uyeda. "Visualizing myosin-actin interaction with a genetically-encoded fluorescent strain sensor." In: *Proceedings of the National Academy of Sciences of the United States of America* 105.44 (Nov. 2008), pp. 16882–7. DOI: 10.1073/pnas.0805513105 (cit. on pp. 10, 11).

[84] I Gautier, M Tramier, C Durieux, J Coppey, R B Pansu, J C Nicolas, K Kemnitz, and M Coppey-Moisan. "Homo-FRET microscopy in living cells to measure monomer-dimer transition of GFP-tagged proteins." In: *Biophysical journal* 80.6 (June 2001), pp. 3000–8. DOI: 10.1016/S0006-3495(01)76265-0 (cit. on p. 10).

[85] Carsten Grashoff et al. "Measuring mechanical tension across vinculin reveals regulation of focal adhesion dynamics." In: *Nature* 466.7303 (July 2010), pp. 263–6. DOI: 10.1038/nature09198 (cit. on p. 10).

[86] Nicolas Borghi, Maria Sorokina, Olga G Shcherbakova, William I Weis, Beth L Pruitt, W James Nelson, and Alexander R Dunn. "E-cadherin is under constitutive actin." In: *Proceedings of the National Academy of Sciences* 31109.10 (2012), pp. 12568–12573 (cit. on p. 10).

[87] Daniel E Conway, Mark T Breckenridge, Elizabeth Hinde, Enrico Gratton, Christopher S Chen, and Martin A Schwartz. "Fluid shear stress on endothelial cells modulates mechanical tension across VE-cadherin and PECAM-1." In: *Current biology : CB* 23.11 (June 2013), pp. 1024–30. DOI: 10.1016/j.cub.2013.04.049. arXiv: NIHMS150003 (cit. on p. 10).

[88] Michael Krieg, Alexander R Dunn, and Miriam B Goodman. "Mechanical control of the sense of touch by β-spectrin." In: *Nature cell biology* 16.3 (Mar. 2014), pp. 224–33. DOI: 10.1038/ncb2915 (cit. on p. 10).

[89] Fanjie Meng and Frederick Sachs. "Visualizing dynamic cytoplasmic forces with a compliance-matched FRET sensor." In: *Journal of cell science* 124.Pt 2 (), pp. 261–9. DOI: 10.1242/jcs.071928 (cit. on p. 11).

[90] Masatoshi Morimatsu, Armen H Mekhdjian, Arjun S Adhikari, and Alexander R Dunn. "Molecular tension sensors report forces generated by single integrin molecules in living cells." In: *Nano letters* 13.9 (Sept. 2013), pp. 3985–9. DOI: 10.1021/nl4005145 (cit. on pp. 11, 12).

[91] Masatoshi Morimatsu, Armen Haig Mekhdjian, Alice Chun-Chii Chang, Steven John Tan, and Alexander R Dunn. "Visualizing the interior architecture of focal adhesions with high-resolution traction maps." In: *Nano Letters* (2015), p. 150302160837001. DOI: 10.1021/nl5047335 (cit. on p. 11).

[92] DR Stabley, Carol Jurchenko, SS Marshall, and Khalid Salaita. "Visualizing mechanical tension across membrane receptors with a fluorescent sensor." In: *Nature methods* 9.1 (2012). DOI: 10.1038/nMeth.1747 (cit. on pp. 11, 22, 23, 25, 69, 78).

[93] Joachim P Spatz, S Mößmer, and M Möller. "Mineralization of gold nanoparticles in a block copolymer microemulsion." In: *Chemistry-A European Journal* 731 (1996), pp. 1552–1555 (cit. on p. 11).

[94] Joachim P Spatz, Sergei Sheiko, and M Möller. "Ion-stabilized block copolymer micelles: film formation and intermicellar interaction." In: *Macromolecules* (1996), pp. 3220–3226 (cit. on p. 11).

[95] Roman Glass, Martin Müller, and Joachim P Spatz. "Block copolymer micelle nanolithography." In: *Nanotechnology* 14.10 (Oct. 2003), pp. 1153–1160. DOI: 10.1088/0957-4484/14/10/314 (cit. on pp. 11, 29).

[96] Majid Mosayebi, Ard A. Louis, Jonathan P. K. Doye, and Thomas E. Ouldridge. "Force-Induced Rupture of a DNA Duplex: From Fundamentals to Force Sensors." In: *ACS Nano* 9.12 (Dec. 2015), pp. 11993–12003. DOI: 10.1021/acsnano.5b04726 (cit. on p. 11).

[97] Yun Zhang, Chenghao Ge, Cheng Zhu, and Khalid Salaita. "DNA-based digital tension probes reveal integrin forces during early cell adhesion." In: *Nature Communications* 5 (Oct. 2014), p. 5167. DOI: 10.1038/ncomms6167 (cit. on pp. 11, 25, 36, 61, 70).

[98] Brandon L Blakely et al. "A DNA-based molecular probe for optically reporting cellular traction forces." In: *Nature Methods* October (Oct. 2014), pp. 1–8. DOI: 10.1038/nmeth.3145 (cit. on p. 11).

[99] Démosthène Mitrossilis, Jonathan Fouchard, David Pereira, François Postic, Alain Richert, Michel Saint-Jean, and Atef Asnacios. "Real-time single-cell response to stiffness." In: *Proceedings of the National Academy of Sciences of the United States of America* 107.38 (2010), pp. 16518–23. DOI: 10.1073/pnas.1007940107 (cit. on p. 11).

[100] Léa Trichet, Jimmy Le Digabel, Rhoda J Hawkins, Sri Ram Krishna Vedula, Mukund Gupta, Claire Ribrault, Pascal Hersen, Raphaël Voituriez, and Benoît Ladoux. "Evidence of a large-scale mechanosensing mechanism for cellular adaptation to substrate stiffness." In: *Proceedings of the National Academy of Sciences of the United States of America* 109.18 (May 2012), pp. 6933–8. DOI: 10.1073/pnas.1117810109 (cit. on p. 11).

[101] Jocelyn Étienne, Jonathan Fouchard, Démosthène Mitrossilis, Nathalie Bufi, Pauline Durand-Smet, and Atef Asnacios. "Cells as liquid motors: mechanosensitivity emerges from collective dynamics of actomyosin cortex." In: *Proceedings of the National Academy of Sciences of the United States of America* 112.9 (2015), pp. 2740–5. DOI: 10.1073/pnas.1417113112. arXiv: 1407.2765 (cit. on p. 11).

[102] Elisabetta Ada Cavalcanti-Adam, Alexandre Micoulet, Jacques Blümmel, Jörg Auernheimer, Horst Kessler, and Joachim P Spatz. "Lateral spacing of integrin ligands influences cell spreading and focal adhesion assembly." In: *European journal of cell biology* 85.3-4 (Apr. 2006), pp. 219–24. DOI: 10.1016/j.ejcb.2005.09.011 (cit. on pp. 12, 29, 56, 95).

[103] Eva Altrock, Christine A Muth, Gerd Klein, Joachim P Spatz, and Cornelia Lee-Thedieck. "The significance of integrin ligand nanopatterning on lipid raft clustering in hematopoietic stem cells." In: *Biomaterials* 33.11 (Apr. 2012), pp. 3107–18. DOI: 10.1016/j.biomaterials.2012.01.002 (cit. on pp. 12, 56).

[104] Katharina Amschler, Luise Erpenbeck, Sebastian Kruss, and Michael P Schön. "Nanoscale integrin ligand patterns determine melanoma cell behavior." In: *ACS nano* 8.9 (Sept. 2014), pp. 9113–25. DOI: 10.1021/nn502690b (cit. on p. 12).

[105] P.P. Lehenkari and M.A. Horton. "Single Integrin Molecule Adhesion Forces in Intact Cells Measured by Atomic Force Microscopy." In: *Biochemical and Biophysical Research Communications* 259.3 (June 1999), pp. 645–650. DOI: 10.1006/bbrc.1999.0827 (cit. on p. 12).

[106] Feiya Li, Sambra D Redick, Harold P Erickson, and Vincent T Moy. "Force Measurements of the $\alpha 5\beta 1$ Integrin–Fibronectin Interaction." In: *Biophysical Journal* 84.2 (Feb. 2003), pp. 1252–1262. DOI: 10.1016/S0006-3495(03)74940-6 (cit. on p. 12).

[107] Sulin Zhang, Huajian Gao, and Gang Bao. "Physical Principles of Nanoparticle Cellular Endocytosis." In: *ACS nano* 9.9 (2015), pp. 8655–8671 (cit. on pp. 13, 14, 21).

[108] Satyajit Mayor and Richard E Pagano. "Pathways of clathrin-independent endocytosis." In: *Nature reviews. Molecular cell biology* 8.8 (Aug. 2007), pp. 603–12. DOI: 10.1038/nrm2216 (cit. on pp. 13, 14).

[109] Katja Kettler, Karin Veltman, Dik van de Meent, Annemarie van Wezel, and A. Jan Hendriks. "Cellular uptake of nanoparticles as determined by particle properties, experimental conditions, and cell type." In: *Environmental Toxicology and Chemistry* 33.3 (2014), pp. 481–492. DOI: 10.1002/etc.2470 (cit. on p. 13).

[110] Huajian Gao, Wendong Shi, and Lambert B Freund. "Mechanics of receptor-mediated endocytosis." In: *Proceedings of the National Academy of Sciences of the United States of America* 102.27 (2005), pp. 9469–9474. DOI: 10.1073/pnas.0503879102 (cit. on p. 13).

[111] Carlos Rosales. *Molecular Mechanisms of Phagocytosis*. Vol. 5. Medical Intelligence Unit 10. Boston, MA: Springer US, Oct. 2005, a023473. DOI: 10.1007/978-0-387-28669-3 (cit. on p. 13).

[112] David M Richards and Robert G Endres. "The mechanism of phagocytosis: two stages of engulfment." In: *Biophysical journal* 107.7 (Oct. 2014), pp. 1542–53. DOI: 10.1016/j.bpj.2014.07.070. arXiv: 1410.7288 (cit. on p. 13).

[113] Harvey T McMahon and Emmanuel Boucrot. "Molecular mechanism and physiological functions of clathrin-mediated endocytosis." In: *Nature reviews. Molecular cell biology* 12.8 (July 2011), pp. 517–33. DOI: 10.1038/nrm3151 (cit. on p. 14).

[114] Ori Avinoam, Martin Schorb, Carsten J Beese, John A G Briggs, and Marko Kaksonen. "Endocytic sites mature by continuous bending and remodeling of the clathrin coat." In: *Science (New York, N.Y.)* 348.6241 (2015), pp. 1369–72. DOI: 10.1126/science.aaa9555 (cit. on p. 14).

[115] Delia Bucher, Felix Frey, Kem A Sochacki, and Susann Kummer. "Flat-to-curved transition during endocytosis correlates with a change in clathrin-adaptor ratio and is regulated by membrane tension." In: *bioRxiv* (2017). DOI: 10.1101/162024 (cit. on p. 14).

[116] Daniela Leyton-Puig, Tadamoto Isogai, Elisabetta Argenzio, Bram van den Broek, Jeffrey Klarenbeek, Hans Janssen, Kees Jalink, and Metello Innocenti. "Flat clathrin lattices are dynamic actin-controlled hubs for clathrin-mediated endocytosis and signalling of specific receptors." In: *Nature Communications* 8 (2017), p. 16068. DOI: 10.1038/ncomms16068 (cit. on p. 14).

[117] Tomas Kirchhausen. "Coated pits and coated vesicles - sorting it all out." In: *Current Opinion in Structural Biology* 3.2 (1993), pp. 182–188. DOI: 10.1016/S0959-440X(05)80150-2 (cit. on p. 14).

[118] Camilla Godlee and Marko Kaksonen. "Review series: From uncertain beginnings: initiation mechanisms of clathrin-mediated endocytosis." In: *The Journal of cell biology* 203.5 (Dec. 2013), pp. 717–25. DOI: 10.1083/jcb.201307100 (cit. on p. 14).

[119] Thorsten Brach, Camilla Godlee, Iben Moeller-Hansen, Dominik Boeke, and Marko Kaksonen. "The initiation of clathrin-mediated endocytosis is mechanistically highly flexible." In: *Current Biology* 24.5 (2014), pp. 548–554. DOI: 10.1016/j.cub.2014.01.048 (cit. on p. 14).

[120] Marko Lampe, Stéphane Vassilopoulos, and Christien Merrifield. "Clathrin coated pits, plaques and adhesion." In: *Journal of structural biology* 196.1 (Oct. 2016), pp. 48–56. DOI: 10.1016/j.jsb.2016.07.009 (cit. on p. 14).

[121] Joanna Rejman, Volker Oberle, Inge S Zuhorn, and Dick Hoekstra. "Size-dependent internalization of particles via the pathways of clathrin- and caveolae-mediated endocytosis." In: *The Biochemical journal* 377.Pt 1 (Jan. 2004), pp. 159–69. DOI: 10.1042/BJ20031253. arXiv: NIHMS150003 (cit. on p. 14).

[122] Satyajit Mayor, Robert G Parton, and Julie G Donaldson. "Clathrin-independent pathways of endocytosis." In: *Cold Spring Harbor Perspectives in Biology* 6.6 (2014). DOI: 10.1101/cshperspect.a016758 (cit. on p. 14).

[123] Gary J Doherty and Harvey T McMahon. "Mechanisms of endocytosis." In: *Annual review of biochemistry* 78.1 (2009), pp. 857–902. DOI: 10.1146/annurev.biochem.78.081307.110540 (cit. on p. 14).

[124] Olivia L Mooren, Brian J Galletta, and John A Cooper. "Roles for actin assembly in endocytosis." In: *Annual review of biochemistry* 81.1 (2012), pp. 661–86. DOI: 10.1146/annurev-biochem-060910-094416 (cit. on pp. 15, 88).

[125] Serge Dmitrieff and François Nédélec. "Membrane Mechanics of Endocytosis in Cells with Turgor." In: *PLoS computational biology* 11.10 (Oct. 2015), e1004538. DOI: 10.1371/journal.pcbi.1004538. arXiv: 1509.00698 (cit. on pp. 15, 18).

[126] Ludger Johannes, Robert G Parton, Patricia Bassereau, and Satyajit Mayor. "Building endocytic pits without clathrin." In: *Nature reviews. Molecular cell biology* 16.5 (2015), pp. 311–21. DOI: 10.1038/nrm3968. arXiv: NIHMS150003 (cit. on pp. 15, 19).

[127] Harvey T McMahon and Jennifer L Gallop. "Membrane curvature and mechanisms of dynamic cell membrane remodelling." In: *Nature* 438.7068 (Dec. 2005), pp. 590–6. DOI: 10.1038/nature04396 (cit. on pp. 15, 18, 89).

[128] Kevin Kendall, Michaela Kendall, and Florian Rehfeldt. *Adhesion of cells, viruses and nanoparticles*. 2011, pp. 1–282. DOI: 10.1007/978-90-481-2585-2. arXiv: arXiv:1011.1669v3 (cit. on pp. 16, 17, 76).

[129] R Lipowsky and H.-G. Döbereiner. "Vesicles in contact with nanoparticles and colloids." In: *Europhysics Letters (EPL)* 43.2 (July 1998), pp. 219–225. DOI: 10.1209/epl/i1998-00343-4 (cit. on p. 17).

[130] Bruno Antonny. "Mechanisms of Membrane Curvature Sensing." In: *Annual Review of Biochemistry* 80.1 (2011), pp. 101–123. DOI: 10.1146/annurev-biochem-052809-155121 (cit. on pp. 17, 18).

[131] Mijo Simunovic, Coline Prévost, Andrew Callan-Jones, and Patricia Bassereau. "Physical basis of some membrane shaping mechanisms." In: *Philosophical transactions. Series A, Mathematical, physical, and engineering sciences* 374.2072 (July 2016), p. 20160034. DOI: 10.1098/rsta.2016.0034 (cit. on pp. 17, 18).

[132] Henri-François Renard et al. "Endophilin-A2 functions in membrane scission in clathrin-independent endocytosis." In: *Nature* 517.7535 (Jan. 2015), pp. 493–6. DOI: 10.1038/nature14064 (cit. on p. 17).

[133] Bruno Marks, Michael H. B. Stowell, Yvonne Vallis, Ian G Mills, Adele Gibson, Colin R Hopkins, and Harvey T McMahon. "GTPase activity of dynamin and resulting conformation change are essential for endocytosis." In: *Nature* 410.6825 (Mar. 2001), pp. 231–235. DOI: 10.1038/35065645 (cit. on p. 17).

[134] Juha Saarikangas, Hongxia Zhao, and Pekka Lappalainen. "Regulation of the actin cytoskeleton-plasma membrane interplay by phosphoinositides." In: *Physiological reviews* 90.1 (Jan. 2010), pp. 259–89. DOI: 10.1152/physrev.00036.2009 (cit. on pp. 17, 18, 88).

[135] Mijo Simunovic, Gregory A Voth, Andrew Callan-Jones, and Patricia Bassereau. *When Physics Takes Over: BAR Proteins and Membrane Curvature*. 2015. DOI: 10.1016/j.tcb.2015.09.005. arXiv: 1401.1790 (cit. on p. 17).

[136] Kathryn R Ayscough, Joel Stryker, Navin Pokala, Miranda Sanders, Phil Crews, and David G Drubin. "High rates of actin filament turnover in budding yeast and roles for actin in establishment and maintenance of cell polarity revealed using the actin inhibitor latrunculin-A." In: *The Journal of cell biology*

137.2 (Apr. 1997), pp. 399–416. DOI: 10.1083/jcb.137.2.399 (cit. on p. 18).

[137] Kathryn R Ayscough. "Endocytosis and the development of cell polarity in yeast require a dynamic F-actin cytoskeleton." In: *Current biology : CB* 10.24 (2000), pp. 1587–90. DOI: 10.1016/S0960-9822(00)00859-9 (cit. on pp. 18, 88).

[138] Marko Kaksonen, Yidi Sun, and David G Drubin. "A Pathway for Association of Receptors, Adaptors, and Actin during Endocytic Internalization." In: *Cell* 115.4 (2003), pp. 475–487. DOI: 10.1016/S0092-8674(03)00883-3 (cit. on p. 18).

[139] Christien J Merrifield, Morris E Feldman, Lei Wan, and Wolfhard Almers. "Imaging actin and dynamin recruitment during invagination of single clathrin-coated pits." In: *Nature cell biology* 4.9 (Sept. 2002), pp. 691–8. DOI: 10.1038/ncb837 (cit. on pp. 18, 88).

[140] Christien J Merrifield, David Perrais, and David Zenisek. "Coupling between clathrin-coated-pit invagination, cortactin recruitment, and membrane scission observed in live cells." In: *Cell* 121.4 (May 2005), pp. 593–606. DOI: 10.1016/j.cell.2005.03.015 (cit. on p. 18).

[141] Defne Yarar, Clare M Waterman-Storer, and Sandra L Schmid. "A dynamic actin cytoskeleton functions at multiple stages of clathrin-mediated endocytosis." In: *Molecular biology of the cell* 16.2 (Feb. 2005), pp. 964–75. DOI: 10.1091/mbc.E04-09-0774 (cit. on p. 18).

[142] Soheil Aghamohammadzadeh and Kathryn R Ayscough. "Differential requirements for actin during yeast and mammalian endocytosis." In: *Nature cell biology* 11.8 (Aug. 2009), pp. 1039–42. DOI: 10.1038/ncb1918 (cit. on p. 18).

[143] Steeve Boulant, Comert Kural, Jean-Christophe Zeeh, Florent Ubelmann, and Tomas Kirchhausen. "Actin dynamics counteract membrane tension during clathrin-mediated endocytosis." In: *Nature Cell Biology* 13.9 (2011), pp. 1124–1131. DOI: 10.1038/ncb2307. arXiv: NIHMS150003 (cit. on pp. 18, 24, 46, 89).

[144] Stefanie Benesch, Simona Polo, Frank P L Lai, Kurt I Anderson, Theresia E B Stradal, Juergen Wehland, and Klemens Rottner. "N-WASP deficiency impairs EGF internalization and actin assembly at clathrin-coated pits." In: *Journal of cell science* 118.Pt 14 (July 2005), pp. 3103–15. DOI: 10.1242/jcs.02444 (cit. on p. 18).

[145] a Durrbach, D Louvard, and E Coudrier. "Actin filaments facilitate two steps of endocytosis." In: *Journal of cell science* 109 (Pt 2 (Feb. 1996), pp. 457–65 (cit. on p. 18).

[146] Christophe Lamaze, L Miya Fujimoto, Helen L Yin, and Sandra L Schmid. "The actin cytoskeleton is required for receptor-mediated endocytosis in mammalian cells." In: *The Journal of biological chemistry* 272.33 (Aug. 1997), pp. 20332–5. DOI: 10.1074/jbc.272.33.20332 (cit. on p. 18).

[147] L Miya Fujimoto, R Roth, J E Heuser, and S L Schmid. "Actin assembly plays a variable, but not obligatory role in receptor-mediated endocytosis in mammalian cells." In: *Traffic* 1.2 (Feb. 2000), pp. 161–71. DOI: tra010208[pii] (cit. on p. 18).

[148] Howard S Moskowitz, John Heuser, Timothy E McGraw, and Timothy A Ryan. "Targeted Chemical Disruption of Clathrin Function in Living Cells." In: *Molecular Biology of the Cell* 14 (Apr. 2004), pp. 4437–4447. DOI: E03-09-0636 (cit. on p. 18).

[149] Bernardo A Mainou, Paula F Zamora, Alison W Ashbrook, Daniel C Dorset, Kwang S Kim, and Terence S Dermody. "Reovirus Cell Entry Requires Functional Microtubules." In: *mBio* 4.4 (July 2013), e00405–13–e00405–13. DOI: 10.1128/mBio.00405-13 (cit. on p. 18).

[150] Stefan Pöhlmann and Graham Simmons. *Viral Entry into Host Cells*. Ed. by Stefan Pöhlmann and Graham Simmons. Vol. 790. Advances in Experimental Medicine and Biology. New York, NY: Springer New York, 2013. DOI: 10.1007/978-1-4614-7651-1 (cit. on p. 19).

[151] Steeve Boulant, Megan Stanifer, and Pierre-Yves Lozach. "Dynamics of Virus-Receptor Interactions in Virus Binding, Signaling, and Endocytosis." In: *Viruses* 7.6 (2015), pp. 2794–2815. DOI: 10.3390/v7062747 (cit. on pp. 19, 83).

[152] Hosni A M Hussein, Lia R. Walker, Usama M. Abdel-Raouf, Sayed A. Desouky, Abdel Khalek M Montasser, and Shaw M. Akula. "Beyond RGD: virus interactions with integrins." In: *Archives of Virology* 160.11 (2015), pp. 2669–2681. DOI: 10.1007/s00705-015-2579-8 (cit. on p. 19).

[153] Cheng-han Yu et al. "Integrin-beta3 clusters recruit clathrin-mediated endocytic machinery in the absence of traction force." In: *Nature Communications* 6 (2015), p. 8672. DOI: 10.1038/ncomms9672 (cit. on p. 19).

[154] Pere Roca-Cusachs, Nils C Gauthier, Armando Del Rio, and Michael P Sheetz. "Clustering of alpha(5)beta(1) integrins determines adhesion strength whereas alpha(v)beta(3) and talin enable mechanotransduction." In: *Proceedings of the National Academy of Sciences of the United States of America* 106.38 (2009), pp. 16245–16250. DOI: 10.1073/pnas.0902818106 (cit. on p. 19).

[155] Elisabetta Ada Cavalcanti-Adam and Joachim P Spatz. "Receptor clustering control and associated force sensing by surface patterning: when force matters." In: *Nanomedicine* 10.5 (Mar. 2015), pp. 681–684. DOI: 10.2217/nnm.14.234 (cit. on pp. 19, 95).

[156] Roger Oria, Tina Wiegand, Jorge Escribano, Alberto Elosegui-Artola, Juan Jose Uriarte, Cristian Moreno-Pulido, Ilia Platzman, ..., Elisabetta Ada Cavalcanti-Adam, and Pere Roca-cusachs. "Force loading explains cell spatial sensing of ligands." In: *Nature* 552.7684 (2017), tba (cit. on pp. 19, 29, 31, 45, 50, 56–59, 104).

[157] Melissa S Maginnis, J Craig Forrest, Sarah A Kopecky-Bromberg, S Kent Dickeson, Samuel A Santoro, Mary M Zutter, Glen R Nemerow, Jeffrey M Bergelson, and Terence S Dermody. "Beta1 Integrin Mediates Internalization of Mammalian Reovirus." In: *Journal of virology* 80.6 (Mar. 2006), pp. 2760–70. DOI: 10.1128/JVI.80.6.2760-2770.2006 (cit. on pp. 20, 21, 24, 46, 80, 84).

[158] Kenneth L Tyler. "Mammalian reoviruses." In: *Fields Virology*. Ed. by Bernard N Fields, Peter M Howley, Diane E Griffin, Robert A Lamb, Martin A Malcolm, Bernard Roizman, Stephen E Straus, and David M Knipe. 4th ed. Lippincott Williams & Wilkins, 2001. Chap. 53, pp. 1729–1745 (cit. on pp. 19, 24).

[159] Jennifer H Tai, John V Williams, Kathryn M Edwards, Peter F Wright, James E Crowe, and Terence S Dermody. "Prevalence of reovirus-specific antibodies in young children in Nashville, Tennessee." In: *The Journal of infectious diseases* 191.8 (Apr. 2005), pp. 1221–4. DOI: 10.1086/428911 (cit. on p. 19).

[160] Wade L Schulz, Amelia K Haj, and Leslie a Schiff. "Reovirus uses multiple endocytic pathways for cell entry." In: *Journal of virology* 86.23 (Dec. 2012), pp. 12665–75. DOI: 10.1128/JVI.01861-12 (cit. on pp. 19, 21, 73, 90, 92).

[161] Chandini M Thirukkumaran et al. "Oncolytic viral therapy for prostate cancer: efficacy of reovirus as a biological therapeutic." In: *Cancer research* 70.6 (Mar. 2010), pp. 2435–44. DOI: 10.1158/0008-5472.CAN-09-2408 (cit. on p. 20).

[162] Kelly A Dryden, Guoji Wang, Mark Yeager, Max L Nibert, Keven M Coombs, Deirdre B Furlong, Bernard N Fields, and Timothy S Baker. "Early Steps in Reovirus Infection Are Associated with Dramatic Changes in Supramolecular Structure and Protein Conformation: Analysis of Virions and Subviral Particles by Cryoelectron Microscopy and Image Reconstruction." In: *The Journal of Cell Biology* 122.5 (1993), pp. 1023–1041 (cit. on p. 20).

[163] Jennifer E. Stencel-Baerenwald, Kerstin Reiss, Dirk M. Reiter, Thilo Stehle, and Terence S Dermody. "The sweet spot: defining virus–sialic acid interactions." In: *Nature Reviews Microbiology* 12.11 (2014), pp. 739–749. DOI: 10.1038/nrmicro3346 (cit. on p. 20).

[164] Dirk M Reiter, Johnna M Frierson, Elizabeth E Halvorson, Takeshi Kobayashi, Terence S Dermody, and Thilo Stehle. "Crystal structure of reovirus attachment protein $\sigma 1$ in complex with sialylated oligosaccharides." In: *PLoS pathogens* 7.8 (Aug. 2011), e1002166. DOI: 10.1371/journal.ppat.1002166 (cit. on p. 20).

[165] Annukka A R Antar, Jennifer L Konopka, Jacquelyn A Campbell, Rachel A Henry, Ana L Perdigoto, Bruce D Carter, Ambra Pozzi, Ty W Abel, and Terence S Dermody. "Junctional adhesion molecule-A is required for hematogenous dissemination of reovirus." In: *Cell host & microbe* 5.1 (Jan. 2009), pp. 59–71. DOI: 10.1016/j.chom.2008.12.001 (cit. on p. 20).

[166] Erik S. Barton, J. Craig Forrest, Jodi L. Connolly, James D. Chappell, Yuan Liu, Frederick J. Schnell, Asma Nusrat, Charles a. Parkos, and Terence S Dermody. "Junction adhesion molecule is a receptor for reovirus." In: *Cell* 104.3 (2001), pp. 441–451. DOI: 10.1016/S0092-8674(01)00231-8 (cit. on pp. 20, 24, 79).

[167] Laurie S Seliger, Keqin Zheng, and A J Shatkin. "Complete nucleotide sequence of reovirus L2 gene and deduced amino acid sequence of viral mRNA guanylyltransferase." In: *The Journal of biological chemistry* 262.34 (Dec. 1987), pp. 16289–93 (cit. on p. 21).

[168] Melissa S Maginnis, Bernardo a Mainou, Aaron Derdowski, Elizabeth M Johnson, Roy Zent, and Terence S Dermody. "NPXY motifs in the beta1 integrin cytoplasmic tail are required for functional reovirus entry." In: *Journal of virology* 82.7 (Apr. 2008), pp. 3181–91. DOI: 10.1128/JVI.01612-07 (cit. on pp. 21, 83, 84).

[169] Steeve Boulant, Megan Stanifer, Comert Kural, David K Cureton, Ramiro Massol, Max L Nibert, and Tomas Kirchhausen. "Similar uptake but different trafficking and escape routes of reovirus virions and infectious subvirion particles imaged in polarized Madin-Darby canine kidney cells." In: *Molecular biology of the cell* 24.8 (Apr. 2013), pp. 1196–207. DOI: 10.1091/mbc.E12-12-0852 (cit. on pp. 21, 42, 73, 90).

[170] Lennart Treuel, Xiue Jiang, and Gerd Ulrich Nienhaus. "New views on cellular uptake and trafficking of manufactured nanoparticles." In: *Journal of The Royal Society Interface* 10.82

(2013), pp. 20120939–20120939. DOI: 10.1098/rsif.2012.0939 (cit. on p. 21).

[171] Shahed Behzadi et al. "Cellular uptake of nanoparticles: journey inside the cell." In: *Chem. Soc. Rev.* 10.46 (2017), p. 1. DOI: 10.1039/C6CS00636A (cit. on p. 21).

[172] Paola Nativo, Ian a Prior, and Mathias Brust. "Uptake and Intracellular Fate of Surface- Modified Gold Nanoparticles." In: *ACS nano* 2.8 (2008), pp. 1639–1644. DOI: 10.1021/nn800330a (cit. on p. 21).

[173] Andreas Herrmann and Christian Sieben. "Single-virus force spectroscopy unravels molecular details of virus infection." In: *Integr. Biol.* (2015). DOI: 10.1039/C5IB00041F (cit. on p. 22).

[174] David Alsteens, Richard Newton, Rajib Schubert, David Martinez-Martin, Martin Delguste, Botond Roska, and Daniel J. Müller. "Nanomechanical mapping of first binding steps of a virus to animal cells." In: *Nature nanotechnology* 12.2 (2016), pp. 177–183. DOI: 10.1038/nnano.2016.228 (cit. on pp. 22, 23, 78, 100).

[175] Yuping Shan, Xian Hao, Xin Shang, Mingjun Cai, Junguang Jiang, Zhiyong Tang, and Hongda Wang. "Recording force events of single quantum-dot endocytosis." In: *Chemical Communications* 47.12 (2011), p. 3377. DOI: 10.1039/c1cc00040c (cit. on pp. 22, 23, 78).

[176] Yuping Shan, Suyong Ma, Liya Nie, Xin Shang, Xian Hao, Zhiyong Tang, and Hongda Wang. "Size-dependent endocytosis of single gold nanoparticles." In: *Chemical Communications* 47.28 (2011), p. 8091. DOI: 10.1039/c1cc11453k (cit. on pp. 22, 23, 78).

[177] Bohua Ding, Yongmei Tian, Yangang Pan, Yuping Shan, Mingjun Cai, Haijiao Xu, Yingchun Sun, and Hongda Wang. "Recording the dynamic endocytosis of single gold nanoparticles by AFM-based force tracing." In: *Nanoscale* 7.17 (2015), pp. 7545–7549. DOI: 10.1039/C5NR01020A (cit. on pp. 22, 23, 78).

[178] Dimitris Missirlis. "The effect of substrate elasticity and actomyosin contractility on different forms of endocytosis." In: *PLoS ONE* 9.5 (2014). DOI: 10.1371/journal.pone.0096548 (cit. on p. 22).

[179] Christian Rankl, Ferry Kienberger, Linda Wildling, Jürgen Wruss, Hermann J Gruber, Dieter Blaas, and Peter Hinterdorfer. "Multiple receptors involved in human rhinovirus attachment to live cells." In: *Proceedings of the National Academy of Sciences of the United States of America* 105.46 (Nov. 2008),

pp. 17778–83. DOI: 10.1073/pnas.0806451105 (cit. on pp. 22, 100).

[180] Christian Sieben, Christian Kappel, Anna Wozniak, Rong Zhu, Christian Rankl, Peter Hinterdorfer, Helmut Grubmüller, and Andreas Herrmann. "Influenza Virus Adhesion to Living Cells Measured by Single Virus Force Spectroscopy (SVFS) and Force Probe MD Simulation." In: *Biophysical Journal* 100.3 (Feb. 2011), 22a–23a. DOI: 10.1016/j.bpj.2010.12.330 (cit. on p. 23).

[181] Christian Sieben, C Kappel, R Zhu, A Wozniak, Christian Rankl, P Hinterdorfer, H Grubmuller, and Andreas Herrmann. "Influenza virus binds its host cell using multiple dynamic interactions." In: *Proceedings of the National Academy of Sciences* 109.34 (2012), pp. 13626–13631. DOI: 10.1073/pnas.1120265109 (cit. on pp. 23, 78, 100).

[182] A Ashkin. "Acceleration and Trapping of Particles by Radiation Pressure." In: *Physical Review Letters* 24.4 (Jan. 1970), pp. 156–159. DOI: 10.1103/PhysRevLett.24.156 (cit. on p. 23).

[183] Bo-ying Tsai, Jyun-yu Chen, Arthur Chiou, and Yueh-hsin Ping. "Using Optical Tweezers to Quantify the Interaction Force of Dengue Virus with Host Cellular Receptors." In: *Microscopy Microanalytics* 21.0110 (2015), pp. 2014–2015. DOI: 10.1017/S1431927615001890 (cit. on pp. 23, 78).

[184] Laurence Meloty-Kapella, Bhupinder Shergill, Jane Kuon, Elliot Botvinick, and Gerry Weinmaster. "Notch Ligand Endocytosis Generates Mechanical Pulling Force Dependent on Dynamin, Epsins, and Actin." In: *Developmental Cell* 22.6 (2012), pp. 1299–1312. DOI: 10.1016/j.devcel.2012.04.005. arXiv: NIHMS150003 (cit. on pp. 23, 78, 88).

[185] Jianwu Dai and Michael P Sheetz. "Membrane tether formation from blebbing cells." In: *Biophysical journal* 77.6 (Dec. 1999), pp. 3363–70. DOI: 10.1016/S0006-3495(99)77168-7 (cit. on p. 24).

[186] Howard L. Weiner, M L Powers, and Bernard N. Fields. "Absolute linkage of virulence and central nervous system cell tropism of reoviruses to viral hemagglutinin." In: *The Journal of infectious diseases* 141.5 (May 1980), pp. 609–16 (cit. on p. 24).

[187] Roman Glass, Marco Arnold, Elisabetta Ada Cavalcanti-Adam, Jacques Blümmel, Christian Haferkemper, Charlotte Dodd, and Joachim P Spatz. "Block copolymer micelle nanolithography on non-conductive substrates." In: *New Journal of Physics* 6 (Aug. 2004), pp. 101–101. DOI: 10.1088/1367-2630/6/1/101 (cit. on p. 29).

[188] Joachim P Spatz, S Mössmer, and Christoph Hartmann. "Ordered deposition of inorganic clusters from micellar block copolymer films." In: *Langmuir* 6 (2000), pp. 407–415 (cit. on p. 29).

[189] Theobald Lohmüller, Daniel Aydin, Marco Schwieder, Christoph Morhard, Ilia Louban, Claudia Pacholski, and Joachim P Spatz. "Nanopatterning by block copolymer micelle nanolithography and bioinspired applications." In: *Biointerphases* 6.1 (Mar. 2011), MR1–12. DOI: 10.1116/1.3536839 (cit. on p. 29).

[190] Kenneth R Brown and Michael J Natan. "Hydroxylamine Seeding of Colloidal Au Nanoparticles in Solution and on Surfaces." In: *Langmuir* 14.4 (Feb. 1998), pp. 726–728. DOI: 10.1021/la970982u (cit. on p. 32).

[191] Theobald Lohmüller, Eva Bock, and Joachim P Spatz. "Synthesis of Quasi-Hexagonal Ordered Arrays of Metallic Nanoparticles with Tuneable Particle Size." In: *Advanced Materials* 20.12 (2008), pp. 2297–2302. DOI: 10.1002/adma.200702635 (cit. on p. 32).

[192] Daniel Aydin et al. "Polymeric substrates with tunable elasticity and nanoscopically controlled biomolecule presentation." In: *Langmuir : the ACS journal of surfaces and colloids* 26.19 (Oct. 2010), pp. 15472–80. DOI: 10.1021/la103065x (cit. on p. 32).

[193] Patrizia Richner, Stephan J P Kress, David Norris, and Dimos Poulikakos. "Charge Effects and Nanoparticle Pattern Formation in Electrohydrodynamic NanoDrip Printing of Colloids." In: *Nanoscale* 8 (2016), pp. 6028–6034. DOI: 10.1039/C5NR08783J (cit. on p. 32).

[194] Patrizia Richner, Hadi Eghlidi, Stephan J P Kress, Martin Schmid, David J Norris, and Dimos Poulikakos. "Printable Nanoscopic Metamaterial Absorbers and Images with Diffraction-Limited Resolution." In: *ACS Applied Materials & Interfaces* 8.18 (May 2016), pp. 11690–11697. DOI: 10.1021/acsami.6b01585 (cit. on p. 32).

[195] Jang-Ung Park et al. "High-resolution electrohydrodynamic jet printing." In: *Nature materials* 6.10 (Oct. 2007), pp. 782–9. DOI: 10.1038/nmat1974 (cit. on p. 32).

[196] P. Galliker, J. Schneider, H. Eghlidi, S. Kress, V. Sandoghdar, and D. Poulikakos. "Direct printing of nanostructures by electrostatic autofocussing of ink nanodroplets." In: *Nature Communications* 3.May (2012), p. 890. DOI: 10.1038/ncomms1891 (cit. on p. 32).

[197] Patrick Galliker, Julian Schneider, L Ruthemann, and Dimos Poulikakos. "Open-atmosphere sustenance of highly volatile attoliter-size droplets on surfaces." In: *Proceedings of the National Academy of Sciences* 110.33 (Aug. 2013), pp. 13255–13260. DOI: 10.1073/pnas.1305886110 (cit. on p. 32).

[198] Jacques Blümmel, Nadine Perschmann, Daniel Aydin, Jovana Drinjakovic, Thomas Surrey, Monica Lopez-garcia, Horst Kessler, and Joachim P Spatz. "Protein repellent properties of covalently attached PEG coatings on nanostructured SiO 2 - based interfaces." In: *Biomater* 28 (2007), pp. 4739–4747. DOI: 10.1016/j.biomaterials.2007.07.038 (cit. on p. 34).

[199] Vu Hong, Stanislav Presolski, Celia Ma, and M.G. Finn. "Analysis and Optimization of Copper-Catalyzed Azide-Alkyne Cycloaddition for Bioconjugation." In: *Angewandte Chemie International Edition* 48.52 (Dec. 2009), pp. 9879–9883. DOI: 10.1002/anie.200905087 (cit. on pp. 39, 43).

[200] Deirdre B Furlong, Max L Nibert, and B N Fields. "Sigma 1 protein of mammalian reoviruses extends from the surfaces of viral particles." In: *Journal of virology* 62.1 (Jan. 1988), pp. 246–56 (cit. on p. 41).

[201] Laurie J Sturzenbecker, Max Nibert, Deirdre Furlong, and B N Fields. "Intracellular digestion of reovirus particles requires a low pH and is an essential step in the viral infectious cycle." In: *Journal of virology* 61.8 (Aug. 1987), pp. 2351–61 (cit. on p. 41).

[202] James D Chappell, Erik S Barton, Trent H Smith, Geoffrey S Baer, David T Duong, Max L Nibert, and Terence S Dermody. "Cleavage susceptibility of reovirus attachment protein sigma1 during proteolytic disassembly of virions is determined by a sequence polymorphism in the sigma1 neck." In: *Journal of virology* 72.10 (Oct. 1998), pp. 8205–13 (cit. on p. 41).

[203] Stanislav I Presolski, Vu Phong Hong, and M G Finn. "Copper-Catalyzed Azide-Alkyne Click Chemistry for Bioconjugation." In: *Current protocols in chemical biology* 3.4 (Dec. 2011), pp. 153–162. DOI: 10.1002/9780470559277.ch110148. arXiv: NIHMS150003 (cit. on p. 43).

[204] Chayasith Uttamapinant, Anupong Tangpeerachaikul, Scott Grecian, Scott Clarke, Upinder Singh, Peter Slade, Kyle R Gee, and Alice Y Ting. "Fast, cell-compatible click chemistry with copper-chelating azides for biomolecular labeling." In: *Angewandte Chemie (International ed. in English)* 51.24 (June 2012), pp. 5852–6. DOI: 10.1002/anie.201108181. arXiv: NIHMS150003 (cit. on p. 43).

[205] Michael D. Allen et al. "Altered microenvironment promotes progression of preinvasive breast cancer: Myoepithelial expression of avb6 integrin in DCIS identifies high-risk patients and predicts recurrence." In: *Clinical Cancer Research* 20.2 (2014), pp. 344–357. DOI: 10.1158/1078-0432.CCR-13-1504 (cit. on p. 45).

[206] Viktoria Schaufler, Helmi Czichos-Medda, Vera Hirschfeld-Warneken, Stefanie Neubauer, Florian Rechenmacher, Rebecca Medda, Horst Kessler, Benjamin Geiger, Joachim P Spatz, and Elisabetta Ada Cavalcanti-Adam. "Selective binding and lateral clustering of α 5 β 1 and α v β 3 integrins: Unraveling the spatial requirements for cell spreading and focal adhesion assembly." In: *Cell Adhesion & Migration* 10.5 (Sept. 2016), pp. 505–515. DOI: 10.1080/19336918.2016.1163453 (cit. on p. 46).

[207] Saveez Saffarian, Emanuele Cocucci, and Tomas Kirchhausen. "Distinct dynamics of endocytic clathrin-coated pits and coated plaques." In: *PLoS Biology* 7.9 (2009). DOI: 10.1371/journal.pbio.1000191 (cit. on p. 46).

[208] Hanna Damke, Takeshi Baba, Dale E Warnock, and Sandra L Schmid. "Induction of mutant dynamin specifically blocks endocytic coated vesicle formation." In: *The Journal of Cell Biology* 127.4 (Nov. 1994), pp. 915–934. DOI: 10.1083/jcb.127.4.915 (cit. on p. 46).

[209] P Thévenaz, U E Ruttimann, and M Unser. "A pyramid approach to subpixel registration based on intensity." In: *IEEE transactions on image processing : a publication of the IEEE Signal Processing Society* 7.1 (Jan. 1998), pp. 27–41. DOI: 10.1109/83.650848 (cit. on p. 51).

[210] Dennis E Discher, Paul A Janmey, and Yu-Li Wang. "Tissue cells feel and respond to the stiffness of their substrate." In: *Science* 310.5751 (Nov. 2005), pp. 1139–43. DOI: 10.1126/science.1116995 (cit. on p. 57).

[211] Penelope C Georges. "Cell type-specific response to growth on soft materials." In: *Journal of Applied Physiology* 98.4 (Apr. 2005), pp. 1547–1553. DOI: 10.1152/japplphysiol.01121.2004 (cit. on p. 57).

[212] Ai Kia Yip, Katsuhiko Iwasaki, Chaitanya Ursekar, Hiroaki Machiyama, Mayur Saxena, Huiling Chen, Ichiro Harada, Keng-Hwee Chiam, and Yasuhiro Sawada. "Cellular response to substrate rigidity is governed by either stress or strain." In: *Biophysical journal* 104.1 (Jan. 2013), pp. 19–29. DOI: 10.1016/j.bpj.2012.11.3805 (cit. on p. 57).

[213] E Clarence Chan and David J Odde. "Traction Dynamics of Filopodia on Compliant Substrates." In: *Science* 322.5908 (Dec. 2008), pp. 1687–1691 (cit. on pp. 58, 104).

[214] Alex G F de Beer, E Ada Cavalcanti-Adam, Günter Majer, M Lopez-García, Horst Kessler, and Joachim P Spatz. "Force-induced destabilization of focal adhesions at defined integrin spacings on nanostructured surfaces." In: *Physical review. E, Statistical, nonlinear, and soft matter physics* 81.5 Pt 1 (May 2010), p. 051914. DOI: 10.1103/PhysRevE.81.051914 (cit. on p. 58).

[215] Sergey V Plotnikov and Clare M Waterman. "Guiding cell migration by tugging." In: *Current Opinion in Cell Biology* Figure 1 (July 2013), pp. 1–8. DOI: 10.1016/j.ceb.2013.06.003 (cit. on p. 58).

[216] Tim Mitchison and M Kirschner. "Cytoskeletal dynamics and nerve growth." In: *Neuron* 1.9 (1988), pp. 761–772. DOI: 0896-6273(88)90124-9[pii] (cit. on p. 58).

[217] A. del Rio, Raul Perez-Jimenez, Ruchuan Liu, Pere Roca-Cusachs, Julio M Fernandez, and Michael P Sheetz. "Stretching Single Talin Rod Molecules Activates Vinculin Binding." In: *Science* 323.5914 (Jan. 2009), pp. 638–641. DOI: 10.1126/science.1162912 (cit. on p. 59).

[218] Pere Roca-Cusachs, Thomas Iskratsch, and Michael P Sheetz. "Finding the weakest link – exploring integrin-mediated mechanical molecular pathways." In: *Journal of Cell Science* 125.13 (July 2012), pp. 3025–3038. DOI: 10.1242/jcs.095794 (cit. on pp. 59, 104).

[219] Phoebe L Stewart and Glen R Nemerow. "Cell integrins: commonly used receptors for diverse viral pathogens." In: *Trends in microbiology* 15.11 (Nov. 2007), pp. 500–7. DOI: 10.1016/j.tim.2007.10.001 (cit. on p. 67).

[220] Marta Fratini, Tina Wiegand, Charlotta Funaya, Zhongxiang Jiang, Pranav N M Shah, Joachim P Spatz, Elisabetta Ada Cavalcanti-Adam, and Steeve Boulant. "Surface Immobilization of Viruses and Nanoparticles Elucidates Early Events in Clathrin-mediated Endocytosis." In: *submitted* (2017) (cit. on pp. 69, 72, 80).

[221] Michael E Drew, Arkadiusz Chworos, Emin Oroudjev, Helen Hansma, and Yoko Yamakoshi. "A tripod molecular tip for single molecule ligand-receptor force spectroscopy by AFM." In: *Langmuir* 26.10 (2010), pp. 7117–7125. DOI: 10.1021/la904151h (cit. on p. 73).

[222] Vincent Tabard-Cossa, Matthew Wiggin, Dhruti Trivedi, Nahid N Jetha, Jason R Dwyer, and Andre Marziali. "Single-molecule bonds characterized by solid-state nanopore force spectroscopy." In: *ACS nano* 3.10 (2009), pp. 3009–14. DOI: 10.1021/nn900713a (cit. on pp. 74, 77).

[223] Joshua R Wayment and Joel M Harris. "Biotin-avidin binding kinetics measured by single-molecule imaging." In: *Analytical Chemistry* 81.1 (2009), pp. 336–342. DOI: 10.1021/ac801818t (cit. on p. 74).

[224] Shulei Zhao and W. M. Reichert. "Influence of biotin lipid surface density and accessibility on avidin binding to the tip of an optical fiber sensor." In: *Langmuir* 8.11 (Nov. 1992), pp. 2785–2791. DOI: 10.1021/la00047a034 (cit. on p. 75).

[225] Linda S Jung, Kjell E Nelson, P S Stayton, and Charles T Campbell. "Binding and Dissociation Kinetics of Wild-Type and Mutant Streptavidins on Mixed Biotin-Containing Alkylthiolate Monolayers." In: *Langmuir* 16.24 (Nov. 2000), pp. 9421–9432. DOI: 10.1021/la000144r (cit. on p. 75).

[226] Hg Döbereiner and B Dubin-Thaler. "Dynamic phase transitions in cell spreading." In: *Physical review ...* Dic (2004). arXiv: 0405008v1 [arXiv:q-bio] (cit. on p. 76).

[227] Damien Cuvelier, Manuel Théry, Yeh-Shiu Chu, Sylvie Dufour, Jean-Paul Thiéry, Michel Bornens, Pierre Nassoy, and L Mahadevan. "The Universal Dynamics of Cell Spreading." In: *Current Biology* 17.8 (Apr. 2007), pp. 694–699. DOI: 10.1016/j.cub.2007.02.058 (cit. on p. 76).

[228] Haguy Wolfenson, Thomas Iskratsch, and Michael P Sheetz. *Early events in cell spreading as a model for quantitative analysis of biomechanical events*. 2015. DOI: 10.1016/j.bpj.2014.10.041 (cit. on p. 76).

[229] Veljko Veljkovic, Sanja Glisic, Claude P. Muller, Matthew Scotch, Donald R. Branch, Vladimir R. Perovic, Milan Sencanski, Nevena Veljkovic, and Alfonso Colombatti. "In silico analysis suggests interaction between Ebola virus and the extracellular matrix." In: *Frontiers in Microbiology* 6.FEB (Feb. 2015). DOI: 10.3389/fmicb.2015.00135 (cit. on p. 76).

[230] Neel Thakkar, Tejabhiram Yadavalli, Dinesh Jaishankar, and Deepak Shukla. "Emerging Roles of Heparanase in Viral Pathogenesis." In: *Pathogens* 6.3 (Sept. 2017), p. 43. DOI: 10.3390/pathogens6030043 (cit. on p. 76).

[231] Livia Stavolone and Vincenzo Lionetti. "Extracellular Matrix in Plants and Animals: Hooks and Locks for Viruses." In: *Frontiers in Microbiology* 8 (Sept. 2017). DOI: 10.3389/fmicb.2017.01760 (cit. on p. 76).

[232] E S Barton, J L Connolly, J C Forrest, J D Chappell, and Terence S Dermody. "Utilization of sialic acid as a coreceptor enhances reovirus attachment by multistep adhesion strengthening." In: *The Journal of biological chemistry* 276.3 (Jan. 2001), pp. 2200–11. DOI: 10.1074/jbc.M004680200 (cit. on p. 79).

[233] Inés Martìn-Padura et al. "Junctional Adhesion Molecule, a Novel Member of the Immunoglobulin Superfamily That Distributes at Intercellular Junctions and Modulates Monocyte Transmigration." In: *The Journal of Cell Biology* 142.1 (July 1998), pp. 117–127. DOI: 10.1083/jcb.142.1.117 (cit. on p. 80).

[234] J Craig Forrest, Jacquelyn A Campbell, Pierre Schelling, Thilo Stehle, and Terence S Dermody. "Structure-Function Analysis of Reovirus Binding to Junctional Adhesion Molecule 1." In: *Journal of Biological Chemistry* 278.48 (Nov. 2003), pp. 48434–48444. DOI: 10.1074/jbc.M305649200 (cit. on p. 80).

[235] C Eberlein et al. "A human monoclonal antibody 264RAD targeting αvβ6 integrin reduces tumour growth and metastasis, and modulates key biomarkers in vivo." In: *Oncogene* 32.37 (2012), pp. 4406–4416. DOI: 10.1038/onc.2012.460 (cit. on p. 81).

[236] Adam Byron, Jonathan D Humphries, Janet A Askari, Sue E Craig, A Paul Mould, and Martin J Humphries. "Anti-integrin monoclonal antibodies." In: *Journal of Cell Science* 122.22 (2009), 4009 LP –4011. DOI: 10.1242/jcs.056770 (cit. on p. 81).

[237] Carolyn B Coyne. "The distinct roles of JAM-A in reovirus pathogenesis." In: *Cell host & microbe* 5.1 (Jan. 2009), pp. 3–5. DOI: 10.1016/j.chom.2008.12.009 (cit. on p. 83).

[238] Jennifer L Konopka-Anstadt, Bernardo A Mainou, Danica M Sutherland, Yuichi Sekine, Stephen M Strittmatter, and Terence S Dermody. "The Nogo receptor NgR1 mediates infection by mammalian reovirus." In: *Cell host & microbe* 15.6 (June 2014), pp. 681–91. DOI: 10.1016/j.chom.2014.05.010. arXiv: NIHMS150003 (cit. on p. 84).

[239] Yareni A Ayala, Bruno Pontes, Barbara Hissa, Ana Carolina M. Monteiro, Marcos Farina, Vivaldo Moura-Neto, Nathan B Viana, and H Moysés Nussenzveig. "Effects of cytoskeletal drugs on actin cortex elasticity." In: *Experimental Cell Research* 351.2 (Feb. 2017), pp. 173–181. DOI: 10.1016/j.yexcr.2016.12.016 (cit. on p. 88).

[240] Alastair S Robertson, Elizabeth Smythe, and Kathryn R Ayscough. "Functions of actin in endocytosis." In: *Cellular and Molecular Life Sciences* 66.13 (July 2009), pp. 2049–2065. DOI: 10.1007/s00018-009-0001-y (cit. on p. 89).

[241] Jason Mercer, Mario Schelhaas, and Ari Helenius. "Virus Entry by Endocytosis." In: *Annual Review of Biochemistry* 79.1 (2010), pp. 803–833. DOI: 10.1146/annurev-biochem-060208-104626 (cit. on p. 89).

[242] Callista B Harper, Michel R Popoff, Adam McCluskey, Phillip J Robinson, and Frédéric A Meunier. "Targeting membrane trafficking in infection prophylaxis: dynamin inhibitors." In: *Trends in Cell Biology* 23.2 (Feb. 2013), pp. 90–101. DOI: 10.1016/j.tcb.2012.10.007 (cit. on p. 92).

[243] K M Guglielmi, E M Johnson, Thilo Stehle, and Terence S Dermody. "Attachment and cell entry of mammalian orthoreovirus." In: *Current topics in microbiology and immunology* 309 (Jan. 2006), pp. 1–38 (cit. on p. 92).

[244] Wei R. Huang, Ying C. Wang, Pei I. Chi, Lai Wang, Chi Y. Wang, Chi H. Lin, and Hung J. Liu. "Cell Entry of Avian Reovirus Follows a Caveolin-1-mediated and Dynamin-2-dependent Endocytic Pathway That Requires Activation of p38 Mitogen-activated Protein Kinase (MAPK) and Src Signaling Pathways as Well as Microtubules and Small GTPase Rab5 Protein." In: *Journal of Biological Chemistry* 286.35 (Sept. 2011), pp. 30780–30794. DOI: 10.1074/jbc.M111.257154 (cit. on p. 92).

[245] Bernardo a Mainou and Terence S Dermody. "Src kinase mediates productive endocytic sorting of reovirus during cell entry." In: *Journal of virology* 85.7 (Apr. 2011), pp. 3203–13. DOI: 10.1128/JVI.02056-10 (cit. on p. 92).

[246] Sung Sik Hur, Yihua Zhao, Yi-Shuan Li, Elliot Botvinick, and Shu Chien. "Live Cells Exert 3-Dimensional Traction Forces on Their Substrata." In: *Cellular and molecular bioengineering* 2.3 (Sept. 2009), pp. 425–436. DOI: 10.1007/s12195-009-0082-6 (cit. on p. 96).

[247] J. E. Molloy, J. E. Burns, J. Kendrick-Jones, R. T. Tregear, and D. C S White. "Movement and force produced by a single myosin head." In: *Nature* 378.6553 (Nov. 1995), pp. 209–212. DOI: 10.1038/378209a0 (cit. on p. 104).

[248] Rustem I Litvinov, Andrey Mekler, Henry Shuman, Joel S Bennett, Valeri Barsegov, and John W Weisel. "Resolving Two-dimensional Kinetics of the Integrin αIIbβ3-Fibrinogen Interactions Using Binding-Unbinding Correlation Spectroscopy." In: *Journal of Biological Chemistry* 287.42 (Oct. 2012), pp. 35275–35285. DOI: 10.1074/jbc.M112.404848 (cit. on p. 104).

LIST OF FIGURES

LIST OF TABLES

ACRONYMS

ECM extracellular matrix

YAP yes-associated protein 1

MRTFA myocardin-related transcription factor A

EG ethylene glycol

PEG polyethylene glycol

RGD Arg-Gly-Asp

cRGD cyclic Arg-Gly-Asp

FA focal adhesion

FAK focal adhesion kinase

TFM traction force microscopy

cTFM confocal reference-free traction force microscopy

Qdots quantum dots

AuNPs gold nanoparticles

FRET Förster resonance energy transfer

NSET nanometal surface energy transfer

PRIM proximitry imaging

PECAM-1 platelet endothelial cell adhesion molecules

WLC worm-like chain

PEG polyethylene glycol

Ab antibody

EGF epidermal growth factor

MTFM molecular tension fluorescence microscopy

BCML block copolymer micelle nanolithography

CME clathrin-mediated endocytosis

CCP clathrin-coated pit

FCHO FCH domain only Proteins

CCV clathrin-coated vesicle

JAM-A junctional adhesion molecule A

GFOGER Gly-Phe-Hyp-Gly-Glu-Arg

ISVP intermediate subviral particle

IDSS Ile-Asp-Ser-Ser

BAR Bin-Amphiphysin-Rvs

PtdIns phosphoinositides

SVFS single-virus force spectroscopy

AFM atomic force microscopy

EGF epidermal growth factor

PBS phosphate buffered saline

NHS N-hydroxysuccinimide

APS ammonium persulfate

TEMED N,N,N´,N´-Tetramethylethylenediamine

HEPES 4-(2-Hydroxyethyl)piperazine-1-ethanesulfonic acid

IF immunofluorescence

RT room temperature

PAA polyacrylamide

RT room temperature

DCM dichloromethane

TFA trifluoracetic acid

DMF N,N-dimethylformamide

HPLC high performance liquid chromatography

DNA deoxyribonucleic acid

CuAAC copper-catalyzed azide-alkyne cycloaddition

TEAA Trietyhlammonium acetate

THPTA tris(3-hydroxypropyltriazolylmethyl)amine

OD optical density

IPTG isopropyl beta-D-1-thiogalactopyranoside

PMSF Phenylmethylsulfonylfluorid

DTT Dithiothreitol

VB virus buffer

TRIS tris(hydroxylmethyl) aminomethane

MW molecular wight

MWCO molecular wight cut-off

DMEM Dulbecco´s modified eagle medium

FBS fetal bovine serum

REF rat embryonic fibroblasts

KO knockout

MALDI matrix-assisted laser desorption/ionization

THF tetrahydrofuran

DHB 2,5-dihydroxybenzoic acid

LUTs lookup tables

YFP yellow fluorescent protein

eGFP enhanced green fluorescent protein

ROCK Rho-associated protein kinase

MMPs matrix metalloproteinases

BSA bovine serum albumin

DMSO dimethyl sulfoxide

SEM Scanning electron microscopy

TIRF total internal reflection fluorescence

TGT tension gauge tethers

CLT clathrin light chain

FTTC Fourier transform traction cytometry

PIV particle image velocimetry

NgR1 Nogo receptor 1

PUBLICATIONS

JOURNAL ARTICLES

Roger Oria, Tina Wiegand, Jorge Escribano, Alberto Elosegui-Artola, Juan Jose Uriarte, Cristian Moreno-Pulido, Ilia Platzman, Daniel Navajas, Xavier Trepat, José Manuel García-Aznar, Elisabetta Ada Cavalcanti-Adam, and Pere Roca- Cusachs. "Force loading explains cell spatial sensing of ligands." In: *Nature* 552.7684 (Dez. 2017)

Marta Fratini, Tina Wiegand, Charlotta Funaya, Zhongxiang Jiang, Pranav N M Shah, Joachim P Spatz, Elisabetta Ada Cavalcanti-Adam and Steeve Boulant. "Surface immobilization of viruses and nanoparticles elucidates early events in clathrin-mediated endocytosis." submitted.

Tina Wiegand, Yang Liu, Kornelia Galior, Khalid Salaita, Marta Fratini, Steeve Boulant, Klaus Yserentant, Felix Frey, Joachim Spatz and Elisabetta Ada Cavalcanti-Adam. "Forces during virus particle uptake at the cell-matrix interface." In preparation.

Tina Wiegand, Tobias Lendenmann, Aldo Ferrari, Ulrich Schwarz, Joachim Spatz and Elisabetta Ada Cavalcanti-Adam. "Combination of traction force microscopy with molecular tension sensors elucidates force load on individual integrin receptors on soft substrates." In preparation.

CONFERENCE CONTRIBUTIONS

5th Heidelberg Forum for Young Life Scientists „A Tale of Cells and Organisms" (Jun. 2017), poster: "Forces during virus particle uptake"

15th Workshop „Cell Biology of Viral Infections" of the Society for Virology (GfV) (Nov. 2016), oral contribution: "Force sensing during virus particle uptake"

18th EMBL PhD Symposium „Life by Numbers: Towards Quantitative Biology" (Nov. 2016), oral contribution and poster: "Force measurements of single virus particle uptake"

Conference: XII Recontres du Vietnam, Quy Nhon: Mechanobiology, from Molecules to Tissue (Jun. 2016), oral contribution: "Forces sensing during virus particle uptake"

6th European Cell Mechanics Meeting, Barcelona (May 2015), poster: "Interplay between integrin expression, clustering, and substrate rigidity in cell mechanical response"

EIDESSTATTLICHE VERSICHERUNG GEMÄSS § 8 DER PROMOTIONSORDNUNG DER NATURWISSENSCHAFTLICH-MATHEMATISCHEN GESAMTFAKULTÄT DER UNIVERSITÄT HEIDELBERG

---

1. Bei der eingereichten Dissertation zu dem Thema *Receptor-mediated Forces for Cell Sensing of Extracellular Ligands and for Virus Particle Uptake* handelt es sich um meine eigenständig erbrachte Leistung.

2. Ich habe nur die angegebenen Quellen und Hilfsmittel benutzt und mich keiner unzulässigen Hilfe Dritter bedient. Insbesondere habe ich wörtlich oder sinngemäß aus anderen Werken übernommene Inhalte als solche kenntlich gemacht.

3. Die Arbeit oder Teile davon habe ich bislang nicht an einer Hochschule des In- oder Auslands als Bestandteil einer Prüfungs- oder Qualifikationsleistung vorgelegt.

4. Die Richtigkeit der vorstehenden Erklärungen bestätige ich.

5. Die Bedeutung der eidesstattlichen Versicherung und die strafrechtlichen Folgen einer unrichtigen oder unvollständigen eidesstattlichen Versicherung sind mir bekannt. Ich versichere an Eides statt, dass ich nach bestem Wissen die reine Wahrheit erklärt und nichts verschwiegen habe.

Heidelberg, December 2017

Tina Wiegand